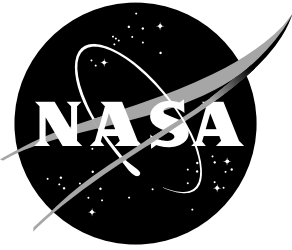


# Sliding Mode Thermal Control System for Space Station Furnace Facility

---

*M.E. Jackson*



# Sliding Mode Thermal Control System for Space Station Furnace Facility

---

*M.E. Jackson*  
*Marshall Space Flight Center • MSFC, Alabama*

## TABLE OF CONTENTS

	Page
I. INTRODUCTION .....	1
II. MODEL FORMULATION .....	3
A. Theory .....	3
B. TCS Model.....	6
1. Flow Path Model.....	7
2. Source Model.....	11
3. Model Disturbances and Assumptions .....	14
C. Summary .....	15
III. BASICS OF SLIDING MODE CONTROL.....	15
A. Background .....	15
B. Theory .....	19
1. System Transformation .....	19
2. Sliding Surface Design .....	22
3. Control Function Design.....	23
C. Summary .....	25
IV. PROBLEM FORMULATION .....	26
V. SLIDING MODE CONTROLLER DESIGN .....	26
A. System Transformation .....	27
B. Sliding Surface Design .....	31
C. Control Function Design.....	32
D. Realization of Control Function .....	35
E. Summary .....	36
VI. SIMULATION RESULTS .....	37
A. Interaction Disturbances .....	37
B. External Disturbances .....	42
C. Plant Uncertainties .....	44
1. Pressure Source .....	44
2. Flow Path .....	45
3. Flow Actuator .....	46
D. Smoothing Function.....	46
E. Summary .....	48
VII. COMPARISON RESULTS .....	49
A. Interaction Disturbance .....	49
B. External Disturbance .....	53
C. Summary .....	55
VIII. CONCLUSION.....	55
A. Performance .....	56
B. Advantages .....	56
APPENDIX: TCS MARSYAS Program .....	57
REFERENCES.....	66

## LIST OF ILLUSTRATIONS

Figure	Title	Page
1.	TCS schematic .....	1
2.	TCS equivalent circuit .....	7
3.	Pump map .....	12
4.	System block diagram .....	16
5.	Phase plane plot for $k(x_1) = -3$ .....	17
6.	Phase plane plot for $k(x_1) = +3$ .....	17
7.	Phase plane plot for $a > 2$ .....	18
8.	Phase plane plot for $a < 2$ .....	19
9.	Time-varying flow profile plots .....	34
10.	Required $u^{eq}(t,x)$ for path plots .....	34
11.	Sliding mode controller block diagram .....	35
12.	Flow response in path 1 with interaction disturbance .....	38
13.	Flow response in path 2 with interaction disturbance .....	38
14.	Flow response in path 3 with interaction disturbance .....	39
15.	Flow response in path 4 with interaction disturbance .....	39
16.	Pressure response with interaction disturbance .....	40
17.	Control input to each path with interaction disturbance .....	40
18.	Moving averages of control inputs with interaction disturbance .....	41
19.	Valve actuator response with interaction disturbance .....	41
20.	Normalized disturbance torque function .....	42
21.	Flow response in path 1 with external disturbance .....	43
22.	Flow response in path 2 with external disturbance .....	43
23.	Flow response in path 3 with external disturbance .....	44
24.	Flow response in path 2 with source uncertainty .....	45
25.	Flow response in path 2 with flow path uncertainty .....	45
26.	Flow response in path 1 with flow actuator uncertainty .....	46

## LIST OF ILLUSTRATIONS

Figure	Title	Page
27.	Flow response in path 2 with discontinuous controller.....	47
28.	Flow response in path 2 with smoothing controller .....	47
29.	Smoothing controller input to path 2 .....	48
30.	Flow response in path 1 for flight controller with interaction disturbance .....	50
31.	Flow response in path 2 for flight controller with interaction disturbance .....	50
32.	Flow response in path 3 for flight controller with interaction disturbance .....	51
33.	Flow response in path 1 for sliding controller with interaction disturbance .....	51
34.	Flow response in path 2 for sliding controller with interaction disturbance .....	52
35.	Flow response in path 3 for sliding controller with interaction disturbance .....	52
36.	Flow response in path 1 for flight controller with external disturbance .....	53
37.	Flow response in path 2 for flight controller with external disturbance .....	54
38.	Flow response in path 3 for flight controller with external disturbance .....	54
39.	System pressure drop for flight controller with external disturbance .....	55

## LIST OF TABLES

Table	Title	Page
1.	Valve loss data .....	9
2.	Source coefficient data .....	14

## LIST OF SYMBOLS

<u>Symbol</u>	<u>Definition</u>
$a$	sliding surface slope for sliding example
$a_p$	pipe cross-sectional area
$\mathbf{B}$	matrix of plant input gains
$C$	system compliance
$d$	inside diameter of pipe
$E$	Young's modulus of elasticity
$e_i$	flow tracking error for each path
$e_p$	pipe wall thickness
$f$	smooth vector field consisting of system states
$\mathbf{G}$	system input matrix
$g_c$	conversion constant
$h$	smooth vector field consisting of system output states
$\mathbf{I}$	identity matrix
$I_a$	pump motor armature current
$J_{\alpha,\beta,\delta}$	least-squares method coefficients
$J_{ml}$	pump rotor plus load inertia
$k_1$	pump speed to load torque gain
$k_2$	pump speed controller feedforward gain
$k_3$	pump speed controller feedforward gain
$k_e$	pump motor back emf gain
$k_f$	valve loss factor
$k_f^*$	valve $k$ -factor
$k_t$	pump motor current torque gain
$k_v$	actuator conversion constant between voltage and position
$l$	length of pipe
lbm/h	pound mass per hour

$L_f^r$	$r$ -th order Lie derivative
$L_m$	pump motor inductance
$L_{P_i}$	lumped flow path inertances
$L_S$	source flow inertance
$M$	matrix of pressure and pump controller gains
$m$	total mass within a defined control volume
$P$	system pressure drop
$P_S$	pressure drop across source pump
$Q$	vector of pressure and pump controller gains
$R_m$	pump motor resistance
$R_{P_i}$	lumped path resistances
$R_S$	source flow resistance
$R_{V_i}$	valve resistances
$t_{r_i}$	sliding surface reaching time
$u_i$	control input signal to each path's actuator
$u_i^{eq}$	equivalent control necessary to linearize the nonlinear system
$u_i^{\max}$	maximum control input to maintain desired profile tracking
$W_i$	path flow rates
$W_S$	source flow rate
$X_c$	vector of pressure and pump controller states
$Z$	phase-variable states in the normal form
$\alpha, \beta, \delta$	curve fit coefficients for the valve k-factor
$\varepsilon$	switching surface boundary layer width
$\eta$	internal dynamic states in the normal form
$\theta_i$	valve position for each path
$\lambda_i$	internal dynamics eigenvalues

$\rho$	density of water
$\rho_i$	switched part of the sliding mode control function
$\sigma_i$	sliding surface definition for each path
$\tau$	actuator plus valve time response delay
$\tau_f$	pump speed filter time constant
$\Omega$	convenience variable to calculate equivalent control
$\omega_{fbk}$	pump speed feedback
$\omega_i$	angular velocity for each path's actuator plus valve combination
$\omega_p$	angular pump speed
$\forall$	symbol that means "for all"

TECHNICAL MEMORANDUM

SLIDING MODE THERMAL CONTROL SYSTEM FOR SPACE STATION FURNACE FACILITY

I. INTRODUCTION

The space station furnace facility (SSFF) is a facility for materials research in the microgravity environment of the *International Space Station Alpha* U.S. Laboratory. The SSFF will accommodate basic research, commercial applications, and studies of phenomena of metals and alloys, electronic and photonic materials, and glasses and ceramics. To support this broad base of research requirements, the SSFF will provide the core systems to operate, regulate, and support a variety of furnaces. The core systems include electrical power, gas distribution, thermal and environmental control, magnetic damping, health monitoring, and sample translation and exchange.

The thermal and environmental control system has as one of its subsystems the thermal control subsystem (TCS). The TCS functions to collect, transport, and reject excess thermal energy from components, subsystems, and furnaces within the SSFF that have an active fluid interface. The TCS utilizes single-phase water as its cooling medium and consists of piping, heat exchangers, coldplates, valves, flow sensors, temperature sensors, pressure sensors, furnace cooling jackets, and a centrifugal pump. The schematic of the TCS is shown in figure 1. The thermal systems are plumbed in parallel paths to conserve water resources and to maintain maximum heat rejection capabilities.

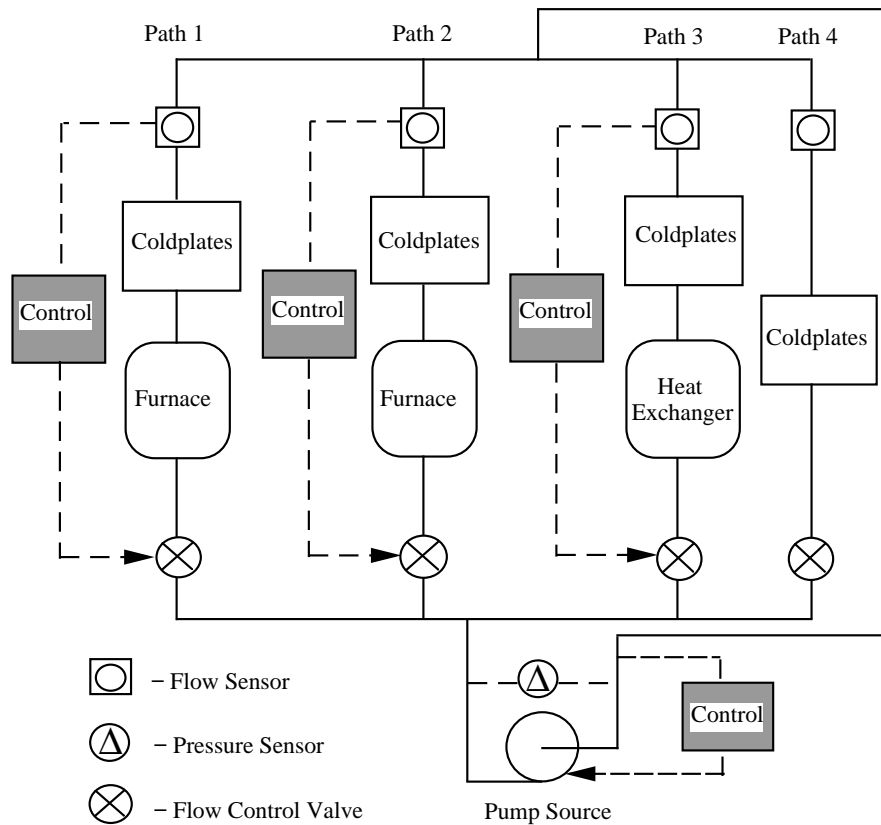


Figure 1. TCS schematic.

The objective of the TCS is to simultaneously control the thermal environments of several furnaces and related subsystems plumbed in parallel. Specifically, the high-accuracy, robust, and decoupled tracking performance of flow rate profiles in the various parallel subsystem paths is desired. Shown in figure 1, the flow rate profiles in paths 1 through 3 are actively controlled by a closed-loop system, and the flow rate profile in path 4 is passively controlled by an open-loop system. The valve in path 4 is fixed to a prescribed position, and the flow rate profile is maintained to a constant by controlling the system pressure drop across the parallel paths. For the specified tracking problem, four control inputs are employed to achieve the flow tracking performance. Three inputs are used to modulate the flow control valves in paths 1 through 3, and one input is used to modulate the pump speed. The pump speed is modulated to control the system pressure drop, which serves to decouple the flow dynamics across the parallel paths.

A mathematical model of the TCS is derived as a means to simulate the dynamic response of the actuators, flows, and pressures within the system. Hydraulic systems such as the TCS usually consist of liquid-filled tanks connected by pipes having orifices, valves, or other flow-restricting devices. The dynamic response of such fluid systems can be analyzed using the fundamental laws of conservation of mass and momentum that govern the flow of liquids. Specifically, there exist three types of basic elements for mathematical modeling of hydraulic systems: resistance, compliance, and inertance elements. These elements can be combined using an electrical analogy to form the mathematical model of the hydraulic system, according to Ogata.<sup>1</sup> The dynamic response of the pump and the flow control actuators are included with the hydraulic model to simulate the integrated system response. For the TCS, physical interconnection of the parallel paths through a common pump source implies that its mathematical model is described by coupled nonlinear differential equations in flow and pressure with partially known parameters and unknown disturbances.

A review of the control system theory that is applicable to systems like the TCS is now discussed. A fundamental problem of interest in control system theory is the design of controllers that yield acceptable performance for not one, but a family of multivariable, nonlinear, coupled, time-varying plants under various types of inputs and disturbances. Over the years, various control approaches have been developed to handle such plants. Two of these approaches, the sensitivity approach<sup>2</sup> and the linear-quadratic-Gaussian (LQG) design approach,<sup>3</sup> have dominated the 1960's and early 1970's and are still in use today. The former approach relies on small perturbations around an accepted model, and the latter approach relies on a statistical description of the disturbances and unknowns. Both approaches utilize frequency shaping filters such as the well-known proportional-plus-derivative-plus-integral (PID) filter to achieve the desired control system performance. Late in the 19th century, the Russian mathematician A.M. Lyapunov<sup>4</sup> developed an approach to control system design and stability analysis of nonlinear systems, now known as the "direct method of Lyapunov." This approach has been widely used in the last 25 years and involves construction of appropriate Lyapunov functions. The approach popularized in the 1970's is that of adaptive control,<sup>5</sup> where the controllers learn the values of the disturbances and unknowns through appropriate feedback or feedforward loops. The  $H^\infty$  (H-infinity) approach<sup>6</sup> has dominated the research in the 1980's. Here, the objective is to obtain a controller that minimizes the maximum norm of a disturbance input-output operator. Two approaches that have attracted a great deal of research interest in recent years are disturbance-accommodating control (DAC) developed by C.D. Johnson<sup>8</sup> and feedback linearization shown by A. Isidori<sup>7</sup> and J.E. Slotine.<sup>9</sup> The former involves dynamic modeling of uncertain disturbances coupled with feedforward/feedback controllers to achieve performance specifications. The latter relies on algebraically transforming a nonlinear system into a linear one, so that linear control techniques can be applied. Finally, an approach that has recently received serious attention in the U.S. is that of variable-structure systems (VSS). Introduced to the U.S. in 1976 by Russian professors U. Itkis<sup>10</sup> and V.I. Utkin,<sup>11</sup> VSS has the distinctive feature of changing the structure of the system during the transient process (hence the term VSS). A special subclass of VSS control is that of sliding mode control. The application of sliding mode control techniques to the TCS is the primary focus of this report.

According to Itkis,<sup>10</sup> Utkin,<sup>11</sup> and DeCarlo,<sup>12</sup> sliding mode control is unique in its ability to achieve accurate, robust, decoupled tracking for a class of nonlinear time-varying multivariable systems

in the presence of disturbances and parameter variations. Unlike the numerous aforementioned control approaches, sliding mode control achieves this unique performance without precise calculations or estimations of the system parameters, nonlinearities, and disturbances. Sliding mode control relies on the presence of a high-speed switching feedback control, and has its roots in relay and bang-bang control theory. The advent of faster switching circuitry, and the many advances in computer technology, have made the implementation of sliding mode control a reality and of increasing interest to control system engineers.

As shown by Itkis,<sup>10</sup> Utkin,<sup>11</sup> and DeCarlo,<sup>12</sup> sliding mode control utilizes a high-speed switched control law to cause the nonlinear plant's state trajectory to move onto a desired linear switching surface called the sliding surface. The objective is to move to this sliding surface and to stay there for all subsequent time. This surface is called the sliding surface because the plant's state trajectory seems to slide along the desired linear surface by the high-speed switching action of the control law. That is, the plant's state trajectory is "above" this surface if the control law is at one gain and "below" this surface at the other gain. The plant's motion along the sliding surface represents the controlled system's behavior. By proper design of the sliding surface, the sliding mode control law attains the desired performance for the system. The "desired" performance of the TCS system is defined or obtained when the system flow tracking error responds as a linear time-invariant homogeneous system with strategically placed eigenvalues.

This report focuses on applying sliding mode techniques to a special operating case for the TCS. The normal operating case for the TCS is represented by the system pressure being tightly controlled. For the normal case, decoupled flow tracking performance is easily maintained by the TCS's flight controllers. However, this pressure control may not always be fully operational. That is, the pressure controller could be poorly designed or operating in a degraded mode due to a system fault. This anomaly would represent the worst-case scenario for coupling between the respective flow paths. Coupling exists in the normal case where the pressure controller is fully operational, but coupling exists much stronger in the anomaly case. This report presents the design and performance of sliding mode controllers for the normal and anomaly cases and, in either case, decoupled tracking performance is maintained.

This report formulates the system equations and develops the sliding mode controllers that cause the interconnected TCS subsystems to operate in the local sliding modes, resulting in control system decoupling and invariance to some external and interaction disturbances, plant uncertainties, and nonlinearities. The desired decoupled flow rate tracking in the local sliding modes is achieved by simple eigenvalue placement of the local linear sliding mode equations. Extensive digital simulation results are presented to show the control system's performance. A comparison against the actual flight TCS PID control algorithm is included to demonstrate improved performance over traditional control techniques.

## **II. MODEL FORMULATION**

### **A. Theory**

The mathematical model of the TCS is derived as a means to simulate the dynamic response of the actuators, flows, and pressures within the system. The basic equations that govern the dynamic response of fluid systems are the equations of continuity of mass and momentum. According to Streeter,<sup>13</sup> these equations can be derived using the control-volume concept. A control volume refers to a region in space where the flow occurs into and out of the space. The size and shape of the control volume usually coincide with the physical boundaries of the system being analyzed. For the TCS, the control volume constitutes a smooth cylindrical pipe.

The law of conservation of mass states that the mass within the system remains constant for all time. This is expressed in equation form as

$$\frac{dm}{dt} = 0 , \quad (1)$$

where  $m$  is the total mass. Streeter<sup>13</sup> derives the continuity of mass equation from the law of conservation of mass stated in equation (1). This is shown as

$$\frac{dm}{dt} = 0 = \frac{d}{dt} \int_{cv} \rho dv + \int_{cs} \rho \mathbf{V} dA , \quad (2)$$

where  $\rho$  is the mass density,  $dv$  is the element of volume,  $\mathbf{V}$  is the velocity of the center of mass of the system, and  $dA$  is an area element of the outflow area. This equation states for a control volume ( $cv$ ) that the time rate of change of the mass in a control volume is equal to the net increase or decrease of mass flowing into the control-volume surface ( $cs$ ).

Newton's second law of motion is usually stated as

$$\sum \mathbf{F} = \frac{d}{dt} (m\mathbf{V}) , \quad (3)$$

where  $\sum \mathbf{F}$  is the sum of all forces acting on the system. Streeter<sup>13</sup> uses Newton's second law of motion stated in equation (3) to derive the continuity of momentum equation for a control volume. This is shown as

$$\sum \mathbf{F} = \frac{d(m\mathbf{V})}{dt} = \frac{d}{dt} \int_{cv} \rho \mathbf{V} dv + \int_{cs} \rho \mathbf{V} \mathbf{V} dA . \quad (4)$$

This equation states for a control volume that the sum of all forces acting on the system is equal to the time rate of change of the linear momentum in a control volume plus the net increase or decrease of linear momentum flowing into the control-volume surface.

The general continuity of mass and momentum relationships shown in equations (2) and (4) are developed specifically for the TCS hydraulic model. Consider a smooth cylindrical pipe with unsteady uniform incompressible fluid flowing through it. Consider that the flow is only in the  $x$  direction, such that the external forces and flow velocities are in the  $x$  direction. Also, consider that the inlet and outlet flow velocities across the control-volume surface are equal, such that the second integral in equation (4) goes to zero. The resulting continuity of momentum equation is shown as

$$\sum F_x = \frac{d}{dt} \int_{cv} \rho V_x dv . \quad (5)$$

The resulting continuity of mass equation is shown as

$$\frac{d}{dt} \int_{cv} \rho dv = \int_{cs} \rho V_x da_p . \quad (6)$$

To derive the basic flow dynamics equation for the TCS, it is useful to start with the continuity of momentum relationship stated in equation (5). The sum of forces in the  $x$  direction acting on the fluid in the pipe is primarily comprised of three pressure forces. Van Wylen<sup>14</sup> defines pressure as the normal component of force per unit area. The first of these pressure forces is the pipe inlet pressure ( $P_{in}$ ) and the second is the pipe outlet pressure ( $P_{out}$ ). The third is the pressure loss ( $P_{loss}$ ) due to the frictional losses

between the fluid and the inner surface area of the pipe. All three pressures are multiplied times the cross-sectional area ( $a_p$ ) of the pipe. The sum of the forces in the  $x$  direction is shown as

$$\sum F_x = (P_{in} - P_{out} - P_{loss}) a_p . \quad (7)$$

According to Streeter,<sup>13</sup> the Darcy-Weisbach equation is generally adopted for pressure loss calculations through a pipe. This is written as

$$P_{loss} = RW , \quad (8)$$

where  $W$  is the average mass flow rate through the pipe in (lbm/h) and  $R$  is the flow resistance in (lbf·h/lbm·ft<sup>2</sup>) defined as

$$R = k_f \frac{W}{2\rho g_c a_p^2} , \quad (9)$$

where  $g_c$  is a conversion constant in (lbm·ft/lbf·s<sup>2</sup>),  $a_p$  is the cross-sectional area of the pipe in ft, and  $k_f$  is the unitless friction loss factor defined as

$$k_f = f \frac{l}{d} , \quad (10)$$

where  $f$  is the unitless friction that is required to cause the equation to produce the correct value for losses,  $l$  is the length of the pipe in ft, and  $d$  is the inside diameter of the pipe in ft.

For a cylindrical pipe, the total volume ( $v$ ) is calculated as

$$v = la_p , \quad (11)$$

and the average mass flow rate ( $W$ ) is calculated as

$$W = \rho a_p V_x . \quad (12)$$

Substituting equations (7), (8), (11), and (12) into equation (5), evaluating the integral, and rearranging terms yields

$$\frac{dW}{dt} = \frac{1}{L} (P_{in} - P_{out} - RW) , \quad (13)$$

where  $L$  is the flow inertance in (lbf·s·h/lbm·ft<sup>2</sup>) defined as

$$L = \frac{l}{a_p g_c} . \quad (14)$$

The resulting flow dynamics relationship stated in equation (13) is a function of the basic resistance ( $R$ ) and inertance ( $L$ ) flow elements and the inlet and outlet pressures. The derivation of the pressure equation is discussed in the following.

To derive the basic pressure dynamics equation for the TCS, it is useful to start with the continuity of mass relationship stated in equation (6). Substituting equation (12) into the right-hand side of equation (6) and integrating the mass flow into and out of the pipe control-surface volume yields

$$\frac{d}{dt} \int_{cv} \rho dv = \sum (W_{in} - W_{out}) . \quad (15)$$

Evaluating the integral results in

$$\frac{d(\rho v)}{dt} = \sum (W_{in} - W_{out}) . \quad (16)$$

Ogata<sup>1</sup> defines the term compliance ( $C$ ) as the change in the quantity of liquid per change in pressure. Another way of representing this is by the relationship

$$C = \frac{d(\rho v)}{dP} , \quad (17)$$

where  $C$  can be expressed in units of (lbm·in<sup>2</sup>·s/h·lbf). Solving this relationship for  $d(\rho v)$ , substituting the resulting expression into equation (16) and dividing through by the compliance ( $C$ ), it is shown that the resulting pressure dynamics equation is

$$\frac{dP}{dt} = \frac{1}{C} \sum (W_{in} - W_{out}) . \quad (18)$$

It should be noted that the compliance term in equation (18) is composed only of the pipe wall compliance, since the fluid is assumed to be incompressible. Compliance for a pipe wall is calculated as

$$C = \frac{ld^3\pi}{4Ee_p} , \quad (19)$$

where  $l$  is the length of the pipe,  $d$  is the diameter of the pipe,  $E$  is Young's modulus of elasticity that relates stress and strain, and  $e_p$  is the pipe wall thickness.

Hydraulic pressure and flow represented by equations (18) and (13), respectively, are now in terms of the three basic elements for mathematical modeling of hydraulic systems: resistance, compliance, and inertance elements. These elements can now be combined using an electrical analogy to form the mathematical model of the hydraulic system.

## B. TCS Model

As seen in figure 1, the TCS has a pump source that forces cold water through four subsystem flow paths plumbed in parallel. Hydraulic systems such as the TCS usually consist of liquid-filled tanks connected by pipes having orifices, valves, or other flow-restricting devices. The dynamic response of such fluid systems can be analyzed using the basic elements for mathematical modeling of hydraulic systems: resistance, compliance, and inertance elements. To form the TCS model, these elements are combined using an electrical circuit analogy. The resulting circuit is shown in figure 2. From this circuit, the flow and pressure equations are written to represent the hydraulic mathematical model of the TCS. The valve and pump actuator equations are included with the hydraulic equations to represent the whole TCS mathematical model. For convenience, the whole TCS mathematical model is divided into two sub-models: the flow path model and the source model.

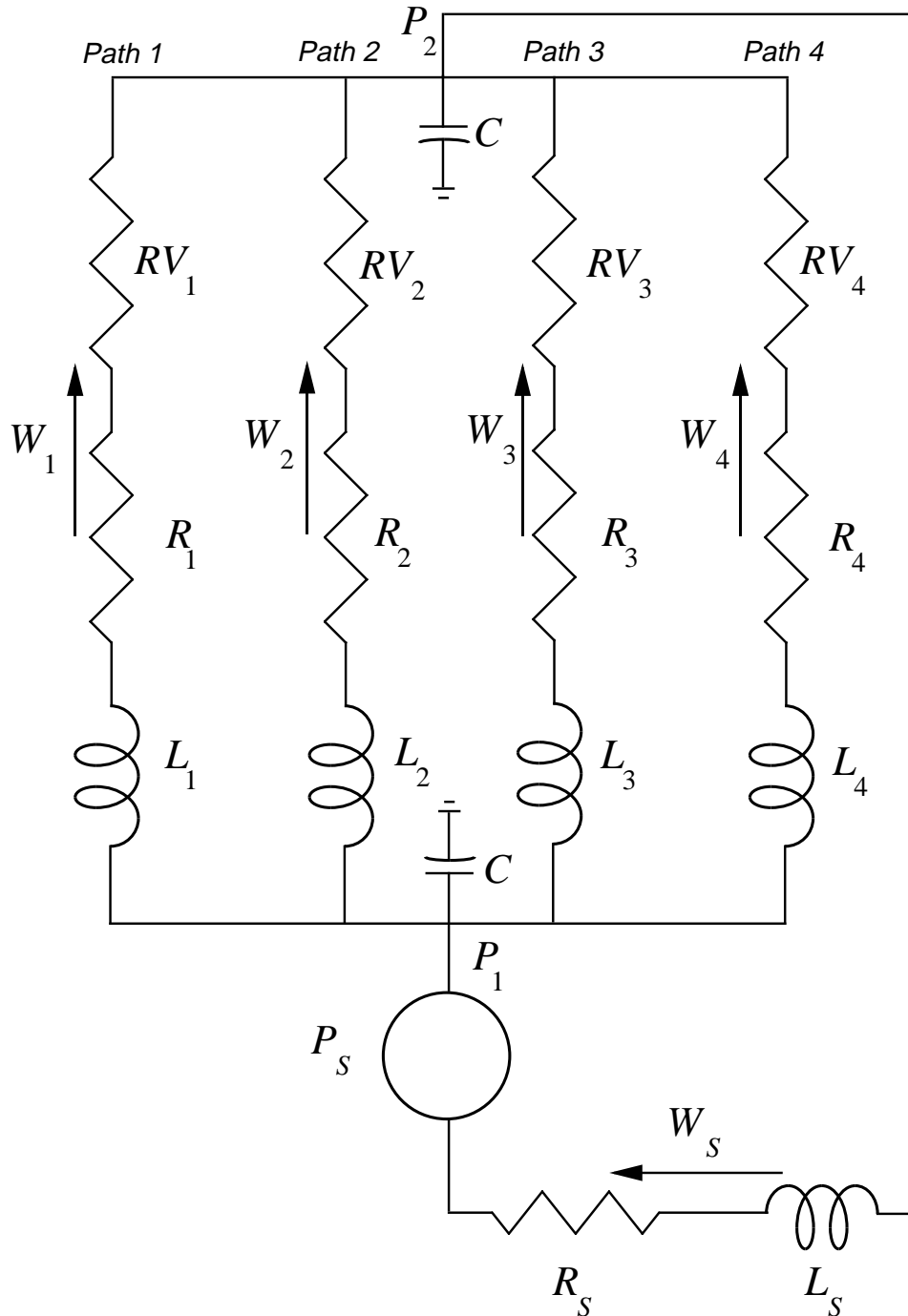


Figure 2. TCS equivalent circuit.

1. **Flow Path Model.** Each of the four flow paths consists of components (for example, cold-plates, heat exchangers, flexible tubing, quick disconnects, furnace cooling jackets, flow sensors, etc.) plumbed in series with a flow control valve. The model of each flow path has one equation that describes the dynamic response of the mass flow rate of water and two equations that describe the dynamic response of the flow control actuator and valve. The four path flow descriptions are presented in equation (20). This equation is derived by applying equation (13) or Kirchhoff's<sup>15</sup> voltage law to each flow path shown in figure 2. Kirchhoff's voltage law states that the algebraic sum of the voltages around

any closed path is zero. Since voltages are analogous to pressures and currents are analogous to flow rates, the resulting path flows are shown as

$$\frac{dW_i}{dt} = \frac{1}{LP_i} [P - (R_{V_i} + R_{P_i})W_i], \quad \forall i = 1, 4, \quad (20)$$

where  $R_{P_i}$  is the lumped path flow resistance,  $LP_i$  is the lumped path flow inertance,  $R_{V_i}$  is the valve resistance, and  $P = P_1 - P_2$  is the system pressure drop across the parallel subsystem paths.

The valve is classified as a variable position valve; moreover, the valve resistance is a nonlinear function of the angular position of the valve. The valve resistance is calculated based on equation (9), where the loss factor ( $k_f$ ) is a nonlinear function of the valve angle ( $\theta_i$ ). The loss factor data are supplied by Allied Signal Aerospace<sup>16</sup> and are shown in table 1. Defining the function

$$k_f^* = k_f \frac{1}{2\rho g_c a_p^2}, \quad (21)$$

and substituting this function into equation (9) simplifies the expression for the valve resistance. This is shown as

$$R_{V_i} = k_f^* W_i. \quad (22)$$

Considering that  $k_f^*$  is a function of the data shown in table 1, it is advantageous to find a concise non-linear curve fit function to represent  $k_f^*$ . This curve fit function is chosen as

$$k_f^* = \alpha e^{-\beta \cdot \theta_i + \delta}, \quad (23)$$

where  $\alpha$ ,  $\beta$ , and  $\delta$  are unknown constants to be determined later.

Minimizing errors between a chosen curve fit function and a given set of data is of utmost concern for engineers. Shown by Strang,<sup>17</sup> one of the best procedures used in minimizing this error is the linear least-squares method. This method is demonstrated by considering the linear system shown as

$$Ax = b, \quad (24)$$

where  $A$  is an  $n \times m$  matrix of known linearly independent column vectors,  $x$  is an  $m \times 1$  column vector of unknown elements, and  $b$  is an  $n \times 1$  column vector of known elements. If the system shown in equation (24) could be solved exactly, there would be no errors. However, since there are more equations than unknowns (i.e.,  $n > m$ ), the system cannot be solved exactly and, hence, the objective is to minimize the resulting errors. According to Strang,<sup>17</sup> the least-squares solution to the inconsistent system  $Ax = b$  of  $n$  equations and  $m$  unknowns satisfies

$$A^T A \bar{x} = A^T b, \quad (25)$$

where the column vector  $\bar{x}$  is the linear least-squared error solution for the system.

Table 1. Valve loss data.

Valve Angle ( $\theta_i$ )	Loss Factor ( $k_f$ )
0.0	5,995,463.0
5.0	1,199,092.0
6.0	599,546.0
7.5	257,805.0
10.0	101,923.0
12.5	38,971.0
15.0	21,584.0
17.5	11,691.0
20.0	8,394.0
30.0	1,559.0
40.0	539.6
50.0	251.0
60.0	125.0
75.0	47.0
90.0	22.0

For the nonlinear function shown in equation (23), the coefficients (unknowns)  $\alpha$ ,  $\beta$ , and  $\delta$  are solved by applying the linear least-squares method just discussed. For convenience, the first step is to rewrite equation (23) in the form

$$f(\alpha, \beta, \delta) = \alpha e^{-\beta \theta_i + \delta} - k_f^* = 0 . \quad (26)$$

The following step is to linearize the above equation using the well-known Taylor series expansion that is shown by Wylie.<sup>18</sup> Taking only the first-order terms of the expansion yields the general result

$$\left[ \frac{\partial f(\alpha, \beta, \delta)}{\partial \alpha} \Delta \alpha + \frac{\partial f(\alpha, \beta, \delta)}{\partial \beta} \Delta \beta + \frac{\partial f(\alpha, \beta, \delta)}{\partial \delta} \Delta \delta \right]_{\substack{\alpha = \alpha_0 \\ \beta = \beta_0 \\ \delta = \delta_0}} + f(\alpha_0, \beta_0, \delta_0) = 0 , \quad (27)$$

where  $\alpha_0$ ,  $\beta_0$ , and  $\delta_0$  are initial guesses or initial conditions for the unknowns, and  $\Delta \alpha$ ,  $\Delta \beta$ , and  $\Delta \delta$  are the deviations or deltas from the initial guesses required to solve the system.

For the next step, the new variable definitions

$$j_{\alpha} = \frac{\partial f(\alpha, \beta, \delta)}{\partial \alpha}, \quad (28)$$

$$j_{\beta} = \frac{\partial f(\alpha, \beta, \delta)}{\partial \beta}, \quad (29)$$

$$j_{\delta} = \frac{\partial f(\alpha, \beta, \delta)}{\partial \delta}, \quad (30)$$

are chosen to simplify the expression in equation (27). Substituting equations (28), (29), and (30) into equation (27) and applying the result to each of the 15 data points shown in table 1 yields the following system of linear equations:

$$\begin{bmatrix} j_{\alpha_1} & j_{\beta_1} & j_{\delta_1} \\ j_{\alpha_2} & j_{\beta_2} & j_{\delta_2} \\ \vdots & \vdots & \vdots \\ j_{\alpha_{15}} & j_{\beta_{15}} & j_{\delta_{15}} \end{bmatrix} \begin{bmatrix} \Delta\alpha \\ \Delta\beta \\ \Delta\delta \end{bmatrix} = - \begin{bmatrix} f_1(\alpha_0, \beta_0, \delta_0) \\ f_2(\alpha_0, \beta_0, \delta_0) \\ \vdots \\ f_{15}(\alpha_0, \beta_0, \delta_0) \end{bmatrix}. \quad (31)$$

The original nonlinear system is now in the standard linear form,  $Ax = b$ , where  $x = [\Delta\alpha \Delta\beta \Delta\delta]^T$  is a  $3 \times 1$  delta column vector of unknown elements. These unknown elements are solved by applying the method described by equation (25) to the system shown in equation (31). The solved elements of the delta column vector are then added to the initial guesses,  $\alpha_0$ ,  $\beta_0$ , and  $\delta_0$ , to obtain updated estimates for  $\alpha$ ,  $\beta$ , and  $\delta$ . These estimates are substituted into equation (26) to verify the resulting curve fit. Several iterations through this method are usually required to obtain the optimum curve fit function for the data. After several iterations, the optimum coefficients are solved as  $\alpha = 0.129$  and  $\delta = 1.14 \times 10^{-5}$ , both in units of  $(\text{lbf} \cdot \text{h}^2 / \text{lbm}^2 \cdot \text{in}^2)$ , and  $\beta = 0.169 \text{ deg}^{-1}$ . Substituting the curve fit function represented by equation (23) and its coefficient values into equation (22) results in the valve resistance equation

$$R_{V_i} = (0.129e^{-0.169\theta_i + 1.14 \times 10^{-5}}) W_i \frac{\text{lbf} \cdot \text{h}^2}{\text{lbm} \cdot \text{in}^2}, \quad \forall i = 1, 4. \quad (32)$$

The plumbing configuration within each respective flow path is assumed to be the same. That is, the component (for example, coldplate, heat exchanger, flexible tubing, quick disconnect, furnace cooling jacket, etc.) configurations are consistent between parallel paths. The component loss data that comprise each flow path are supplied by the respective component vendors. Each flow path resistance ( $R_{P_i}$ ) is calculated by adding (in series) the individual component loss data. The resulting summation is calculated as

$$R_{P_i} = 3.57 \times 10^{-5} W_i \frac{\text{lbf} \cdot \text{h}^2}{\text{lbm} \cdot \text{in}^2}, \quad \forall i = 1, 4. \quad (33)$$

The line lengths and pipe cross-sectional areas are also assumed to be consistent between flow paths. The flow inertance ( $L_{P_i}$ ) for each path is calculated according to equation (14). Specifically, the flow inertance for each component is calculated and added (in series) to yield the total inertance for each path. The resulting summation is calculated as

$$L_{P_i} = 7.03 \times 10^{-4} \frac{\text{h} \cdot \text{s} \cdot \text{lbf}}{\text{lbm} \cdot \text{in}^2}, \quad \forall i = 1, 4. \quad (34)$$

The flow control actuator that is located in each flow path consists of an analog speed controller and a brushless dc motor. The flow control actuator is connected through a common shaft to the sculptured ball valve to provide the desired valve movement. The valve integrates its commanded rate ( $\omega_i$ ) to achieve the desired valve position ( $\theta_i$ ). Hence, the response of the valve position is modeled as an ideal integrator. This is shown as

$$\frac{d\theta_i}{dt} = \omega_i, \quad \forall i = 1, 4. \quad (35)$$

The angular valve speed ( $\omega_i$ ) response of the analog speed controller and brushless dc motor combination to the commanded valve speed ( $u_i$ ) is modeled as a first-order delay. This is shown as

$$\frac{d\omega_i}{dt} = \frac{1}{\tau} (k_v u_i - \omega_i), \quad \forall i = 1, 4, \quad (36)$$

where  $\tau$  is the time constant delay equal to 0.01 s, and  $k_v$  is the conversion constant between voltage and degrees per second, equal to 1.0 (deg/s·V).

The composite flow path model is represented by equations (20), (35), and (36). These equations are combined with the source model to represent the whole TCS model. The source model equations are presented in the next section.

2. Source Model. The source model consists of the system flow and pressure drop, pump motor, pump speed controller, and system pressure controller equations. The pump source functions to force cold water through the four subsystem paths. This source also functions to control the system pressure drop across the parallel subsystem paths. Modeling the dynamic response of the source is important because the four flow paths are dynamically coupled through this common source.

The system flow ( $W_S$ ) description is presented in equation (37). This equation is derived by applying equation (13) or Kirchhoff's<sup>15</sup> voltage law to the source flow path shown in figure 2. This is shown as

$$\frac{dW_S}{dt} = \frac{1}{L_S} (P_S - P - R_S W_S), \quad (37)$$

where  $L_S$  is the lumped source inertance,  $R_S$  is the lumped source resistance,  $P_S$  is the pressure rise across the pump source, and  $P = P_1 - P_2$  is the system pressure drop across the parallel subsystem paths.

The pump package assembly that houses the centrifugal pump source consists of many fluid loss components (for example, coarse and fine filters, temperature, flow, and pressure sensors, gas trap, check valve, etc.). The combined resistance associated with these components is added to that of the source heat exchanger and the source line losses to represent the total source resistance ( $R_S$ ). The component loss data that comprise the total source resistance are supplied by the respective component vendors. The resulting summation is calculated as

$$R_S = 1.0 \times 10^{-5} \frac{\text{lbf} \cdot \text{h}^2}{\text{lbm} \cdot \text{in}^2}. \quad (38)$$

The source line lengths, including the supply and return lines to the parallel flow paths, and the pipe cross-sectional areas are determined. The flow inductance for each source component is calculated according to equation (14) and summed together to determine the total source inductance ( $L_S$ ). The resulting summation is calculated as

$$L_S = 1.13 \times 10^{-3} \frac{\text{h} \cdot \text{s} \cdot \text{lb} \cdot \text{f}}{\text{lb} \cdot \text{m} \cdot \text{in}^2} . \quad (39)$$

The pressure rise ( $P_S$ ) across the pump is described by a pump map function that is a function of the pump speed ( $\omega_p$ ) and the system flow ( $W_S$ ) at any given time. This pump map function is a nonlinear family of curves as seen in figure 3. Each curve represents a different operating speed of the pump.

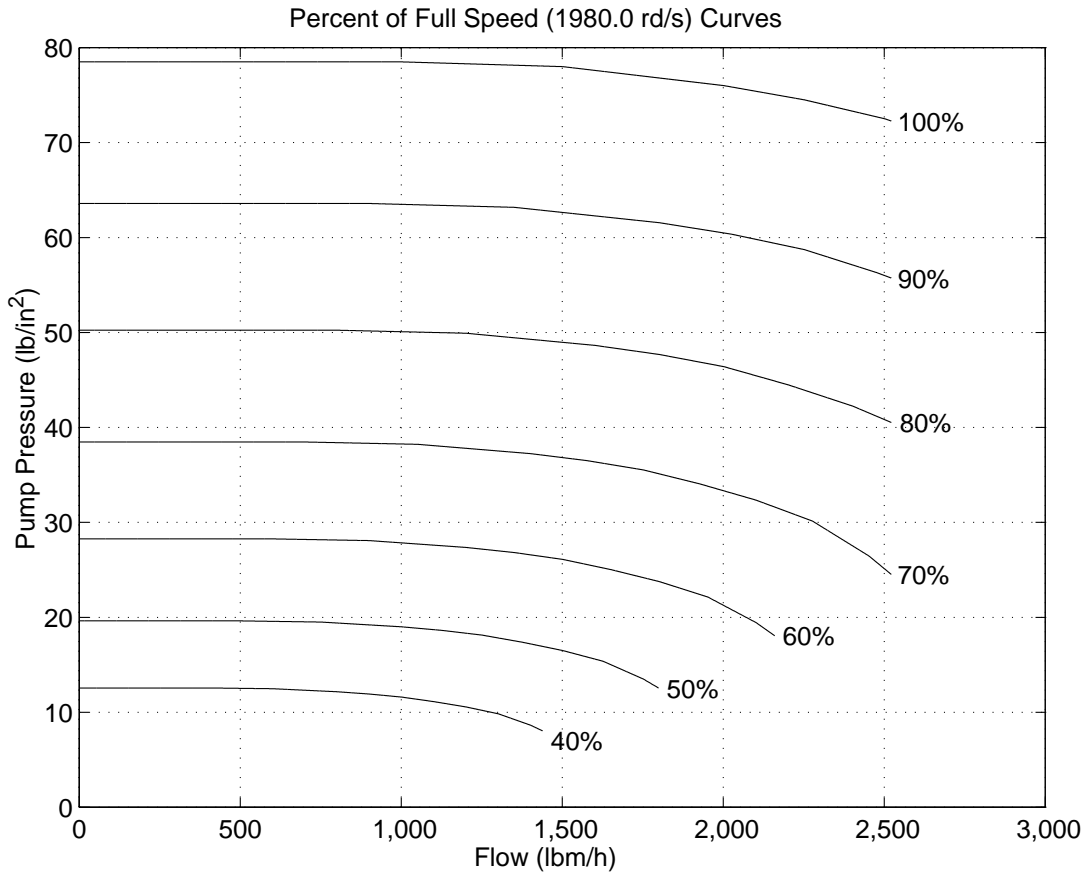


Figure 3. Pump map.

The system pressure drop ( $P$ ) description is presented in equation (40). This equation is derived by applying equation (18) or Kirchhoff's<sup>15</sup> voltage law to the source flow path shown in figure 2. This is shown as

$$\frac{dP}{dt} = \frac{d(P_1 - P_2)}{dt} = \frac{2}{C} \left( W_S - \sum_{i=1}^4 W_i \right) , \quad (40)$$

where  $C$  is the system compliance. The individual compliance for each path is first calculated according to equation (19); however, the resulting values for compliance are so small (approximately  $10^{-5}$ ), they cause unnecessary high-frequency dynamics in the model. Moreover, the flow dynamics are shown to be insensitive to these high-frequency terms. Hence, the compliance values are not calculated, but artificially selected for the model. This is to allow for expansion and contraction of the fluid system at the fluid merge and split junctions. The resulting system compliance is chosen as

$$C = 0.1 \frac{\text{lbf}\cdot\text{h}}{\text{lbf}\cdot\text{in}^2\cdot\text{s}} . \quad (41)$$

The dynamic model representing the pump source is obtained from the pump vendor, Allied Signal Aerospace.<sup>16</sup> The pump source model consists of a pump motor model, a pump speed controller model, and a system pressure controller model. For convenience, the equations representing these models are compressed into a compact form consisting of four differential equations. These are shown as

$$\frac{d\omega_p}{dt} = \frac{1}{j_{ml}} (k_t I_a - k_1 \omega_p^2) , \quad (42)$$

$$\frac{dI_a}{dt} = \frac{1}{L_m} [-R_m I_a - k_e \omega_p - k_2 (P - P_{\text{set}}) - k_3 \omega_{fbk} + \mathbf{Q} \mathbf{X}_c] , \quad (43)$$

$$\frac{d\omega_{fbk}}{dt} = \frac{1}{\tau_f} (\omega_p - \omega_{fbk}) , \quad (44)$$

$$\frac{d\mathbf{X}_c}{dt} = \mathbf{M} \mathbf{X}_c + \mathbf{B} \cdot [\omega_{fbk} \quad P \quad P_{\text{set}}]^T , \quad (45)$$

where  $\omega_p$  is the pump speed,  $I_a$  is the pump motor armature current,  $\omega_{fbk}$  is the pump speed feedback,  $\mathbf{X}_c$  is the  $2 \times 1$  row vector of controller states,  $j_{ml}$  is the rotor plus load inertia,  $k_t$  is the current to motor torque gain,  $k_1$  is the speed to load torque gain,  $L_m$  is the pump motor inductance,  $R_m$  is the pump motor resistance,  $k_e$  is the motor back emf gain,  $k_2$  is one pump speed controller feedforward gain,  $k_3$  is the other pump speed controller feedforward gain,  $\mathbf{Q}$  is the  $1 \times 2$  row vector of controller gains,  $\tau_f$  is the pump speed filter time constant,  $\mathbf{M}$  is the  $2 \times 2$  matrix of controller gains, and  $\mathbf{B}$  is the  $2 \times 3$  plant state input matrix. The constants in equations (42) through (45) are defined in table 2.

The following are the matrix definitions for equations (42) through (45):

$$\mathbf{Q} = [0.0213 \quad 400.0] , \quad (46)$$

$$\mathbf{M} = \begin{bmatrix} 0 & 0 \\ 4.3 \times 10^{-4} & 0 \end{bmatrix} , \quad (47)$$

$$\mathbf{B} = \begin{bmatrix} 0 & -0.1 & 0.1 \\ -4.3 \times 10^{-4} & -4.3 \times 10^{-5} & 4.3 \times 10^{-5} \end{bmatrix} . \quad (48)$$

In summary, the source model is an important part of the overall system model because of the dynamic coupling present through the nonlinear pump source. The composite source model is represented by equations (37), (40), (42), (43), (44), and (45). These equations describe the response of

the system flow and pressure drop, pump speed controller, and system pressure controller. The next section discusses the disturbances and assumptions that are considered in solving the TCS problem.

Table 2. Source coefficient data.

Coefficient Name	Coefficient Value
$j_{ml}$	$3.125 \times 10^{-5}$ in·lbf·s <sup>2</sup>
$kt$	0.3312 in·lbf/A
$L_m$	0.0012 henrys
$R_m$	0.618 ohms
$\tau_f$	0.00796 s
$ke$	0.0418 V/rad·s
$k_1$	$5.07 \times 10^{-7}$ in·lbf·s <sup>2</sup> /rad <sup>2</sup>
$k_2$	0.00213 A/rad
$k_3$	0.021 A·in <sup>2</sup> /s·lbf

3. Model Disturbances and Assumptions. This section discusses the major sources of disturbances and operating assumptions for the TCS model. This section also serves to provide some insight into the more important dynamics within the model. It is certainly beneficial to consider potential disturbances and important dynamics when determining the optimum controllers for a problem like the TCS.

The most important dynamic effect within the TCS can actually be classified as an internal disturbance. Internal coupling of the flow dynamics is a major disturbance to maintaining decoupled flow tracking performance. That is, modulating a valve in one path not only affects the flow in one path but also the flow in all the other paths. This is because the parallel paths are dynamically coupled through the nonlinear pump source. Dynamic coupling between the respective parallel paths is seen mathematically from equations (20) and (40), where the system pressure is a function of the path flows and the path flows are functions of the system pressure. Dynamic coupling is considered the most significant disturbance to controlling flow in the TCS.

While dynamic coupling is an obvious disturbance to the TCS, there exist other disturbances that are not so obvious. One of these disturbances is that of parameter uncertainties. As in most physical systems, it is difficult to accurately model the system under investigation. That is, model coefficients usually deviate from their actual values due to measurement inaccuracies, imprecise measurement instruments, incorrect measurement procedures, and measurement constraints (i.e., it is sometimes too costly or impractical to accurately measure a certain coefficient). Moreover, these coefficients usually vary or drift over the operational life of the system. Since control systems such as the TCS are designed, analyzed, and simulated using a computer mathematical model, it is important to consider potential parameter uncertainties and variations seen in the model of the physical system.

Another disturbance worth consideration is that of disturbance torques. Disturbance torques occur external as well as internal to the TCS control valve actuator and originate from a variety of sources such as power delivery spikes, electromagnetic interference, and flow turbulence variations. Such torques are unmeasured and can greatly affect the performance of the TCS. It is important to design the control system robust to unwanted disturbance torques present in the physical system.

Some operating assumptions for this model are now addressed. As discussed by Brogan,<sup>4</sup> the important properties of complete observability and controllability are assumed valid for the flow path model around the nominal operating point. These properties assure for  $i = 1, m$  that (1) the path flow  $W_i$  can be determined from the outputs  $y_i$  and (2) the flow reaches its set-point (i.e.,  $W_i(t) \rightarrow W_i^{\text{set}}(t)$ ) in a finite amount of time. For the source model, it is assumed that the system pressure drop controller is poorly designed or operating in a degraded mode. This assumption is useful in simulating the worst-case scenario for controlling flow rate profiles in the respective parallel paths.

This section identifies most of the major disturbance sources and addresses some of the major operating assumptions, both for the TCS mathematical model. This section also gives some insight into the important dynamics to consider when designing and verifying the controllers used to achieve the control system goals.

### C. Summary

The TCS mathematical model consisting of flow path and source equations were developed in this section. All equation parameters were included for model completeness. Values for these parameters were either obtained from the vendor, derived using first principles, or assumed using a conservative estimate. This section also addressed the major sources of disturbances and discussed the major operating assumptions. This section formulated the set of nonlinear differential equations with partially known parameters and unknown disturbances that describe the TCS system. The next section discusses the basics of sliding mode control theory, which is used to control the TCS mathematical model.

## III. BASICS OF SLIDING MODEL CONTROL

Variable-structure systems (VSS) have the distinctive feature of changing the structure of the system during the transient process (hence, the name VSS). A special subclass of VSS is that of sliding mode control. In sliding mode control, as in all VSS, the structure of the system is changed by a high-speed switching control law, i.e., the control gain is toggled between two values depending on some rule. Sliding mode control is unique in its ability to achieve accurate, robust, decoupled tracking for a class of nonlinear time-varying multivariable systems in the presence of disturbances and parameter variations. Sliding mode control achieves this performance without precise calculations or estimations of the system parameters, nonlinearities, and disturbances.

Sliding mode control relies on the presence of a high-speed switched control law. This law causes the nonlinear plant's state trajectory to move onto a user-specified state space surface (called the sliding or switching surface), and maintains the plant's state trajectory on this surface for all subsequent time. When operating in this surface, the controlled system is said to be in its "sliding mode." The surface is called the sliding surface because the plant's state trajectory seems to slide along this surface by the high-speed switching action of the control law. That is, the plant's state trajectory is "above" this surface at one gain and "below" this surface at the other gain. The plant's motion along this surface represents the controlled system's output behavior. By proper design of this sliding surface, the sliding mode control law attains the desired decoupled, linear, set-point tracking performance for the system.

### A. Background

Fundamental to VSS is that a nonlinear control law causes the plant's closed-loop dynamics to change its structure according to some user-chosen rule. If properly designed, the resulting nonlinear feedback control system achieves the desired output tracking solution for the given problem. As an example of VSS, consider the unstable linear second-order plant state model

$$\begin{bmatrix} \dot{x}_1 \\ \dot{x}_2 \end{bmatrix} = \begin{bmatrix} 0.0 & 1.0 \\ 2.0 & 0.5 \end{bmatrix} \begin{bmatrix} x_1 \\ x_2 \end{bmatrix} + \begin{bmatrix} 0.0 \\ 1.0 \end{bmatrix} u , \quad (49)$$

with one measurable state  $x_1$  and one control input of the form  $u = k(x_1)$ , where the control gain  $k(x_1)$  takes on two possible values,  $+3$  or  $-3$ . This system is illustrated in block diagram form in figure 4. As seen in the block diagram, a switch represents the toggling of the control gain  $k(x_1)$  between its respective values. For both positions of the switch, the system has a linear structure; moreover, the system has complex eigenvalues when  $k(x_1) = +3$  and real eigenvalues when  $k(x_1) = -3$ .

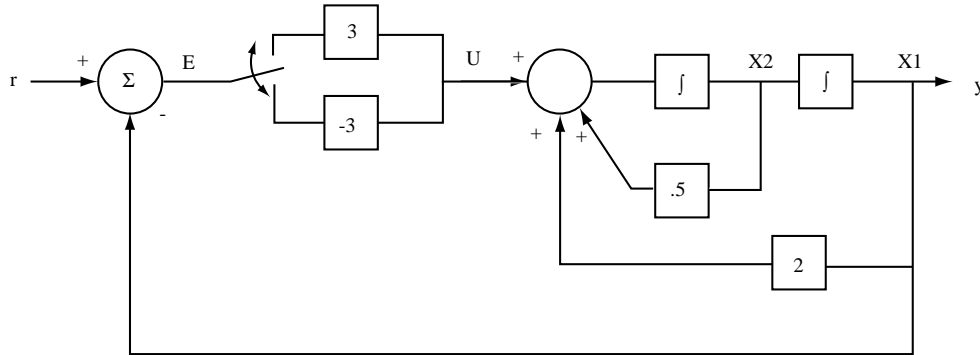


Figure 4. System block diagram.

When the switch is in the lower position, the unstable, unforced motion of the system is described by the model

$$\begin{bmatrix} \dot{x}_1 \\ \dot{x}_2 \end{bmatrix} = \begin{bmatrix} 0.0 & 1.0 \\ -1.0 & 0.5 \end{bmatrix} \begin{bmatrix} x_1 \\ x_2 \end{bmatrix} . \quad (50)$$

The phase plane plot of equation (50) is shown in figure 5. The plot shows the plant state's trajectory spiraling toward infinity.

When the switch is in the upper position, the unstable, unforced motion of the system is described by the model

$$\begin{bmatrix} \dot{x}_1 \\ \dot{x}_2 \end{bmatrix} = \begin{bmatrix} 0.0 & 1.0 \\ 5.0 & 0.5 \end{bmatrix} \begin{bmatrix} x_1 \\ x_2 \end{bmatrix} . \quad (51)$$

The phase plane plot of equation (51) is shown in figure 6. The plant's state trajectory asymptotically goes toward infinity according to the straight line boundary equations  $2.5x_1 - x_2 = 0$  and  $2.0x_1 + x_2 = 0$ . These boundary equations are solved as the eigenvectors of the system described by equation (51).

The position of the switch for a given system is determined according to a user-chosen switching rule. This rule utilizes a sliding or switching surface, denoted as  $\sigma = 0$ . Typically, this surface represents the desired output tracking trajectory for the system. For the given example, the sliding or switching surface is chosen of the form

$$\sigma = ax_1 + x_2 , \quad (52)$$

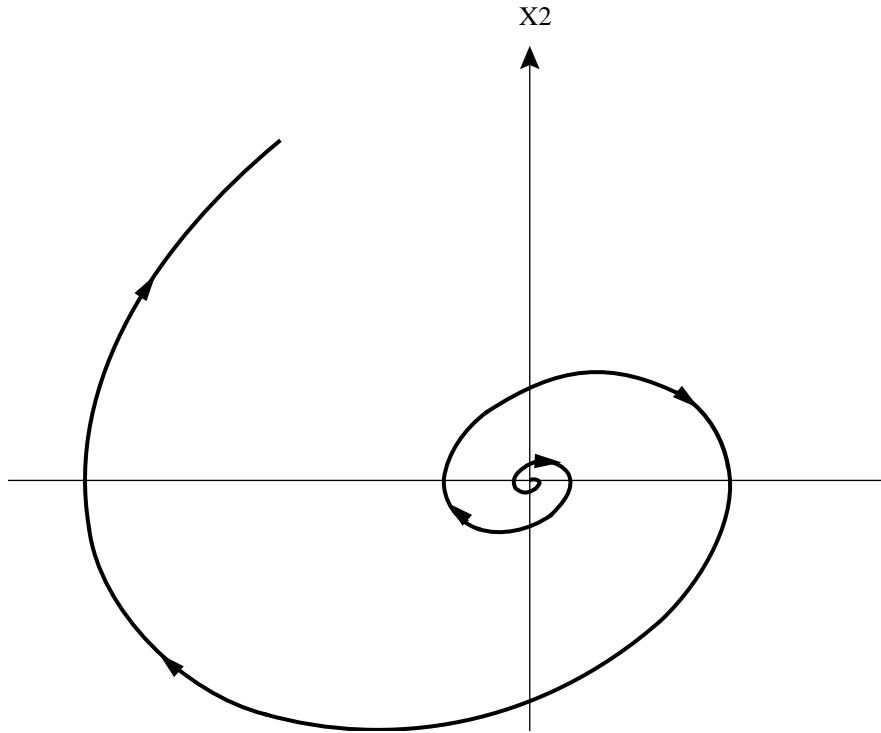


Figure 5. Phase plane plot for  $k(x_1) = -3$ .

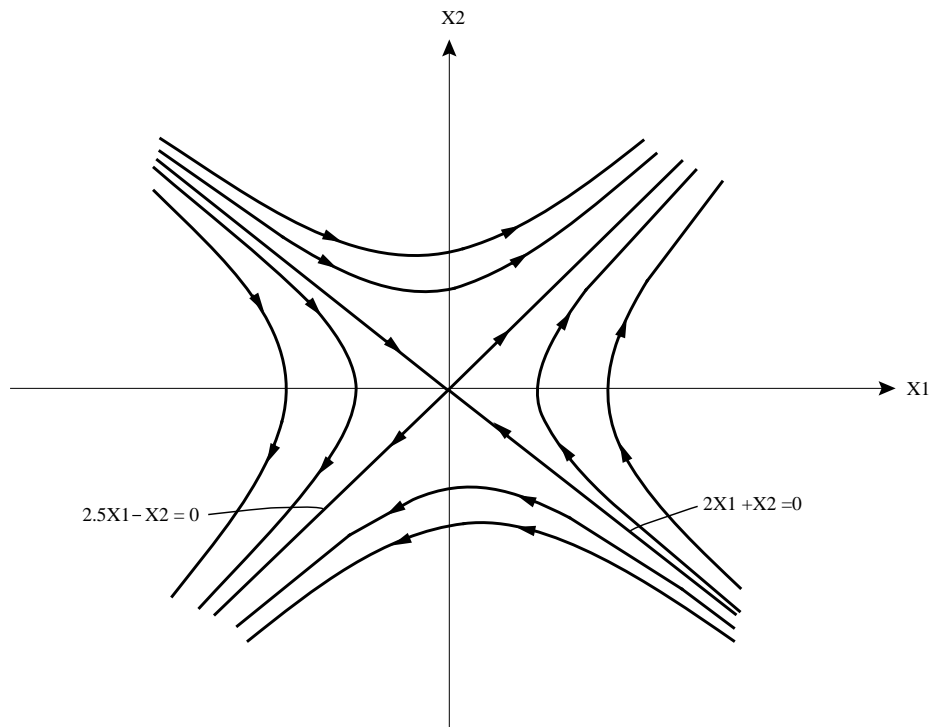


Figure 6. Phase plane plot for  $k(x_1) = +3$ .

where  $a \neq 2$ . For the given example, the switching rule is chosen as

$$k(x_1) = \begin{cases} -3, & \text{if } \sigma x_1 > 0 \\ +3, & \text{if } \sigma x_1 < 0 \end{cases} \quad (53)$$

Selecting the design parameter “ $a$ ” is now investigated. For  $a > 2$ , the resulting system’s phase plane trajectory is shown in figure 7. The shaded and unshaded regions represent the system’s trajectory when the switch is set to the upper and lower positions, respectively. As seen in figure 7, a perturbation below the switching surface causes a clockwise encirclement of the phase plane until the switching surface is encountered again. The trajectory may or may not stay on the switching surface once encountered. For the given example, the trajectory will encircle the phase plane in a clockwise decaying fashion until it finally steadies out to zero—similar to a lightly damped sinusoid.

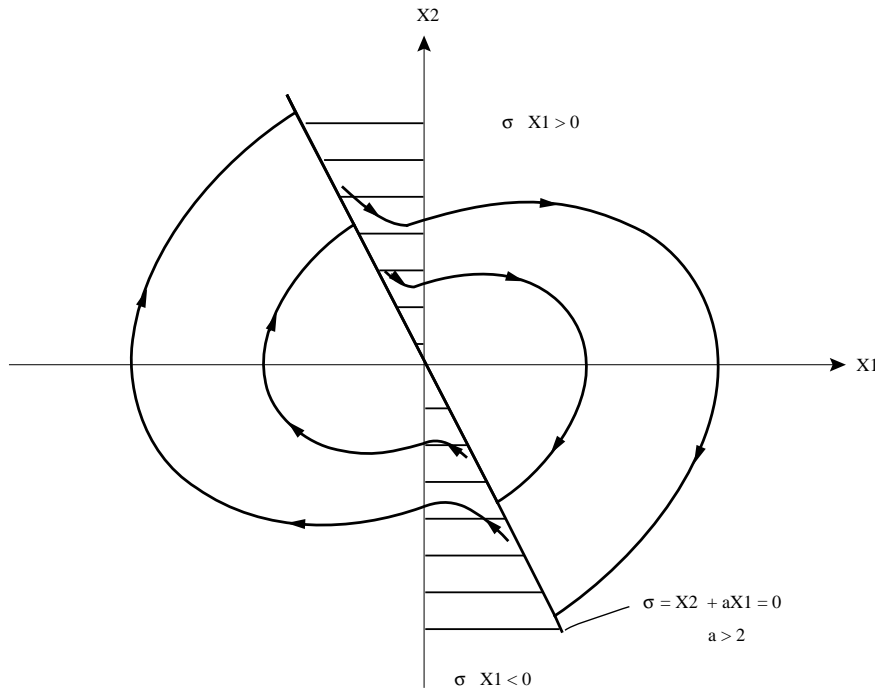


Figure 7. Phase plane plot for  $a > 2$ .

For  $a < 2$ , the resulting system’s phase plane trajectory is shown in figure 8. Again, the shaded and unshaded regions represent the system’s trajectory when the switch is set to the upper and lower positions, respectively. However, in this case, a perturbation off the switching surface is always immediately forced back to the surface since the phase plane trajectories always point toward the switching surface.

In the given example, an interesting observation of VSS is that the closed-loop system is unstable for both gains in the control law; nevertheless, with proper switching timing, the resultant response of the system is stable. Another interesting observation is that the response of a system varies greatly depending on the selection of the switching law and surface. That is, selection of the switching surface  $\sigma = ax_1 + x_2$  where  $a < 2$  results in the unique property that, once the system’s trajectory intercepts the switching surface, it remains there for all subsequent time. This property is referred to as a sliding mode. Sliding mode control is a special subclass of VSS control. The next section discusses in more depth the design theory for sliding mode control.

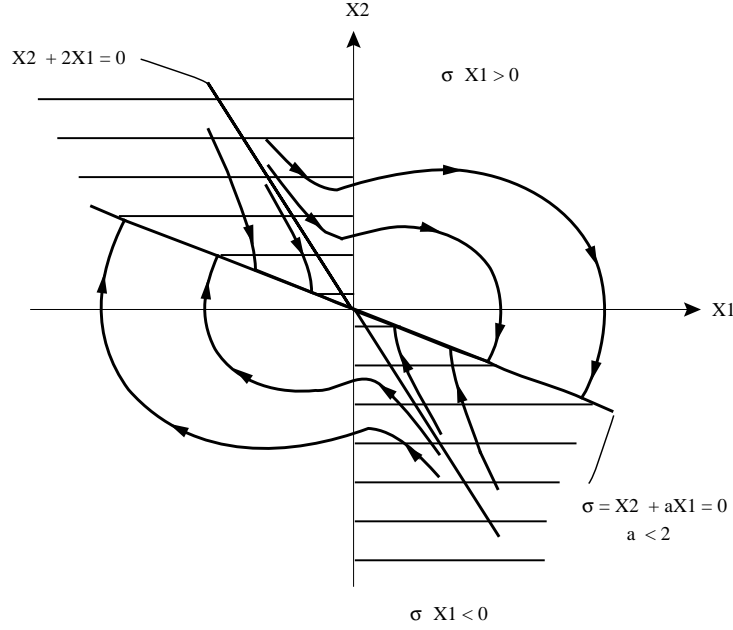


Figure 8. Phase plane plot for  $a < 2$ .

## B. Theory

In this section, the theory of sliding mode control is reviewed, including some key concepts borrowed from feedback linearization techniques. This section (1) describes the system transformation that is most useful in describing the system under consideration, (2) synthesizes the sliding surface upon which the desired output response is restricted, and (3) develops some useful control functions that force the system to move to the sliding surface and to maintain the sliding surface for all subsequent time.

1. System Transformation. It seems reasonable to discuss the sliding mode control theory as it is applied to a generic nonlinear multi-input, multi-output (MIMO) system. This theory extends to other systems such as linear and nonlinear single-input, single-output (SISO) and MIMO systems with unknown disturbances, time-varying parameters, uncertain parameters, and any combinations thereof without loss of generality. Consider the nonlinear MIMO system represented by the two vector equations

$$\begin{cases} \dot{\mathbf{x}} = \mathbf{f}(\mathbf{x}) + \mathbf{G}(\mathbf{x})\mathbf{u} \\ \mathbf{y} = \mathbf{h}(\mathbf{x}) \end{cases}, \quad (54)$$

where  $\mathbf{x}$  is the  $n \times 1$  state vector,  $\mathbf{u}$  is the  $m \times 1$  control input vector (or components  $u_i$ ),  $\mathbf{y}$  is the  $m \times 1$  vector of system outputs (of components  $y_i$ ),  $\mathbf{f}(\mathbf{x})$  and  $\mathbf{h}(\mathbf{x})$  are smooth vector fields, and  $\mathbf{G}(\mathbf{x})$  is a  $n \times m$  matrix whose columns are smooth vector fields  $g_i$ .

According to Elmali,<sup>19</sup> the sliding mode control design process is initiated by the transformation of the given system to a canonical form. Discussed in this section, this form is convenient in determining the vector relative degree and the stability of the internal dynamics for the system. The transformation is accomplished by applying the input-output linearization technique shown by Isidori<sup>7</sup> and Slotine.<sup>9</sup> This technique involves differentiating the outputs  $y_i$  until at least one of the inputs  $u_i$  appear. This technique

is performed as a means to find a direct and simple relation between the system outputs  $y_i$  and the system inputs  $u_i$ . This technique is shown as

$$y_i^{(r_i)} = L_f^{r_i} h_i(\mathbf{x}) + \sum_{j=1}^m L_{g_j} L_f^{r_i-1} h_i(\mathbf{x}) u_j, \quad \forall i = 1, m, \quad (55)$$

where  $L_{g_j} L_f^{r_i-1} h_i(\mathbf{x}) \neq 0$  for at least one  $j$ . The number  $r_i$  of differentiations required for the input  $u_j$  to appear is called the “relative degree” of the  $i$ th system channel. Performing the procedure described in equation (55) for each output  $y_i$  of equation (54) yields an  $m$ -dimensional set of output derivative equations shown as

$$\begin{bmatrix} y_1^{(r_1)} \\ \dots \\ y_m^{(r_m)} \end{bmatrix} = \begin{bmatrix} L_f^{r_1} h_1(\mathbf{x}) \\ \dots \\ L_f^{r_m} h_m(\mathbf{x}) \end{bmatrix} + \Delta(\mathbf{x}) \begin{bmatrix} u_1 \\ \dots \\ u_m \end{bmatrix}, \quad (56)$$

where

$$\Delta(\mathbf{x}) = \begin{bmatrix} L_{g_1} L_f^{r_1-1} h_1(\mathbf{x}) & \dots & \dots & L_{g_m} L_f^{r_1-1} h_1(\mathbf{x}) \\ \dots & \ddots & & \dots \\ \dots & & \ddots & \dots \\ L_{g_1} L_f^{r_m-1} h_m(\mathbf{x}) & \dots & \dots & L_{g_m} L_f^{r_m-1} h_m(\mathbf{x}) \end{bmatrix}. \quad (57)$$

According to Elmali,<sup>19</sup> the system described by equation (54) is guaranteed to have vector relative degree  $\mathbf{r} = [r_1, \dots, r_m]$  and is therefore linearizable at  $\mathbf{x}_0$  if (1)

$$L_{g_j} L_f^k h_i(\mathbf{x}) = 0, \quad (58)$$

for  $i = 1, \dots, m, j = 1, \dots, m, k = 1, \dots, r_i-1$ , and for all  $\mathbf{x}$  is the neighborhood of  $\mathbf{x}_0$ ; and (2) the matrix  $\Delta(\mathbf{x})$  is a nonsingular at  $\mathbf{x} = \mathbf{x}_0$ . It is fundamental to the theory of sliding mode and feedback linearization control that the original system be linearizable by a proper choice of the control functions  $u_i$ . In the above equations, the function  $L^k$  denotes the  $k$ th successive Lie derivative. This is defined in the first-order case as

$$L_{f(\mathbf{x})} h(\mathbf{x}) = \frac{\partial h(\mathbf{x})}{\partial \mathbf{x}} \dot{\mathbf{x}}, \quad (59)$$

and in the second-order case as

$$L_{f(\mathbf{x})}^2 h(\mathbf{x}) = \frac{\partial [L_{f(\mathbf{x})} h(\mathbf{x})]}{\partial \mathbf{x}} \dot{\mathbf{x}}, \quad (60)$$

and so on.

Shown by Slotine,<sup>9</sup> systems like the one represented in equation (54) can be transformed, using the phase-variable canonical form developed by Johnson,<sup>20</sup> to the so-called “normal form.” This allows

for a more formal look into the notions of internal dynamics and zero dynamics. Internal dynamics are defined as the dynamics of the original system that are not involved in the phase-variable canonical form description. The normal form description of the system is shown as

$$\left\{ \begin{array}{l} \dot{Z}_{1i} = Z_{2i} \\ \dot{Z}_{2i} = Z_{3i} \\ \vdots \\ \dot{Z}_{(r_{m-1})i} = Z_{r_{mi}} \\ \dot{Z}_{r_{mi}} = L_f^r h_i + L_{g_i} L_f^{r_i-1} h_i u_i \\ y_i = Z_{1i}, \quad \forall i = 1, m \\ \dot{\eta}_i = q_i(\mathbf{Z}, \eta), \quad \forall i = (\sum_{j=1}^m r_j) + 1, n \end{array} \right. , \quad (61)$$

where  $\mathbf{Z}$  is the phase-variable state vector and  $\eta$  is the internal state vector.

In the transformed system shown above, it is required that the internal dynamics described by

$$\dot{\eta}_i = q_i(\mathbf{Z}, \eta), \quad \forall i = r_i + 1, n, \quad (62)$$

be bounded-input bounded-state (BIBS) stable. As discussed in Byrnes and Isidori,<sup>21</sup> one method of determining BIBS stability is to analyze the zero dynamics defined as

$$\dot{\eta} = q(0, \eta), \quad (63)$$

for exponential stability. For output tracking problems, Slotine<sup>9</sup> determines BIBS stability by analyzing the nominal zero dynamics defined as

$$\dot{\eta} = q(\mathbf{Z}^*, \eta), \quad (64)$$

for exponential stability, where  $\mathbf{Z}^*$  is the desired phase-variable trajectory.

Lyapunov<sup>4</sup> developed two methods for analyzing the exponential stability of nonlinear systems such as the one shown in equation (64). The first method involves linearizing the nonlinear system around some operating point(s) to analyze stability. The resulting linearized system

$$\Delta \dot{\eta} = \mathbf{A} \Delta \eta + \mathbf{B} \Delta \mathbf{Z}^*, \quad (65)$$

is then analyzed by finding the roots of the characteristic polynomial

$$\det [\lambda \mathbf{I} - \mathbf{A}] = 0. \quad (66)$$

The stability is only dependent upon the matrix  $\mathbf{A}$ , where the term  $\mathbf{B} \Delta \mathbf{Z}^*$  is assumed bounded. For each operating point analyzed, (1) if the characteristic roots all have negative real parts, the operating point is asymptotically stable; (2) if at least one of the characteristic roots has a positive real part, the operating point is unstable; (3) if one or more of the characteristic roots have a zero real part, with the remaining characteristic roots having negative real parts, no conclusions can be drawn by the study of the linearized model. Note that Lyapunov's first method is limited to determining stability in small regions about the operating points.

The second method, called the direct method, makes use of Lyapunov functions  $V(x)$ . If a positive definite function  $V(x)$  can be determined such that (1)  $V(x) > 0$  for all  $x \neq 0$  and  $V(0) = 0$ , (2)  $\dot{V}(x) < 0$  for all  $x \neq 0$ , and (3)  $V(x) \infty \rightarrow \infty$  as  $\|x\| \rightarrow \infty$ , then the origin is a globally asymptotically stable operating point. In summary, whichever method is used to investigate stability, if the resulting analysis shows that the internal dynamics are unstable, sliding mode control as well as feedback linearization techniques are not applicable to the system.

Procedures to determine the vector relative degree and the stability of the internal dynamics are discussed in this section. The next section discusses the sliding surface design upon which the output motion is restricted.

2. Sliding Surface Design. This section synthesizes the sliding surface upon which the desired output tracking motion is restricted for the MIMO system represented by equation (61). The motion of the system operating in the sliding surface is invariant to disturbances, parameter uncertainties, coupling between channels, and nonlinearities seen in the system.

In general, the set-point tracking control problem is defined as

$$\lim_{t \rightarrow \infty} \|y_i^{\text{set}}(t) - y_i(t)\| = 0, \quad \forall i = 1, m, \quad (67)$$

where  $y_i^{\text{set}}(t)$  represents the time-varying output set-point profile. According to Utkin<sup>11</sup> and DeCarlo,<sup>12</sup> the solution of this control problem using sliding mode implies that the synthesis of the sliding surface defined as  $\sigma_i(x) = 0$  in the subspace of the output errors and its derivatives is such that the output responses of the system in this surface are desirable.

For the MIMO system under consideration, it is desired that the tracking error for each output responds as a linear homogeneous differential equation with constant coefficients and with optimal eigenvalues placement. According to Shtessel and Jackson,<sup>22</sup> the desired tracking error response equation is chosen as the sliding surface. This is defined as

$$\sigma_i(t) = \sum_{j=0}^{r_m-1} c_{ji} e_i^{(j)}(t) = 0, \quad \forall i = 1, m, \quad (68)$$

where  $c_{ji}$  are constant coefficients and  $e_i(t)$  are the dynamic tracking errors defined as

$$e_i(t) = y_i^{\text{set}}(t) - y_i(t), \quad \forall i = 1, m, \quad (69)$$

or

$$e_i(t) = Z_{li}^{\text{set}}(t) - Z_{li}(t), \quad \forall i = 1, m, \quad (70)$$

using the phase-variable canonical form variables. The order  $r_m - 1$  of the sliding surface equation shown in equation (68) is chosen as one less than the relative degree for each output channel.

As shown by Utkin,<sup>11</sup> Itkis,<sup>10</sup> and DeCarlo,<sup>12</sup> an interesting result of the system operating on the sliding surface is that the motion is governed by a reduced-order set of equations. This result is derived from the state variable constraints imposed by the sliding surface equation,  $\sigma(x) = 0$ . Determining the reduced order set of equations is accomplished by first substituting equation (70) into the sliding surface equation represented in equation (68) and then solving for the highest-order state variable. This results in

$$Z_{rmi} = \sum_{j=0}^{r_m-1} c_{ji} Z_{1i}^{\text{set}(j)} - \sum_{j=0}^{r_m-2} c_{ji} Z_{(j+1)i}, \quad \forall i = 1, m, \quad (71)$$

where  $c_{(r_m-1)i} = 1$ . The next step involves substituting the algebraic expression for the highest-order state variable  $Z_{rmi}$ , shown in equation (71), into the transformed system represented by equation (61). The resulting reduced-order set of equations that describe the motion of the system on the sliding surface are shown as

$$\begin{cases} \dot{Z}_{1i} = Z_{2i} \\ \dot{Z}_{2i} = Z_{3i} \\ \vdots \\ \dot{Z}_{(r_m-1)i} = \sum_{j=0}^{r_m-1} c_{ji} Z_{1j}^{\text{set}(j)} - \sum_{j=0}^{r_m-2} c_{ji} Z_{(j+1)i} \\ y_i = Z_{1i}, \end{cases} \quad \forall i = 1, m \quad (72)$$

The constant coefficients  $c_{ji}$  of the linear sliding surface described by equation (68) or (72) are chosen to provide the desired output tracking motion in sliding mode. As shown by Dorf,<sup>23</sup> this is accomplished through simple linear design techniques such as pole placement or application of the ITAE criterion.

In summary, the system description in the sliding surface shown in equation (68) or (72) does not exhibit coupling between the various output channels. It is also invariant to the system parameter uncertainties and variations, as well as external and internal disturbances. The next section discusses the control function designs that cause the system to move to and operate in the local linear sliding surfaces.

**3. Control Function Design.** This section discusses the control function designs that force the system to the sliding surface and that maintain the system in the sliding surface for all subsequent time. Thus far in the discussion of sliding mode control theory, it can be stated that the theories of sliding mode and feedback linearization control parallel each other. In this section, however, these two theories deviate from each other in the application of the control function design.

Feedback linearization control relies on the real-time calculation of the control function  $u_i(t, \mathbf{x})$  to cancel the nonlinear system dynamics and to achieve the desired output tracking performance; whereas, the application of sliding mode control does not. Typically, the expression for the control function  $u_i(t, \mathbf{x})$  is very difficult and expensive to accurately calculate; moreover, if successfully calculated, this expression is very complicated and calculation intensive. Also, calculation errors for the control function can potentially cause an instability in the system. Unlike feedback linearization, the application of sliding mode control utilizes a bounded amount of control magnitude or a combination of a calculated and fixed amount of control to achieve output tracking performance.

According to Utkin,<sup>11</sup> each component  $u_i(t, \mathbf{x})$  of the high-speed switched control function  $u(t, \mathbf{x})$  has the nonlinear structure described by

$$u_i(t, \mathbf{x}) = \begin{cases} u_i^+(t, \mathbf{x}), & \sigma_i(\mathbf{x}) > 0 \\ u_i^-(t, \mathbf{x}), & \sigma_i(\mathbf{x}) < 0 \end{cases}, \quad \forall i = 1, m, \quad (73)$$

where  $\sigma_i(\mathbf{x}) = 0$  is the  $i$ th switching surface component associated with the  $(n-m)$ -dimensional switching surface

$$\sigma(\mathbf{x}) = [\sigma_1(\mathbf{x}), \dots, \sigma_m(\mathbf{x})]^T = 0. \quad (74)$$

Discussed in the previous section, the switching surfaces  $\sigma_i(\mathbf{x})$  are defined such that the motion restricted to  $\sigma(\mathbf{x}) = 0$  is the desired linear response of the system.

According to Slotine,<sup>9</sup> if a nonlinear control function of the form shown in equation (73) is chosen such that

$$\sigma_i(\mathbf{x}) \cdot \dot{\sigma}_i(\mathbf{x}) \leq -\rho_i |\sigma_i(\mathbf{x})|, \quad \forall i = 1, m, \quad (75)$$

for  $\rho_i > 0$ , then the system will reach the sliding surface  $\sigma(\mathbf{x}) = 0$  within a finite amount of time  $t_r$  defined as

$$t_{r_i} = \frac{|\sigma_i(0)|}{\rho_i}, \quad \forall i = 1, m. \quad (76)$$

The inequality represented by equation (75) is the existence condition for sliding mode control. This condition assures that the state derivatives point toward the sliding surface in the region of attraction. Shown by Slotine,<sup>9</sup> a sliding mode control function that satisfies the inequality shown in equation (75) is

$$u_i(t, \mathbf{x}) = \begin{cases} u_i^{eq}(t, \mathbf{x}) + \rho_i, & \sigma_i(\mathbf{x}) > 0 \\ u_i^{eq}(t, \mathbf{x}) - \rho_i, & \sigma_i(\mathbf{x}) < 0 \end{cases}, \quad \forall i = 1, m, \quad (77)$$

where  $u_i^{eq}(t, \mathbf{x})$  is the continuous equivalent control necessary to linearize the system and  $\rho_i$  is an arbitrary constant that represents the discontinuous or switched part of the control function.

According to Utkin,<sup>24</sup> the so-called equivalent control concept evolved from an equality first proposed by Wonham and Johnson<sup>25</sup> for describing the motion of the system in sliding mode. This equality is shown as

$$\sigma_i(\mathbf{x}) = \dot{\sigma}_i(\mathbf{x}) = 0. \quad (78)$$

Applying the chain rule to this equality yields

$$\frac{\partial \sigma_i(\mathbf{x})}{\partial \mathbf{x}} \dot{\mathbf{x}} = 0. \quad (79)$$

Substituting the expression for  $\dot{\mathbf{x}}$  shown in equation (54) into equation (79) yields

$$\frac{\partial \sigma_i(\mathbf{x})}{\partial \mathbf{x}} \dot{\mathbf{x}} = \frac{\partial \sigma_i(\mathbf{x})}{\partial \mathbf{x}} [\mathbf{f}(\mathbf{x}) + \mathbf{G}(\mathbf{x}) u_i^{eq}(t, \mathbf{x})] = 0, \quad (80)$$

where  $u_i^{eq}(t, \mathbf{x})$  is the equivalent control that solves this equation. Assuming the matrix product  $[\partial \sigma_i(\mathbf{x}) / \partial \mathbf{x}] \mathbf{G}(\mathbf{x})$  is nonsingular for all  $t$  and  $\mathbf{x}$ , the equivalent control is computed from equation (80) as

$$u_i^{eq}(t, \mathbf{x}) = - \left[ \frac{\partial \sigma_i(\mathbf{x})}{\partial \mathbf{x}} \mathbf{G}(\mathbf{x}) \right]^{-1} \left[ \frac{\partial \sigma_i(\mathbf{x})}{\partial \mathbf{x}} \mathbf{f}(\mathbf{x}) + \frac{\partial \sigma_i(\mathbf{x})}{\partial \mathbf{x}} \right]. \quad (81)$$

The control function defined in equation (77) provides the existence of sliding mode in the presence of parameter variations and uncertainties, as well as external and internal disturbances.

The sliding mode control functions rely on high-speed switching to achieve performance. The phenomenon of nonideal but high-speed switching is labeled as chattering. The high-speed switched components of this chattering are usually undesirable because they may excite unmodeled high-frequency plant dynamics, which could result in unforeseen instabilities. Shown by Slotine,<sup>9</sup> this “chattering” may be eliminated by choosing a boundary layer of width  $\varepsilon$  about  $\sigma = 0$  such that the discontinuous control function shown in equation (77) is redefined as

$$u_i(t, \mathbf{x}) = \begin{cases} u_i^{\text{eq}}(t, \mathbf{x}) + \rho_i \text{sgn}[\sigma_i(\mathbf{x})], & |\sigma_i(\mathbf{x})| \geq \varepsilon \\ u_i^{\text{eq}}(t, \mathbf{x}) + \hat{\rho}_i, & |\sigma_i(\mathbf{x})| < \varepsilon \end{cases}, \quad \forall i = 1, m, \quad (82)$$

where

$$\hat{\rho}_i = \frac{\rho_i}{\varepsilon} \sigma_i(\mathbf{x}), \quad \forall i = 1, m. \quad (83)$$

This redefined smoothing control function has the advantage of an attractive switching boundary.

Another possible form of the control function structure expressed in equation (73) is

$$u_i(t, \mathbf{x}) = \begin{cases} +u_i^{\text{max}}, & \sigma_i(\mathbf{x}) > 0 \\ -u_i^{\text{max}}, & \sigma_i(\mathbf{x}) < 0 \end{cases}, \quad \forall i = 1, m, \quad (84)$$

where  $u_i^{\text{max}}$  is a bounding constant that is obtained from an extension of the existence condition shown in equation (75). According to Slotine,<sup>9</sup> this extension is defined by the inequality

$$u_i^{\text{max}} \geq |u_i^{\text{eq}}(t, \mathbf{x})| + \rho_i, \quad \forall i = 1, m. \quad (85)$$

Meeting this inequality guarantees that the output motion moves to and stays on the sliding surface for all time. The bounding control value  $u_i^{\text{max}}$  represents the maximum amount of control necessary to maintain the desired set-point tracking for the specified problem. If this amount of control is not available (i.e., it is too costly or because of physical constraints), satisfactory tracking performance is usually achieved by setting  $u_i^-$  and  $u_i^+$  to a nominal control value that is somewhat less than  $u_i^{\text{max}}$ .

### C. Summary

This section reviewed the major concepts of VSS, specifically that of sliding mode control. This section identified some techniques common between feedback linearization control and sliding mode control and pointed out the differences between the two. This section also illustrated the application of sliding mode control to a generic nonlinear MIMO system. Sliding mode control is unique in its ability to achieve accurate, robust, decoupled tracking for a class of nonlinear time-varying multivariable systems in the presence of disturbances and parameter variations. The next section will formulate the specific TCS control problem upon which the sliding mode theory is applied.

## IV. PROBLEM FORMULATION

This section will formalize the TCS control problem that the sliding mode controllers are designed to solve. The problem formalization begins with a description of the TCS by a mathematical model. This mathematical model is represented by the nonlinear MIMO system with partially known parameters shown in equations (20), (35), (36), (37), (40), and (42) through (45). These equations model the salient dynamics within the TCS, which include the response of each valve actuator, each path flow rate, the system pressure drop, and the source flow rate through the pump. The TCS mathematical model is very useful in determining the sliding surfaces and control functions designed to meet and even exceed the control system objective discussed in the following.

The control system objective of the TCS is to simultaneously control the thermal environments of several furnaces and related subsystems plumbed in parallel. Specifically, the high accuracy, robust, and decoupled tracking performance of time-varying flow rate profiles  $W^{\text{set}}(t)$  in the various parallel subsystem paths is desired. It is assumed that each individual path flow rate profile  $W_i^{\text{set}}(t)$  is formed or conceived beforehand or in real time.

The TCS set-point tracking control problem is defined as

$$\lim_{t \rightarrow \infty} \|e_i(t)\| = 0, \quad \forall i = 1, 3, \quad (86)$$

where

$$e_i(t) = W_i^{\text{set}}(t) - W_i(t), \quad \forall i = 1, 3. \quad (87)$$

The solution of this control problem using sliding mode is twofold. First, equations  $\sigma_i(x) = 0$  are chosen such that the sliding mode tracking errors defined in equation (87) are the outputs of linear homogeneous systems with constant coefficients and with desired eigenvalue placements. Secondly, discontinuous control laws of the form

$$u_i(t, \mathbf{x}) = \begin{cases} u_i^+(t, \mathbf{x}), & \sigma_i(\mathbf{x}) > 0 \\ u_i^-(t, \mathbf{x}), & \sigma_i(\mathbf{x}) < 0 \end{cases}, \quad \forall i = 1, 3, \quad (88)$$

are chosen such that desired output tracking motion goes to and stays on the sliding surfaces defined as  $\sigma_i(x) = 0$ .

In summary, the goal of the control system design is to achieve decoupled output tracking in the presence of system nonlinearities, parameter variations, and external and internal disturbances. This section formulated the problem upon which the sliding mode control strategy is to be applied. The next section will detail the design process for the sliding mode controllers.

## V. SLIDING MODE CONTROLLER DESIGN

This section discusses the synthesis of the sliding mode controllers designed to track defined flow rate profiles for the TCS. The TCS sliding mode controller synthesis process consists of three major steps. The first step is to transform the original system to a convenient canonical form to determine the vector relative degree of the system and to analyze the stability of the internal dynamics. The second step is to design the desired linear sliding surface upon which the output motion is restricted. The

third step is to select the control function to provide the existence of the motion in the sliding surface. Several sliding mode control implementation issues are also discussed.

### A. System Transformation

The first step in the sliding mode controller design process is to transform the TCS MIMO non-linear system to a form convenient for the determination of the vector relative degree and for the stability analysis of the internal dynamics. The original TCS system is presented in matrix form as follows:

$$\begin{cases} \dot{\mathbf{x}} = \mathbf{f}(\mathbf{x}) + \mathbf{G}\mathbf{u} \\ \mathbf{y} = \mathbf{h}(\mathbf{x}) \end{cases}, \quad (89)$$

where  $\mathbf{x}$  is the  $16 \times 1$  state vector defined as

$$\mathbf{x} = [W_1 \quad \theta_1 \quad \omega_1 \quad W_2 \quad \theta_2 \quad \omega_2 \quad W_3 \quad \theta_3 \quad \omega_3 \quad W_S \quad P \quad \omega_p \quad I_a \quad \omega_{fbk} \quad X_{c1} \quad X_{c2}]^T. \quad (90)$$

$\mathbf{u}$  is the  $3 \times 1$  control input vector defined as

$$\mathbf{u} = [u_1 \quad u_2 \quad u_3]^T. \quad (91)$$

$\mathbf{y}$  is the  $3 \times 1$  output vector defined as

$$\mathbf{y} = [y_1 \quad y_2 \quad y_3]^T. \quad (92)$$

$\mathbf{h}(\mathbf{x})$  is the smooth  $3 \times 1$  vector defined as

$$\mathbf{h}(\mathbf{x}) = [W_1 \quad W_2 \quad W_3]^T.$$

$\mathbf{f}(\mathbf{x})$  is the smooth  $16 \times 1$  vector field defined as

$$\mathbf{f}(\mathbf{x}) = [f_1(\mathbf{x}) \quad \cdots \quad f_{16}(\mathbf{x})]^T, \quad (93)$$

where

$$f_i(\mathbf{x}) = \frac{1}{L_{P_i}} [P - (R_{V_i} + R_{P_i})W_i], \quad \forall i = 1, 4, 7, \quad (94)$$

$$f_i(\mathbf{x}) = \omega_i, \quad \forall i = 2, 5, 8, \quad (95)$$

$$f_i(\mathbf{x}) = -\frac{1}{\tau} \omega_i, \quad \forall i = 3, 6, 9, \quad (96)$$

$$f_{10}(\mathbf{x}) = \frac{1}{L_S} (P_S - P - R_S W_S), \quad (97)$$

$$f_{11}(\mathbf{x}) = \frac{2}{C} \left( W_S - \sum_{i=1}^4 W_i \right), \quad (98)$$

$$f_{12}(\mathbf{x}) = \frac{1}{j_{ml}} (k_t I_a - k_1 \omega_p^2), \quad (99)$$

$$f_{13}(\mathbf{x}) = \frac{1}{L_m} [-R_m I_a - k_e \omega_p - k_2 (P - P_{\text{set}}) - k_3 \omega_{fbk} + \mathbf{QX}_c], \quad (100)$$

$$f_{14}(\mathbf{x}) = \frac{1}{\tau_f} (\omega_p - \omega_{fbk}), \quad (101)$$

$$[f_{15}(\mathbf{x}) \quad f_{16}(\mathbf{x})]^T = \mathbf{MX}_c + \mathbf{B} \cdot [\omega_{fbk} \quad P \quad P_{\text{set}}]^T, \quad (102)$$

and  $\mathbf{G}$  is the constant  $16 \times 3$  matrix defined as

$$\mathbf{G} = \begin{bmatrix} 0 & 0 & 0 & 0 & 0 & 0 & 0 & 0 & \frac{k_v}{\tau} & 0 & \dots & 0 \\ 0 & 0 & 0 & 0 & 0 & \frac{k_v}{\tau} & 0 & 0 & 0 & 0 & \dots & 0 \\ 0 & 0 & \frac{k_v}{\tau} & 0 & 0 & 0 & 0 & 0 & 0 & 0 & \dots & 0 \end{bmatrix}^T. \quad (103)$$

Transformation to a convenient canonical form is accomplished by first applying a technique borrowed from input-output linearization. This technique, shown in equation (55), is applied to the system shown in equation (89). This technique involves taking successive derivatives of each output  $y_i$  until at least one input  $u_i$  appears. The first derivative is calculated as

$$L_{f(x)} h_i(\mathbf{x}) = -\frac{1}{L_{P_i}} \Omega_{li}, \quad \forall i = 1, 3, \quad (104)$$

where

$$\Omega_{li} = \Omega_{2i} W_i^2 + P, \quad \forall i = 1, 3. \quad (105)$$

and

$$\Omega_{2i} = -\left[ (\alpha e^{-\beta \cdot \theta_i} + \delta) + K_i \right], \quad \forall i = 1, 3. \quad (106)$$

It is obvious that the control inputs  $u_i$  do not appear in the first derivative; therefore, it is necessary to take the second derivative. This is calculated as

$$L_{f(x)}^2 h_i(\mathbf{x}) = -\frac{1}{L_{P_i}} \left[ \alpha \beta \omega_i W_i^2 e^{-\beta \cdot \theta_i} + \frac{2}{L_{P_i}} W_i \Omega_{li} \Omega_{2i} + \frac{2}{C} \left( W_S - \sum_{k=1}^4 W_k \right) \right], \quad \forall i = 1, 3. \quad (107)$$

Again, the control inputs  $u_i$  do not appear; therefore, the third derivative is calculated as

$$L_{f(x)}^3 h_i(\mathbf{x}) = -\frac{1}{L_{P_i}} \left[ \sum_{j=1}^4 \Psi_{ji} + \frac{1}{\tau} \alpha \beta W_i^2 e^{-\beta \theta_i} (\omega_i + K_v u_i) \right], \quad \forall i = 1, 3, \quad (108)$$

where

$$\Psi_{1i} = -\alpha \beta^2 \omega_i^2 W_i^2 e^{-\beta \theta_i} + \frac{1}{L_{P_i}} (2\Omega_{2i} W_i^3 + 2\Omega_{1i} W_i) \alpha \beta \omega_i e^{-\beta \theta_i}, \quad (109)$$

$$\Psi_{2i} = \frac{2}{L_{P_i}} \alpha \beta \omega_i W_i \Omega_{1i} e^{-\beta \theta_i} + \frac{1}{L_{P_i}^2} (4W_i^2 \Theta_{2i}^2 + 2\Omega_{1i} \Omega_{2i}) f_{1i} - \frac{2}{L_i C} \Omega_{1i}, \quad (110)$$

$$\Psi_{3i} = \frac{4}{L_{P_i} C} \Omega_{2i} W_i \left( W_S - \sum_{j=1}^4 W_j \right), \quad (111)$$

$$\Psi_{4i} = \frac{2}{C} \left[ \frac{1}{L_S} (P_S - R_S W_S^2 - P) - \sum_{\substack{k=1 \\ k \neq i}}^4 \frac{1}{L_{P_K}} \Omega_{ki} \right]. \quad (112)$$

The control input appears after the third derivative of the output function. The resulting 3-dimensional set of output derivative equations is shown as

$$\begin{bmatrix} \ddot{y}_1 \\ \ddot{y}_2 \\ \ddot{y}_3 \end{bmatrix} = \begin{bmatrix} -\frac{1}{L_{P_1}} \left[ \sum_{i=1}^4 \Psi_{i1} + \frac{1}{\tau} \alpha \beta W_1^2 e^{-\beta \theta_1} \omega_1 \right] \\ -\frac{1}{L_{P_i}} \left[ \sum_{i=1}^4 \Psi_{i2} + \frac{1}{\tau} \alpha \beta W_2^2 e^{-\beta \theta_2} \omega_2 \right] \\ -\frac{1}{L_{P_i}} \left[ \sum_{i=1}^4 \Psi_{i3} + \frac{1}{\tau} \alpha \beta W_3^2 e^{-\beta \theta_3} \omega_3 \right] \end{bmatrix} + \Delta(\mathbf{x}) \begin{bmatrix} u_1 \\ u_2 \\ u_3 \end{bmatrix}, \quad (113)$$

where

$$\Delta(\mathbf{x}) = \begin{bmatrix} \frac{1}{\tau} \alpha \beta W_1^2 e^{-\beta \theta_1} K_v & 0 & 0 \\ 0 & \frac{1}{\tau} \alpha \beta W_2^2 e^{-\beta \theta_2} K_v & 0 \\ 0 & 0 & \frac{1}{\tau} \alpha \beta W_3^2 e^{-\beta \theta_3} K_v \end{bmatrix}. \quad (114)$$

The matrix  $\Delta(\mathbf{x})$  is nonsingular at  $\mathbf{x} = \mathbf{x}_0$ ; therefore, the system is linearizable at  $\mathbf{x}_0$  and has a vector relative degree  $\mathbf{r} = [3, 3, 3]$ . It is noted that the input matrix  $\Delta(\mathbf{x})$  decouples the control function from each path.

The system represented by equation (113) is transformed, using the phase-variable canonical form developed by Johnson<sup>20</sup> to the so-called “normal form.” This allows for a more formal look into the notions of internal dynamics and zero dynamics. Internal dynamics are defined as the dynamics of the original system that are not involved in the phase-variable canonical form description. The normal form description of the system is shown as

$$\begin{cases} \dot{Z}_{1i} = Z_{2i} \\ \dot{Z}_{2i} = Z_{3i} \\ \dot{Z}_{3i} = -\frac{1}{L_{P_i}} \left[ \sum_{j=1}^4 \Psi_{ji} + \frac{1}{\tau} \alpha \beta Z_{1i}^2 e^{-\beta Z_{2i}} (Z_{3i} + K_{v_i} u_i) \right] + \frac{1}{\tau} \alpha \beta Z_{1i}^2 e^{-\beta Z_{2i}} K_{v_i} u_i, \\ y_i = Z_{1i}, \quad \forall i = 1,3 \\ \dot{\eta}_i = q_i(\mathbf{Z}, \eta), \quad \forall i = 10,16 \end{cases} \quad (115)$$

where  $\mathbf{Z}$  is the  $9 \times 1$  phase-variable state vector defined by

$$\mathbf{Z} = [W_1 \quad \theta_1 \quad \omega_1 \quad W_2 \quad \theta_2 \quad \omega_2 \quad W_3 \quad \theta_3 \quad \omega_3]^T, \quad (116)$$

and  $\eta$  is the  $7 \times 1$  internal state vector defined by

$$\eta = [W_S \quad P \quad \omega_p \quad I_a \quad \omega_{fbk} \quad X_{c1} \quad X_{c2}]^T. \quad (117)$$

Stability of the internal dynamics is required to assure that sliding mode techniques are applicable to the TCS system. According to Slotine,<sup>9</sup> it is required that the internal dynamics described by

$$\dot{\eta}_i = q_i(\mathbf{Z}, \eta), \quad \forall i = 10,16, \quad (118)$$

are bounded-input bounded-state (BIBS) stable. This stability is determined by analyzing the nominal zero dynamics defined by

$$\dot{\eta}_i = q_i(\mathbf{Z}^*, \eta), \quad \forall i = 10,16, \quad (119)$$

for exponential stability, where  $\mathbf{Z}^*$  is the desired phase-variable trajectory

$$\mathbf{Z}^* = [W_1^{\text{set}}(t) \quad W_2^{\text{set}}(t) \quad W_3^{\text{set}}(t)]^T. \quad (120)$$

Defined in section III. Lyapunov’s first method is performed on the system shown in equation (119). Since two equations of the internal dynamics are nonlinear, this method involves selecting nominal operating point(s) at which the local stability is analyzed. The nominal operating point for the internal states is shown as

$$\eta = \eta_0 = [1,004.1 \quad 10.0 \quad 1,016.2 \quad 1.58 \quad 1,016.2 \quad 1,016.2 \quad 0.1078]^T. \quad (121)$$

An analysis program is used to linearize the system at a desired phase-variable trajectory

$$\mathbf{Z}^* = [260.0 \quad 300.0 \quad 260.0]^T, \quad (122)$$

and the result is shown as

$$\Delta\dot{\eta} = A\Delta\eta + B\Delta Z^* , \quad (123)$$

where

$$A = \begin{bmatrix} 0.0 & 20.0 & 0.0 & 0.0 & 0.0 & 0.0 & 0.0 \\ -890.0 & -19.6 & 36.8 & 0.0 & 0.0 & 0.0 & 0.0 \\ 0.0 & 0.0 & -33.0 & 1.1E+4 & 0.0 & 0.0 & 0.0 \\ -1.8 & 0.0 & -34.8 & -51.5 & -17.5 & 17.8 & 3.3E+5 \\ 0.0 & 0.0 & 130.0 & 0.0 & -130.0 & 0.0 & 0.0 \\ -0.1 & 0.0 & 0.0 & 0.0 & 0.0 & 0.0 & 0.0 \\ -4.3E-5 & 0.0 & 0.0 & 0.0 & -4.3E-4 & 4.3E-4 & 0.0 \end{bmatrix} , \quad (124)$$

and  $B\Delta Z^*$  is bounded. The roots of the characteristic equation are calculated according to equation (66) as

$$\lambda_1 = -0.00414 , \quad (125)$$

$$\lambda_2 = -2.708 , \quad (126)$$

$$\lambda_{3,4} = -9.801 \pm j132.84 , \quad (127)$$

$$\lambda_5 = -196.0 , \quad (128)$$

$$\lambda_{6,7} = -237.4 \pm j551.1 . \quad (129)$$

These roots all have negative real parts; therefore, the linearized system is stable for the defined operating point and the desired phase-variable vector. Multiple operating points and phase-variable vectors are subsequently used to analyze stability, and the results indicate that the linearized system around the local operating points is always BIBS stable. Time simulations confirm that the internal dynamics are BIBS stable for the analyzed operating points. Hence, sliding-mode techniques are certainly applicable to the TCS system.

In summary, this section presented the original TCS system equations in a compact matrix form. This section transformed the original system, using input-output linearization techniques, to the output derivative form to determine the system's relative degree. Lastly, the original system was presented in the normal form to identify the internal dynamics and to analyze the stability using Lyapunov's first method. The internal dynamics are shown to be stable for the system. The next section discusses the sliding surface design upon which the output motion is restricted.

## B. Sliding Surface Design

The second major step in the design process is to choose the desired linear homogeneous sliding surface upon which each path's error dynamics are restricted. The degree (order) of each sliding surface is chosen as one less than the relative degree for each path's output expression. The relative degree for each path's output expression is calculated as the number of differentiations required such that one or more of the system inputs appears in the resulting output differentiation. For the whole TCS system, the vector relative degree is a combination of the relative degrees for each output. The vector relative degree

is calculated in the previous section as  $\mathbf{r} = [3, 3, 3]$ , hence, the vector degree of the sliding surfaces is chosen as  $\mathbf{r}_s = [2, 2, 2]$ .

The sliding surface  $\sigma_i$  equations are chosen as the set of second-order linear homogeneous differential equations of the form

$$\sigma_i = \ddot{e}_i + c_{2i}\dot{e}_i + c_{1i}e = 0, \quad \forall i = 1,3, \quad (130)$$

with constant coefficients. Shown by Shtessel and Jackson,<sup>22</sup> the coefficients of equation (130) are selected to obtain the desired transient response of the error dynamics within the TCS. These coefficients are chosen as  $c_{1i} = 225.0$  and  $c_{2i} = 21.0$ ,  $\forall i = 1,3$ , using the ITAE method shown by Dorf.<sup>23</sup> The resulting system has a damping ratio  $\zeta = 0.7$  and a natural frequency  $\omega_n = 15.0$ , according to the standard second-order form

$$\ddot{e} + 2\zeta\omega_n\dot{e} + \omega_n^2e = 0. \quad (131)$$

The eigenvalues of the system are solved as  $\lambda_{1,2} = -10.5 \pm j10.7$ , which gives the desired optimal transient response of the system operating in sliding mode.

In summary, the linear homogeneous sliding surface equations with desired optimal eigenvalues placement are chosen for each path. The system response in the sliding surface shown by equation (130) is linear and invariant to internal and external disturbances, parameter uncertainties, and variations. The next section will discuss the control function designs that cause the system to move to and operate in the local linear sliding surfaces.

### C. Control Function Design

The third major step of the design process involves selecting the control functions  $u_i(t, \mathbf{x})$  to provide the existence of the motion described by equation (130) in sliding mode. According to Utkin,<sup>24</sup> the sliding mode control function judiciously switches back and forth at a high speed between the positive and negative value of a chosen magnitude according to some prescribed control function. That is, each component  $u_i(t, \mathbf{x})$ ,  $i = 1,3$ , of the high-speed switched control function has the nonlinear structure described by

$$u_i(t, \mathbf{x}) = \begin{cases} u_i^+(t, \mathbf{x}), & \sigma_i(\mathbf{x}) > 0 \\ u_i^-(t, \mathbf{x}), & \sigma_i(\mathbf{x}) < 0 \end{cases}, \quad \forall i = 1,3. \quad (132)$$

Specifically, the nonlinear form of the control function is chosen as

$$u_i(t, \mathbf{x}) = u_i^{\max}(t, \mathbf{x}) \text{sign} [\sigma_i(\mathbf{x})], \quad \forall i = 1,3, \quad (133)$$

where  $\sigma_i(\mathbf{x}) = 0$  are the desired linear homogeneous switching surfaces defined by equation (130).

As explained in section III of this report, the existence of sliding mode requires that the state derivative must point toward the sliding surface in the region of attraction. This is shown mathematically as

$$\sigma_i(\mathbf{x}) \cdot \dot{\sigma}_i(\mathbf{x}) < 0, \quad \forall i = 1,3. \quad (134)$$

Appropriate selection of the control functions  $u_i^{\max}(t, \mathbf{x})$  assures that the above inequality is satisfied. This is accomplished by choosing the value of these control functions greater than or equal to the absolute value of the so-called equivalent control  $u_i^{eq}(t, \mathbf{x})$ . This is shown mathematically as

$$u_i^{\max}(t, \mathbf{x}) > |u_i^{eq}(t, \mathbf{x})|, \quad \forall i = 1, 3, \quad (135)$$

where the equivalent control  $u_i^{eq}(t, \mathbf{x})$  is the amount of control necessary to maintain desired set-point tracking. In other words, it is the amount of control necessary to maintain the motion of the system on the sliding surface in the presence of system nonlinearities, parameter variations, and external and internal disturbances. Mathematically, equivalent control is the amount of control necessary to solve the equality defined as

$$\sigma_i(\mathbf{x}) = \dot{\sigma}_i(\mathbf{x}) = 0, \quad \forall i = 1, 3. \quad (136)$$

Substituting the sliding surface  $\sigma_i(\mathbf{x})$  shown in equation (130) into the above equality yields

$$\dot{\sigma}_i(\mathbf{x}) = \ddot{y}_i + c_{2i}\dot{y}_i + c_{1i}y_i = 0, \quad \forall i = 1, 3. \quad (137)$$

Substituting the definition for  $\ddot{y}_i$  shown in equation (107) into the above equation and solving for the equivalent control  $u_i^{eq}(t, \mathbf{x})$  yields

$$u_i^{eq}(t, \mathbf{x}) \geq \frac{-\ddot{W}_i^{\text{set}} + \frac{1}{L_{P_i}} \left( \sum_{j=1}^4 \Psi_{ji} + \frac{1}{\tau} \alpha \beta \omega_i W_i^2 e^{-\beta \theta_i} \right) - c_{2i}\dot{y}_i - c_{1i}y_i}{\frac{1}{L_{P_i}} \frac{\alpha \beta}{\tau} K_v W_i^2 e^{-\beta \theta_i}}, \quad (138)$$

for all  $i = 1, 3$ . Substituting the above expression for  $u_i^{eq}(t, \mathbf{x})$  into the inequality defined in equation (135) results in

$$u_i^{\max}(t, \mathbf{x}) \geq \left| \frac{-\ddot{W}_i^{\text{set}} + \frac{1}{L_{P_i}} \left( \sum_{j=1}^4 \Psi_{ji} + \frac{1}{\tau} \alpha \beta \omega_i W_i^2 e^{-\beta \theta_i} \right) - c_{2i}\dot{y}_i - c_{1i}y_i}{\frac{1}{L_{P_i}} \frac{\alpha \beta}{\tau} K_v W_i^2 e^{-\beta \theta_i}} \right|, \quad (139)$$

for all  $i = 1, 3$ .

The control function represented by equation (139) is the maximum amount of control necessary to maintain desired set-point tracking for the MIMO nonlinear TCS system in the face of time-varying flow profiles, parameter variations, and internal flow and pressure disturbances. This calculated control function does not contain external disturbance torque terms; however, these terms could be added to improve the calculation.

Nonlinear control methods like feedback linearization require accurate real-time calculations of functions like the one shown in equation (139) to achieve control system performance. Unlike these nonlinear control methods, the sliding mode control method does not require such calculations to achieve performance. The sliding mode control method only requires that the boundary values of these type functions be calculated or approximated to achieve sliding mode performance. Furthermore, sliding mode control usually achieves control system performance using control function values much less than these boundary values. Not relying on these function calculations is a unique advantage for sliding mode

control because functions such as the one shown in equation (139) are usually very difficult and expensive to accurately calculate.

For the sliding mode control function shown in equation (133), the  $u_i^{\max}(t, \mathbf{x})$  values are chosen by calculating the  $u_i^{eq}(t, \mathbf{x})$  expression shown in equation (138) during a computer simulation of the TCS. As shown in figure 9, this simulation involves simultaneously changing flow set-points in the respective paths. During the simulation, the time-varying system parameters and states are calculated and substituted into equation (138). The resulting  $u_i^{eq}(t, \mathbf{x})$  calculations for each of the three flow paths are shown in figure 10.

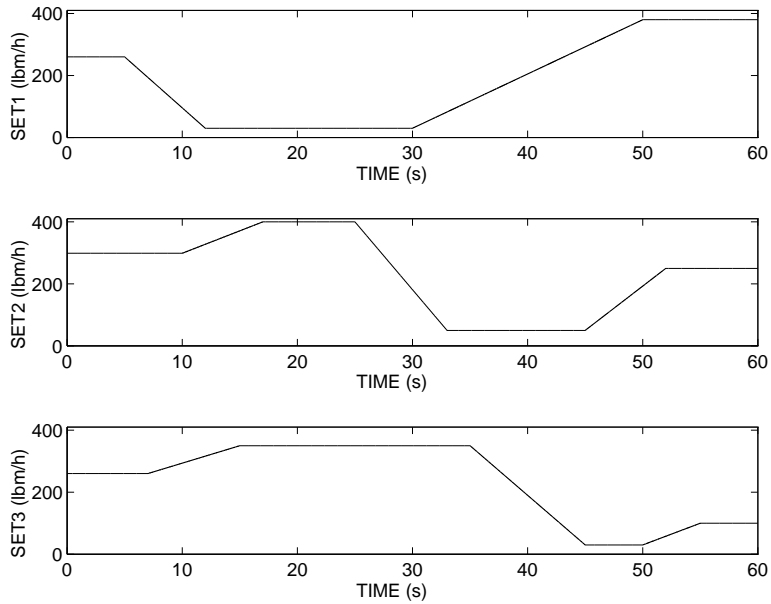


Figure 9. Time-varying flow profile plots.

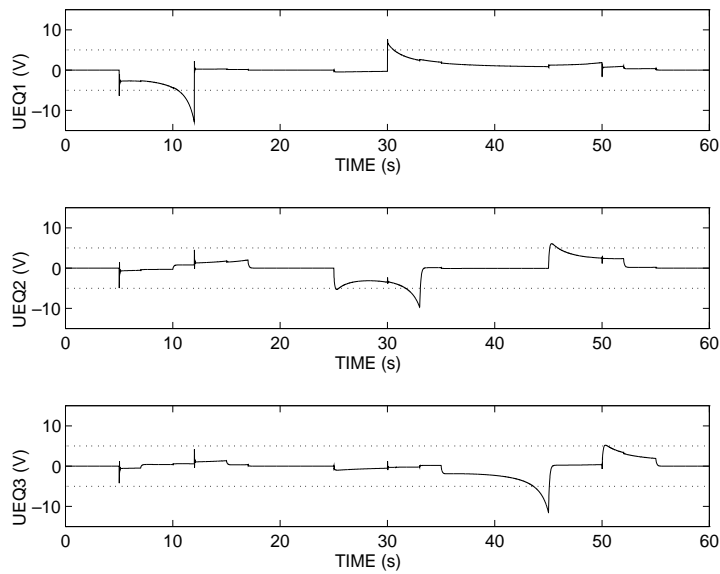


Figure 10. Required  $u_i^{eq}(t, \mathbf{x})$  for path plots.

The specifications for the TCS flight valve actuators call for a maximum and minimum command voltage of  $\pm 5$  V. From the plots of  $u_i^{eq}(t, \mathbf{x})$  shown in figure 10, it is observed that the equivalent control necessary to achieve sliding surface tracking is mostly contained within the  $\pm 5$ -V threshold. This voltage threshold is shown by the horizontal dotted lines in the plots of  $u_i^{eq}(t, \mathbf{x})$  control functions. Therefore, the resulting sliding mode control function is chosen as

$$u_i(t, \mathbf{x}) = \begin{cases} +5, & \sigma_i(\mathbf{x}) > 0 \\ -5, & \sigma_i(\mathbf{x}) < 0 \end{cases}, \quad \forall i = 1, 3, \quad (140)$$

or equivalently by

$$u_i(t, \mathbf{x}) = 5 \cdot \text{sign} [\sigma_i(\mathbf{x})], \quad \forall i = 1, 3. \quad (141)$$

The discontinuous sliding mode control function is defined by the above equations. The next section discusses several issues related to the realization of the above equations.

#### D. Realization of Control Function

The realization of the sliding mode controller is accomplished by first comparing the desired flow path signal  $W_i^{\text{set}}(t)$  with the actual (sensed) flow signal  $W_i(t)$  to generate the error signal  $e_i(t)$ . This error signal is then passed through two differentiators to compute the first and second derivatives of the error, respectively. Each of these differentiators is realized by a first-order transfer function of the form

$$\frac{S}{\tau S + 1}, \quad (142)$$

where the time constant  $\tau = 0.01$  s. The time constant  $\tau$  is a design parameter chosen to filter noise seen on the error signal. The error signal and its derivatives are then combined to form the sliding surface equation. This is shown as

$$\sigma_i = \ddot{e}_i + 21.0 \dot{e}_i + 225.0 e = 0, \quad \forall i = 1, 3. \quad (143)$$

Finally, the sliding surface equation output  $\sigma_i$  is passed into the control function shown in equation (140) to compute the necessary input  $u_i(t, \mathbf{x})$ . This control input actuates the flow control valve to track defined flow rate profiles. The composite sliding mode controller is illustrated in block diagram form in figure 11.

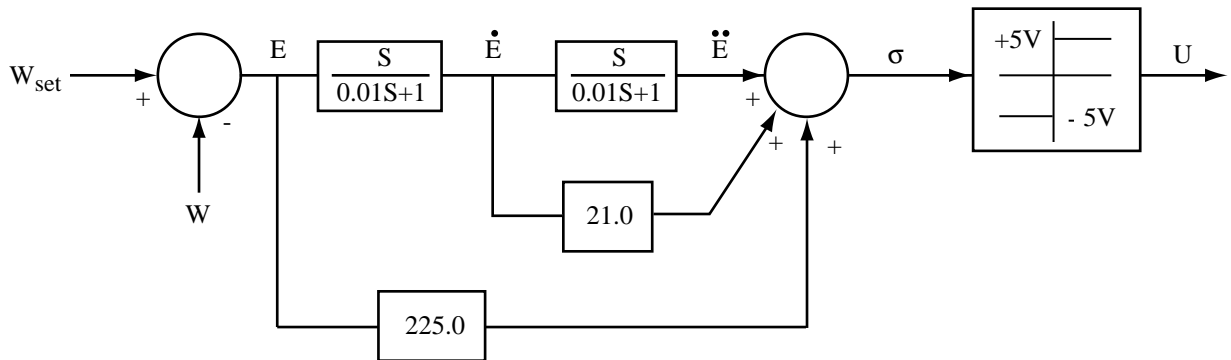


Figure 11. Sliding mode controller block diagram.

The sliding mode controller shown in figure 11 is realized through a continuous circuit. Equivalently, this system may also be realized through a discrete circuit that involves a control computer and sample-and-hold circuits. The sliding mode control theory is equivalent for both the continuous and discrete realizations with one exception. For continuous realization, the necessary and sufficient condition for the existence of sliding mode is given as

$$\dot{\sigma}(t, \mathbf{x}) \cdot \sigma(t, \mathbf{x}) < 0 . \quad (144)$$

Whereas, according to Sarpturk,<sup>26</sup> the necessary condition for the existence of sliding mode for discrete realization is given as

$$[\sigma[(k+1)T, \mathbf{x}] - \sigma(kT, \mathbf{x})] \cdot \sigma(kT, \mathbf{x}) < 0 , \quad (145)$$

and the sufficient condition is given as

$$|\sigma[(k+1)T, \mathbf{x}]| < |\sigma(kT, \mathbf{x})| . \quad (146)$$

The two existence conditions shown above for the discrete realization are dependent upon the discrete sample period  $T$ . As this period becomes smaller, the two existence conditions are easier to satisfy.

The sliding mode controller shown in figure 11 relies on high-speed switching to achieve performance. The phenomenon of nonideal but high-speed switching is labeled as chattering. In general, chattering must be eliminated for the controller to perform properly. This is accomplished by modifying the discontinuous control function shown in equation (140) according to the smoothing function defined by equations (82) and (83). The resulting smoothed control function is

$$u_i(t, \mathbf{x}) = \begin{cases} 5 \cdot \text{sign} [\sigma_i(\mathbf{x})] , & |\sigma_i(\mathbf{x})| \geq \varepsilon \\ \hat{\rho}_i , & |\sigma_i(\mathbf{x})| < \varepsilon \end{cases} , \quad \forall i = 1, 3 , \quad (147)$$

where

$$\hat{\rho}_i = \frac{5}{\varepsilon} \sigma_i(\mathbf{x}) , \quad \forall i = 1, 3 . \quad (148)$$

Implementation of the smoothing function leads to operation in the sliding surface to within a guaranteed precision  $\sigma = \varepsilon$ , rather than perfect sliding surface operation. The boundary width  $\varepsilon = 0.1$  is chosen to tune the control function to achieve a trade-off between tracking precision and robustness to unmodeled dynamics.

## E. Summary

This section discussed the synthesis of the sliding mode controllers designed to track defined flow rate profiles for the TCS. This synthesis consists of transforming the system mathematical model to the normal form to determine the vector relative degree and to analyze the stability of the internal dynamics, designing the desired linear sliding surface upon which the output motion is restricted, and selecting the control function to provide the existence of the motion in the sliding surface. Sliding mode controller realization issues such as continuous versus discrete implementations and chattering suppression were discussed. The next section will show that the synthesized sliding mode controllers achieve decoupled output tracking in the presence of system nonlinearities, parameter variations, and external and internal disturbances.

## VI. SIMULATION RESULTS

This section presents the results of continuous time simulations of the TCS under various operating conditions. The time simulations are performed using the Marshall System for Aerospace Simulation (MARSYAS) software package. The MARSYAS software package is designed for easy setup and control of the simulation of continuous dynamics of physical systems on a digital computer. The differential equations and corresponding coefficient definitions developed in section II of this report are entered into MARSYAS to build the TCS simulation model. The MARSYAS code representing the TCS model is shown in the appendix. The Runge Kutta fourth-order algorithm with a 0.001-s step size is used for the numerical solutions of the differential equations during the simulations.

The performance of the TCS sliding mode controller is assessed under various operating conditions within the TCS. These operating conditions are divided into three categories: (1) simultaneous flow set-point changes in each of the three parallel paths, (2) normalized disturbance torques applied to the flow actuators, and (3) parameter variations occurring in each of the three paths as well as the source. For this section, multiple time simulations are performed exercising each of the three operating categories within the TCS. These simulations assess the ability of the sliding mode controllers to cause the interconnected TCS subsystems to operate in their local sliding modes in the face of external and interaction disturbances, plant uncertainties, and nonlinearities seen in the TCS. The next three sections present the results of exercising the three operating categories within the TCS.

### A. Interaction Disturbances

The category of interaction disturbances within the TCS is the first of three operating conditions discussed. Interaction disturbances are caused by internal flow set-point changes in each of the three flow paths. As a result of these flow set-point changes (also called defined flow profiles), each path's flow controller modulates its flow control valve to track defined flow profiles. This causes the driving source pressure to deviate from its set-point—an effect referred to as an interaction disturbance. This section simulates the sliding mode controller's ability to track defined flow profiles in each of the three paths.

The defined flow profiles consist of a series of randomly spaced ramps with time-varying slopes and magnitudes. The control system objective is to achieve decoupled tracking performance of these flow profiles in the face of the interaction disturbances. The simulation results of paths 1, 2, and 3 to the defined flow profiles is shown in figures 12, 13, and 14, respectively. The dotted lines represent the defined flow profiles and the solid lines represent the actual flow tracking responses. The flow errors remain less than 0.1 lbm/h for all three paths when the system is operating in its sliding mode. For a few short time intervals (less than 4 s in duration), lack of control resources causes sliding mode to be destroyed; however, the system error remains less than 8.0 lbm/h for these short intervals.

The flow response through path 4 is shown in figure 15. This flow is uncontrolled and is included to demonstrate the effect of interaction disturbances caused by the flow profile changes in the other three paths. These interaction disturbances are dynamically coupled through a common pressure source. Ideally, the common pressure source is controlled to 10 lb/in<sup>2</sup>; however, for this simulation, the pressure controller is degraded to simulate a worst-case scenario for controlling defined flow profiles in the respective parallel paths. Shown in figure 16, the source pressure deviates from its desired set-point by over 60 percent, thereby providing a tremendous interaction disturbance within the TCS.

The sliding mode controller utilizes high-speed switching of the control input to realize tracking performance. The plots shown in figure 17 are of the high-speed switched control inputs to the flow control valve actuators in paths 1, 2, and 3. The TCS flow control valve actuator is typical of most control actuators in that it is low pass in nature. Consequently, the TCS flow control valve actuator responds to

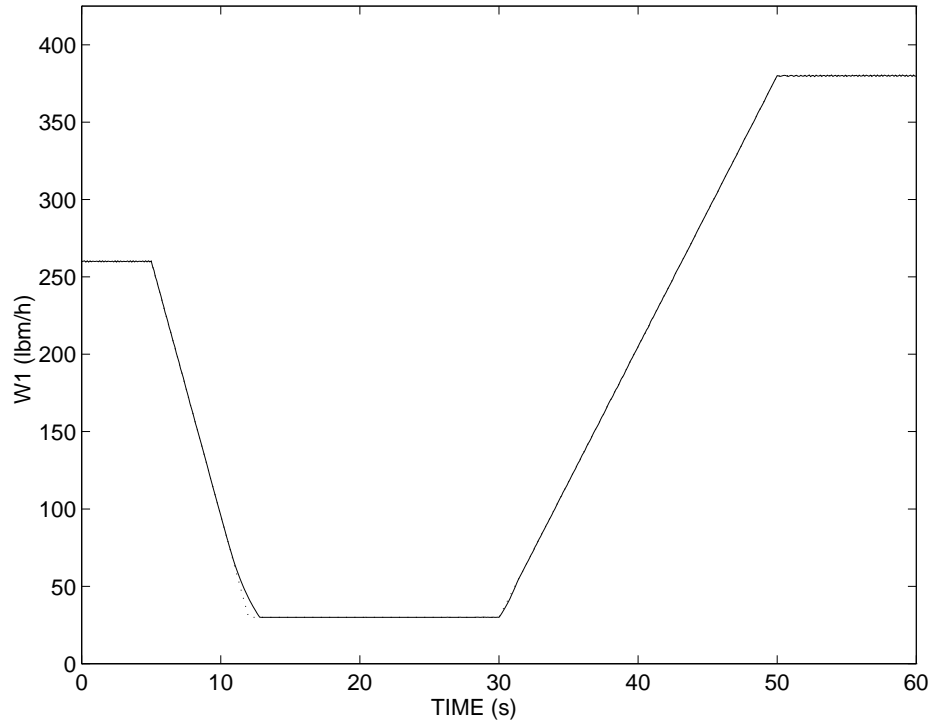


Figure 12. Flow response in path 1 with interaction disturbance.

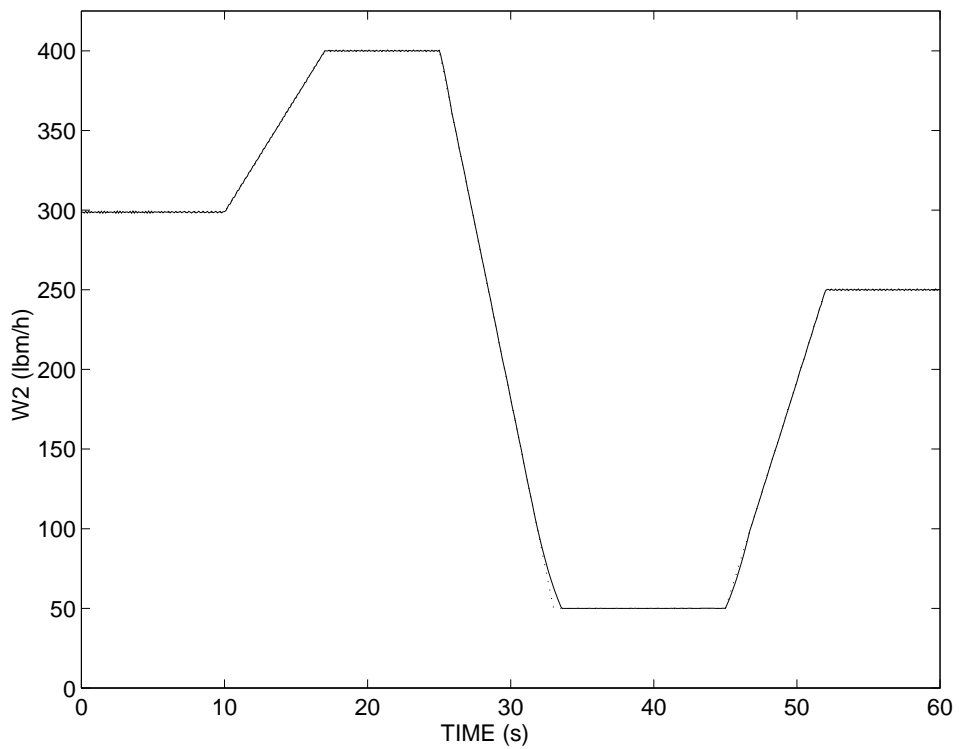


Figure 13. Flow response in path 2 with interaction disturbance.

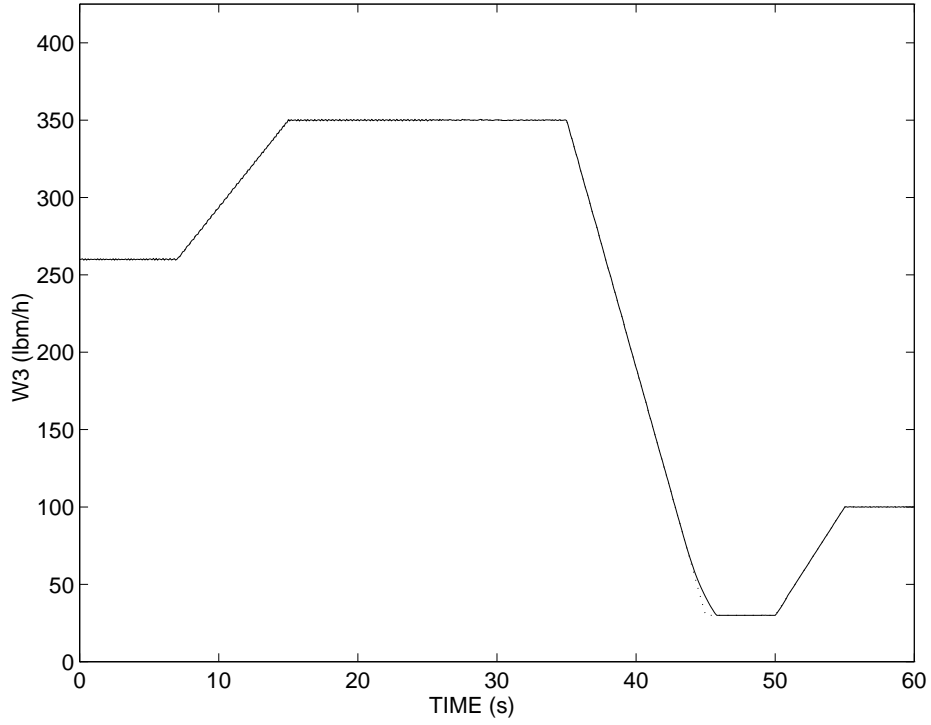


Figure 14. Flow response in path 3 with interaction disturbance.

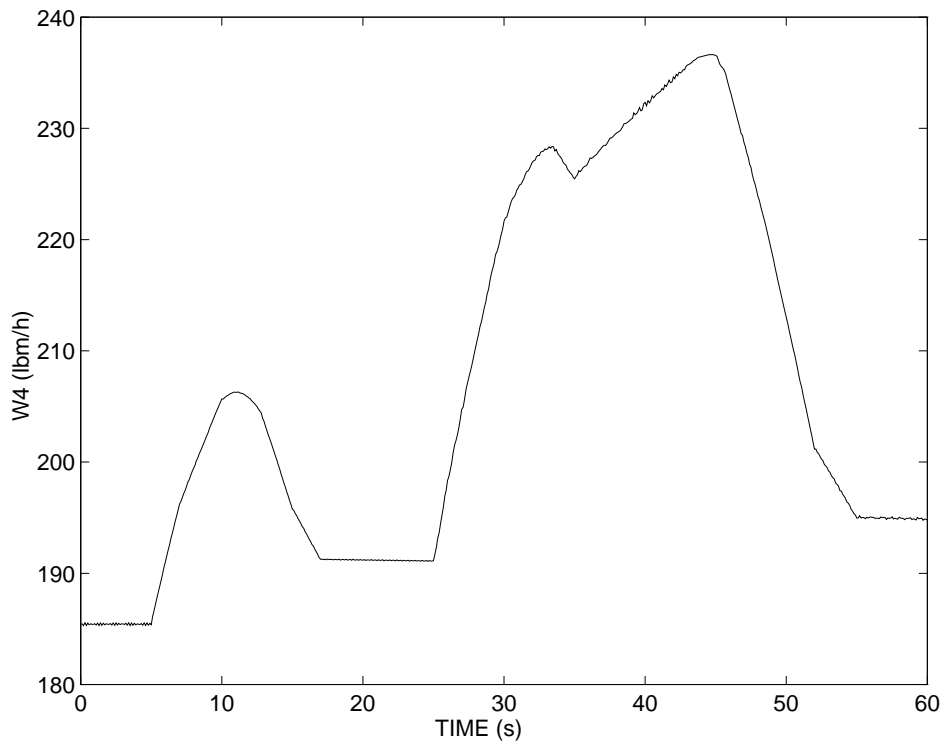


Figure 15. Flow response in path 4 with interaction disturbance.

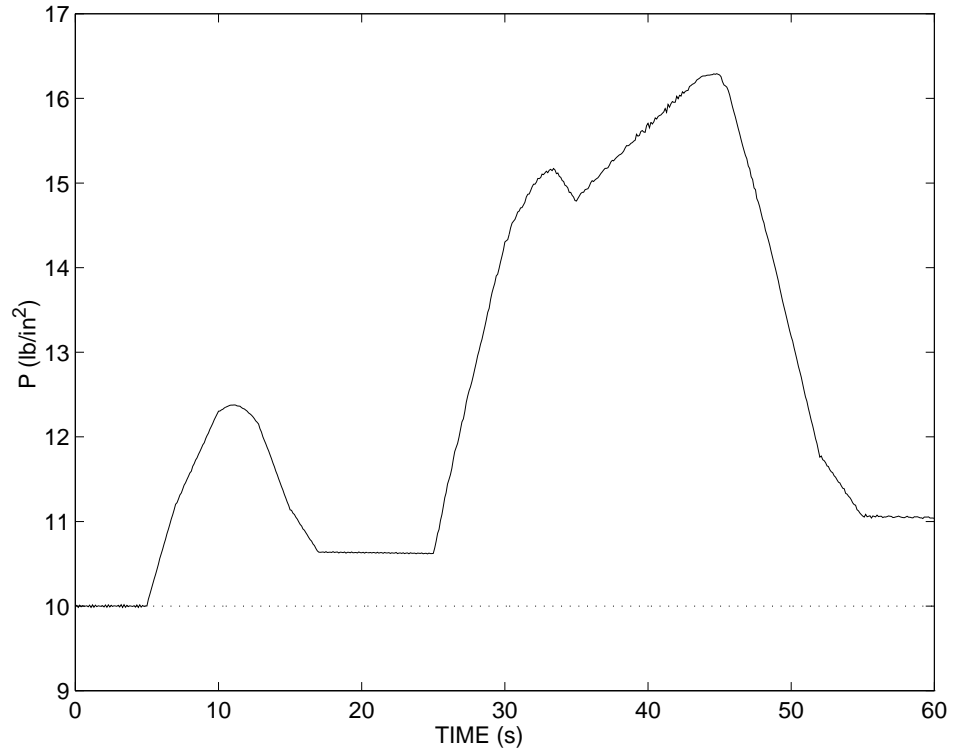


Figure 16. Pressure response with interaction disturbance.

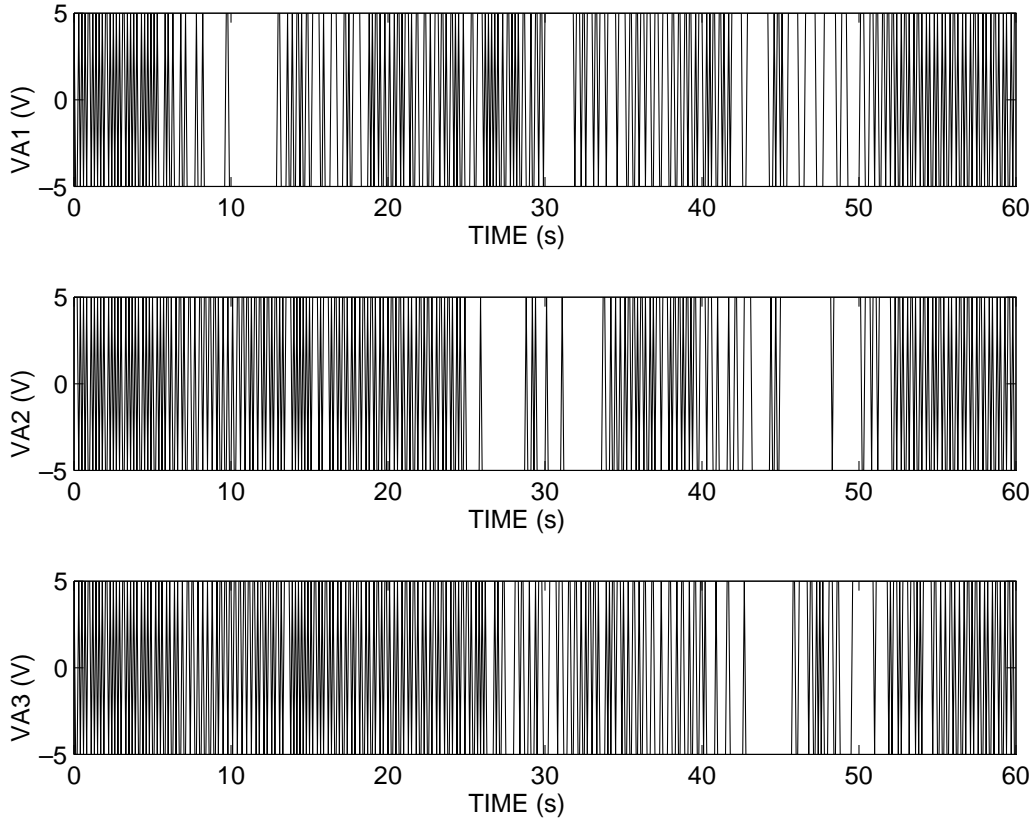


Figure 17. Control input to each path with interaction disturbance.

the moving average rather than to every back and forth motion of the high-frequency switched sliding mode control inputs. The plots in figure 18 show the moving averages of the control inputs in paths 1, 2, and 3. The TCS valve actuator responses to these control inputs are shown in figure 19. It is observed that the valve responses are very smooth and exhibit almost no chatter to the high-speed switched control inputs.

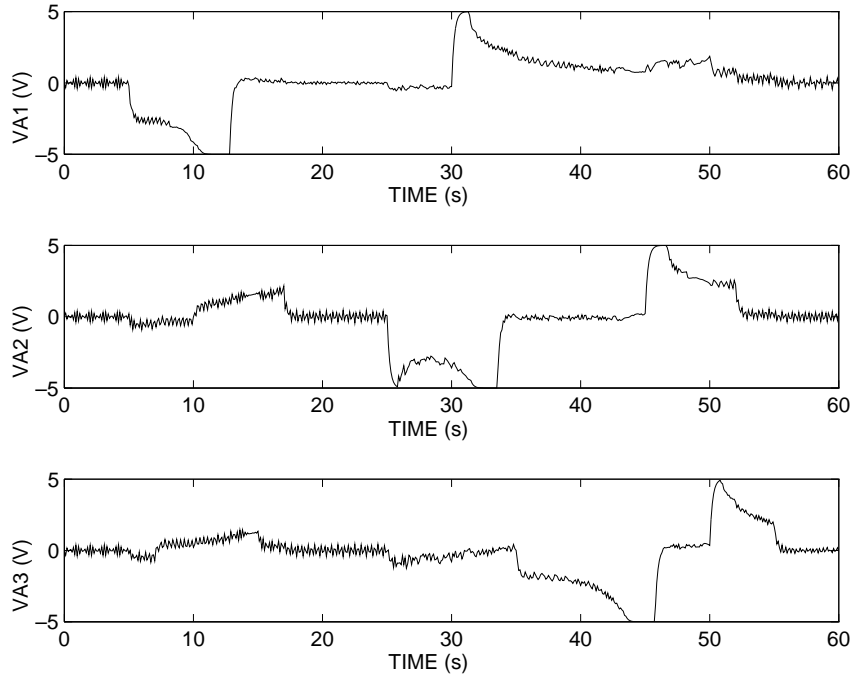


Figure 18. Moving averages of control inputs with interaction disturbance.

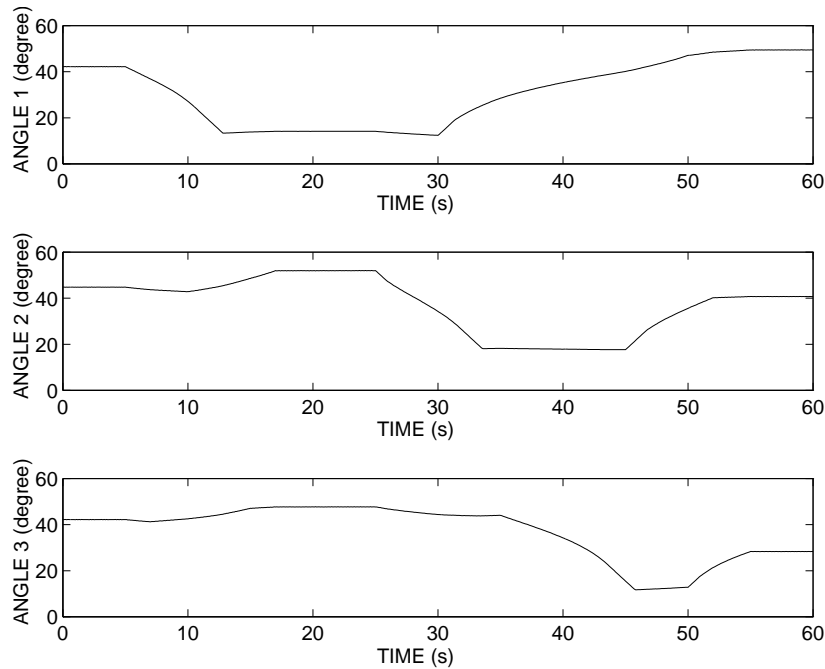


Figure 19. Valve actuator response with interaction disturbance.

Shown in figure 18, the moving averages of the control inputs are pegged at the maximum of +5 V and the minimum of -5 V for short time intervals during the simulation. Within these intervals, the system is operating outside of its sliding mode; as a result, the system exhibits imperfect set-point tracking. However, these time intervals are so short and the tracking errors so small that the composite performance is more than acceptable for the TCS.

In summary, the sliding mode controllers are shown to be robust to the interaction disturbances caused by the set-point changes within the TCS. The next section will discuss the results of external disturbances to the TCS.

## B. External Disturbances

The category of external disturbances within the TCS is the second of the three operating conditions discussed. External disturbances are defined as unwanted torques to the TCS control valve actuators and originate from a variety of sources such as power delivery spikes, electromagnetic interference, and flow turbulence variations. Such torques are unmeasured and can greatly affect the performance of the TCS. It is important to show that the sliding mode controllers are robust to unwanted disturbance torques seen in the physical system.

For this simulation, disturbance torques are injected into the TCS through so-called normalized control forces that are added to the sliding mode control input functions. In reality, these disturbance torques occur internal to the valve actuators; however, they are normalized and applied at the control inputs for simulation purposes. Shown in the previous section, the sliding mode control input functions consist of a high-frequency signal that is switched between a maximum value of +5 V and a minimum value of -5 V. This control input signal can potentially be modified by the addition of an external input signal, which serves to simulate the effect of a disturbance torque. This effect is accomplished by injecting the signal shown in figure 20 to the second high-frequency control input signal shown in figure 17. This external signal causes the actual control input signal to deviate by 30 percent from the nominal control input signal, shown in figures 17 and 18. A time simulation is used to assess the performance of the sliding mode controllers to this potentially devastating disturbance torque.

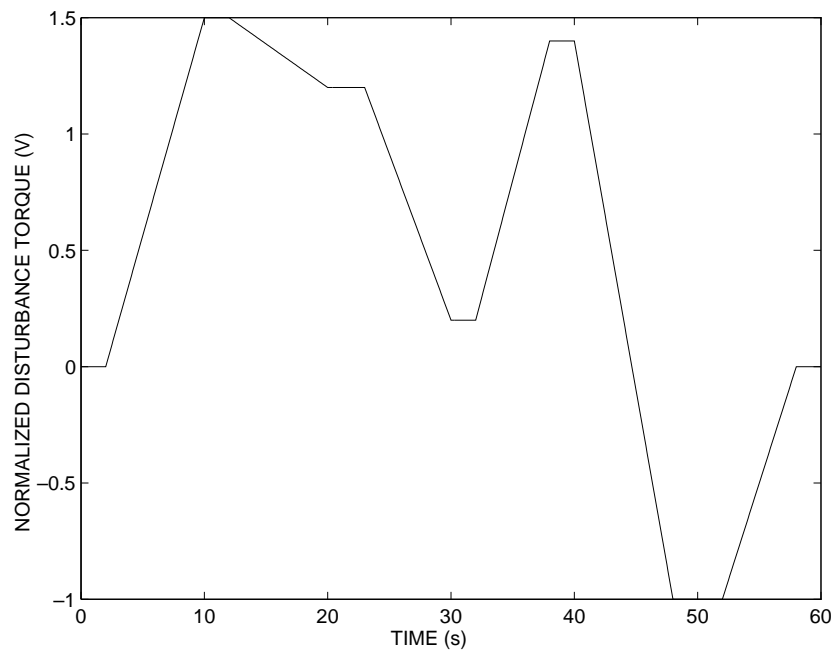


Figure 20. Normalized disturbance torque function.

The simulation results of paths 1, 2, and 3 to the injected disturbance torque are shown in figures 21, 22, and 23, respectively. The dotted lines represent the defined flow profiles and the solid lines represent the actual flow tracking responses. The flow errors remain less than 0.1 lbm/h for all three paths when the system is operating in its sliding mode. For a few short time intervals (less than 4 s in duration), lack of control resources causes sliding mode to be destroyed; however, the system error remains less than 10.0 lbm/h for these short intervals.

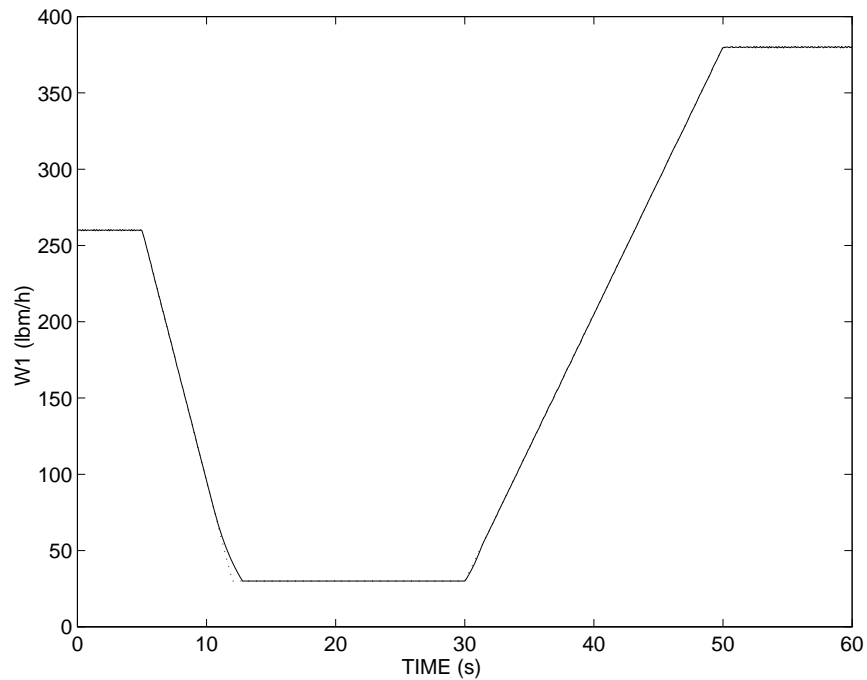


Figure 21. Flow response in path 1 with external disturbance.

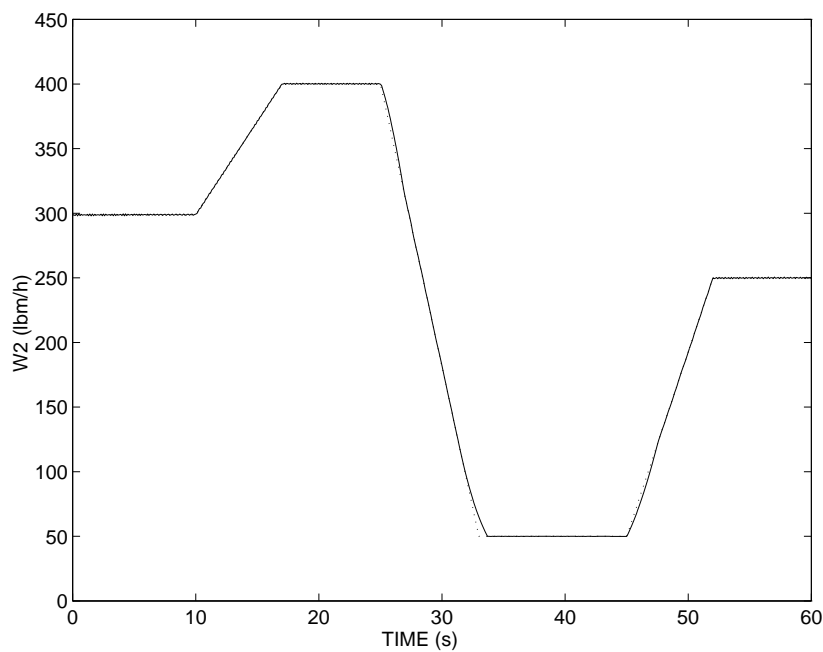


Figure 22. Flow response in path 2 with external disturbance.

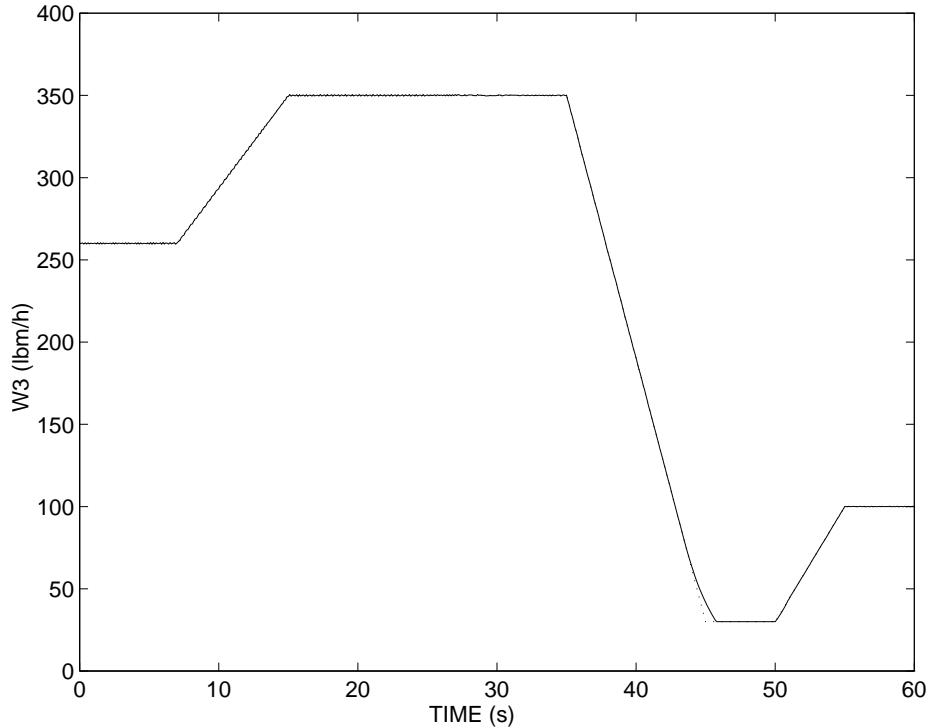


Figure 23. Flow response in path 3 with external disturbance.

In summary, the TCS sliding mode controllers are shown to be robust to the interaction disturbances caused by the set-point changes and to the external disturbance torques applied to the actuator valves. The next section discusses the results of plant uncertainties within the TCS model.

### C. Plant Uncertainties

The category of plant uncertainties within the TCS is the last of the three operating conditions discussed. Plant uncertainties are present because of the difficulty in accurately modeling the system under investigation. That is, model coefficients usually deviate from their actual values due to measurement inaccuracies, imprecise measurement instruments, incorrect measurement procedures, and measurement constraints, where it is too costly or impractical to measure a parameter. Since the sliding mode controllers are designed using a mathematical model, it is important to design the controllers robust to potential plant uncertainties seen in the model of the TCS system. The next three subsections discuss parameter uncertainties in the pressure source, flow path, and flow actuator, respectively.

1. **Pressure Source.** The pressure source's resistance  $R_S$  to flow, defined by equation (37), is an important parameter used in the determination of the sliding mode controllers designed to achieve set-point tracking performance. For this simulation, the source resistance parameter is varied by plus and minus 20 percent to verify the robustness of each path's sliding mode controller. A change of  $-20$  percent results in no noticeable increases in flow tracking errors in all three paths over previously presented plots. A change of  $+20$  percent results in no noticeable increases in flow tracking errors in paths 1 and 3 over identical simulation runs presented in section VI.B of this report; however, the resulting flow tracking error in path 2 increases slightly in two short time intervals as shown in figure 24. Nevertheless, in the presence of this parameter uncertainty, the resulting set-point tracking performance is very acceptable.

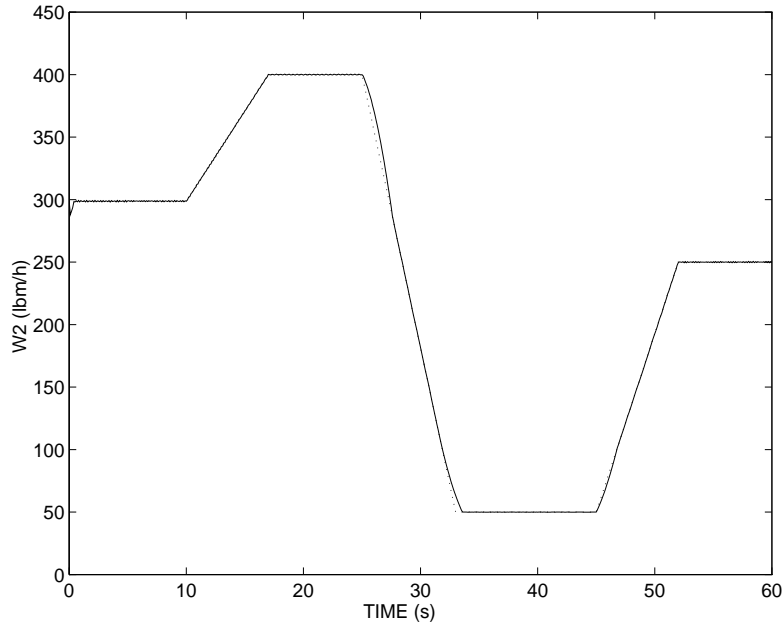


Figure 24. Flow response in path 2 with source uncertainty.

2. Flow Path. The flow path inertia  $L_1$  in path 1, defined by equation (20), is another important parameter used in the determination of the sliding mode controllers designed to achieve set-point tracking performance. For this simulation, the flow path inertia in path 1 is varied by  $\pm 50$  percent to verify the robustness of the sliding mode controller in path 1. A change of  $+50$  percent results in no noticeable increases in flow tracking errors in path 1 over similar runs shown in section VI.A of this report. A change of  $-50$  percent results in a short deviation at 28 s as shown in figure 25. In summary, in the presence of this parameter uncertainty, the resulting set-point tracking performance is very acceptable.

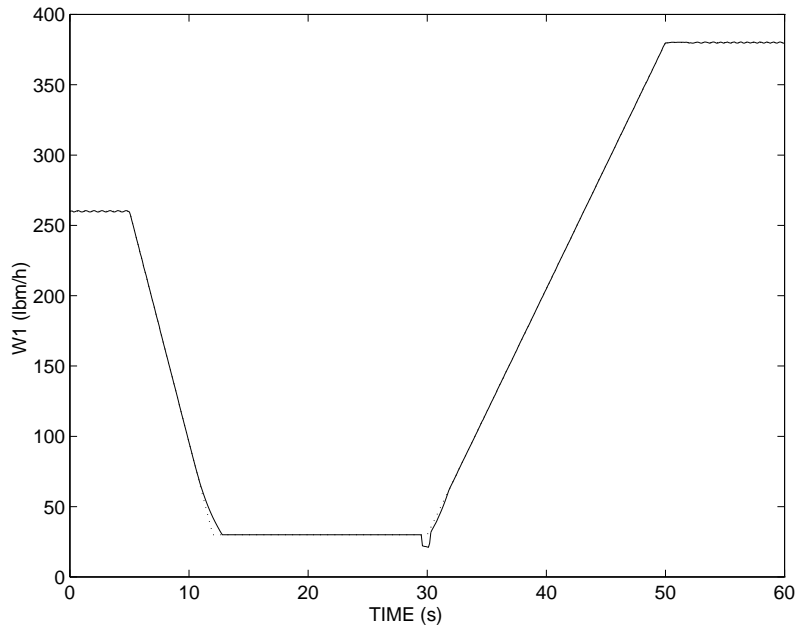


Figure 25. Flow response in path 2 with flow path uncertainty.

3. **Flow Actuator.** The flow control actuator gain  $K_v$  in path 2, defined by equation (36), is the final parameter that is modified to verify the robustness of the sliding mode controllers designed to achieve set-point tracking performance. For this simulation, the actuator gain in path 2 is varied by  $\pm 20$  percent. A change of +20 percent results in no noticeable increases in flow tracking errors in path 2 over similar runs shown in section VI.A of this report. A change of -20 percent results in slight flow tracking error increases in two short time intervals as shown in figure 26. Again, in the presence of a parameter uncertainty, the resulting set-point tracking performance is more than acceptable for this problem.

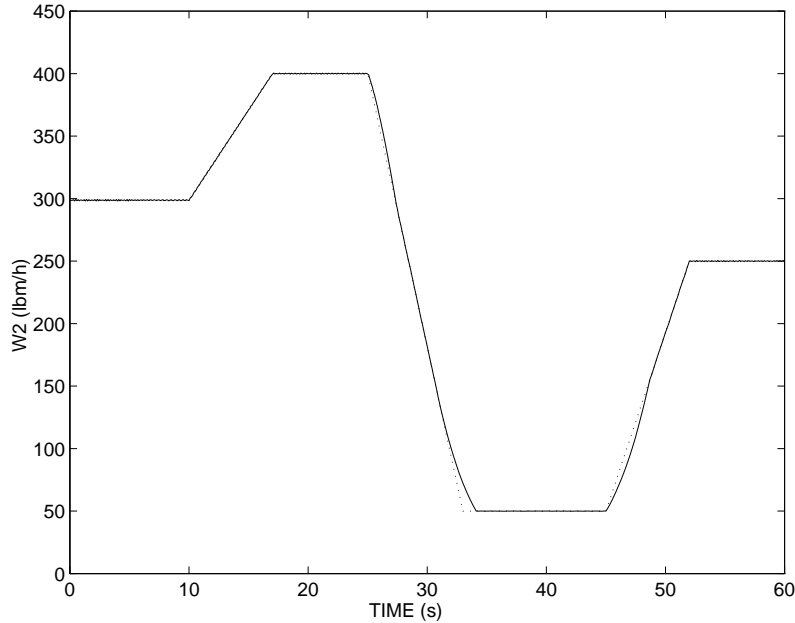


Figure 26. Flow response in path 1 with flow actuator uncertainty.

#### D. Smoothing Function

The simulation results presented thus far in section VI are produced with the implementation of the discontinuous sliding mode controller shown in equation (140). This section addresses the simulation results with the implementation of the smoothed sliding mode controller represented by equations (147) and (148). In general, the tradeoff of using the smoothed sliding mode controller rather than the discontinuous sliding mode controller is the loss of robustness to disturbances and parameter variations and the loss of tracking precision versus the reduction of output chattering and power usage. An analysis of this tradeoff is presented in the following.

The first simulation category addressed is that of interaction disturbances. Interaction disturbances are caused by internal flow set-point changes in each of the three flow paths. Using the discontinuous sliding mode controller, the simulation results of paths 1, 2, and 3 to defined set-point changes are shown in figures 12, 13, and 14, respectively. The dotted lines represent the set-point profiles and the solid lines represent the actual flow tracking responses. From these plots, chattering does not seem present in the output responses; however, magnification of the ordinate scale between 0 and 10 s shows that small amplitude output chattering is indeed present. This chattering is shown in figure 27.

Using the smoothed sliding mode controller, the simulation results of paths 1, 2, and 3 to defined set-point changes seem equivalent to those shown in figures 12, 13, and 14 for the discontinuous sliding mode controller; however, magnification of the ordinate scale between 0 and 10 s shows that no chattering is present, as shown in figure 28. Moreover, tracking precision results are not compromised by the

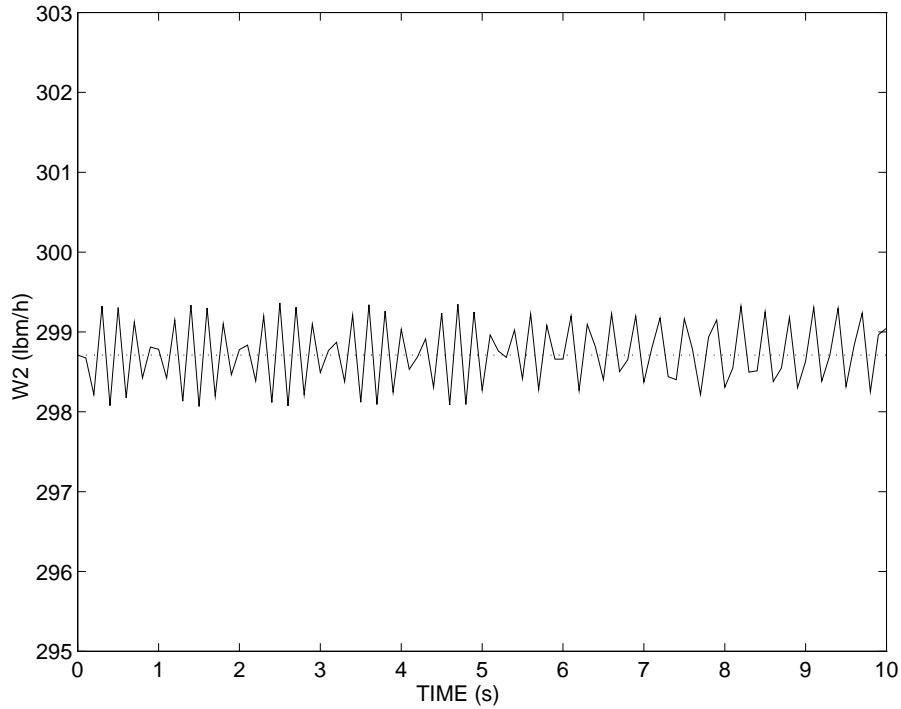


Figure 27. Flow response in path 2 with discontinuous controller.

implementation of this smoothed sliding mode controller. The control input signal generated from using the smoothed sliding mode controller to track the flow in path 2 is shown in figure 29. This smooth signal is contrasted with the high-frequency switched control input signal for path 2 shown in figure 17; it is compared with the filtered control input signal for path 2 shown in figure 18. Implementation of the smoothed sliding mode controller not only smoothes the output response, but also saves control power without noticeable loss of performance.

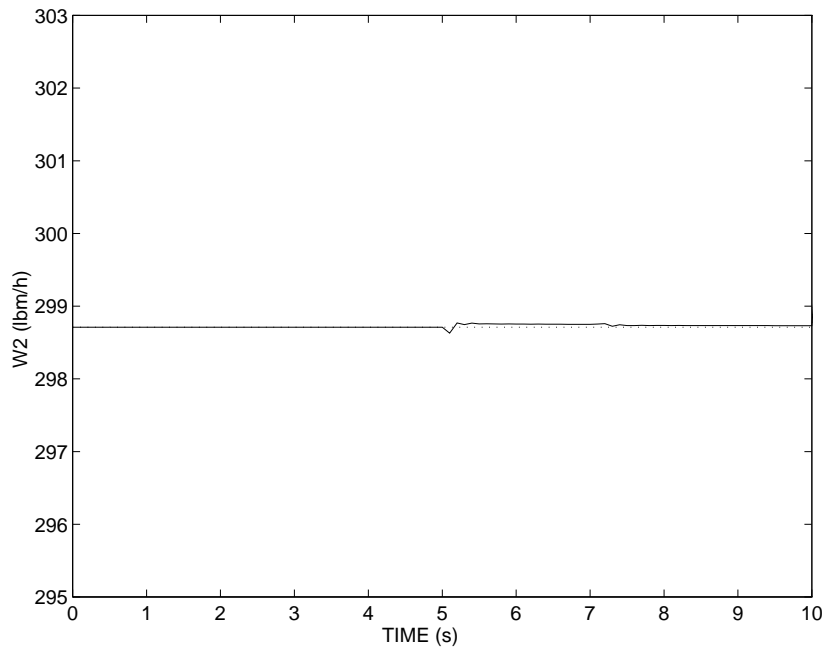


Figure 28. Flow response in path 2 with smoothing controller.

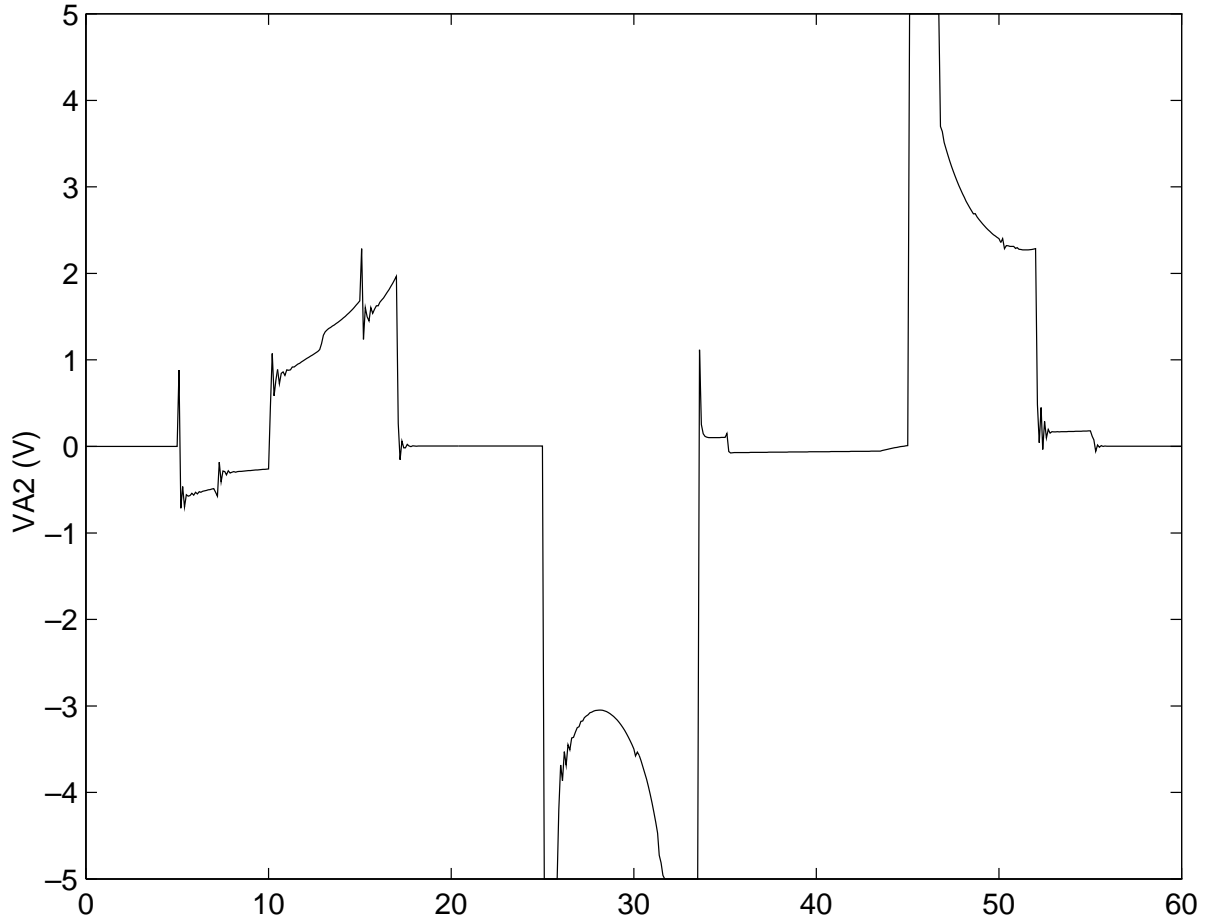


Figure 29. Smoothing controller input to path 2.

The simulation categories of external disturbances and plant uncertainties are also exercised with the implementation of the smoothed sliding mode controller. The output tracking results are shown to be very similar to those results obtained from the discontinuous sliding mode controller presented in the previous two sections. The only noticeable difference in performance is the reduction of output chattering and power usage in both simulation categories. The implementation of the smoothed sliding mode controller maintains robustness to disturbances and parameter variations without loss of tracking precision.

### E. Summary

This section presented the results of continuous time simulations of the TCS using both the discontinuous and smoothing sliding mode controllers subjected to the three defined operating conditions. Exercising the three operating conditions confirms the ability of both sliding mode controllers to perform decoupled set-point tracking in the presence of simultaneous flow set-point changes, normalized disturbance torques, parameter variations, as well as inherent nonlinearities of the system. The smoothing sliding mode controller exhibits increased performance in reducing output chattering and power usage. The next section will discuss the comparison of sliding mode controller performance to that of the popular proportional-plus-integral-plus-derivative controller.

## VII. COMPARISON RESULTS

This section will compare the simulation results of the TCS sliding mode controller against that of the TCS flight controller. The TCS flight controller is in the PID family of controllers that are probably the most commonly used controllers in feedback control systems. Comparison of sliding mode control with traditional methods such as PID control amplifies the uniqueness of sliding mode control's ability to provide accurate, robust, decoupled tracking for the class of nonlinear time-varying multivariable systems in the presence of disturbances and parameter variations.

The TCS flight controller is fine-tuned to provide the best transient and steady-state response of the system over its full operating range. The design of the flight controller involves linearizing and simulating the system at multiple operating points to verify and fine-tune stability and performance, respectively. Moreover, the controller gains are chosen to operate the controller in a linear fashion. The resulting controller, with  $e_i(t)$  the controller input and  $u_i(t)$  the output, is defined by the equation

$$u_i(t) = 0.05e_i(t) + 1.0 \frac{d}{dt} e_i(t) . \quad (149)$$

This controller is classified as a PD controller; however, when coupled with the type 1 system plant, this controller performs as a PI controller. This is shown as

$$u_i(t) = 1.00e_i(t) + 0.05 \int_0^t e_i(\tau) d\tau . \quad (150)$$

This PI controller has a pole at the origin and a zero at  $-0.05$ . Since the pole is nearer to the origin than is the zero, the controller is phase-lag and the controller adds a negative angle to the angle criterion of the root locus. Hence, this controller is used to improve the steady-state response of the system.

A comparison of the TCS flight and sliding mode controllers is performed using the MARSYAS computer simulation of the TCS. The objective of this comparison is to verify the ability of the controllers to achieve accurate, robust, decoupled flow tracking performance in the presence of interaction and external disturbances. It is again noted that the flow path dynamics are dynamically coupled through a common nonlinear pressure source. This source is normally controlled in a feedback loop to a constant 10 lb/in<sup>2</sup>; however, for this simulation, the pressure controller is considered poorly designed or operating in a degraded mode to simulate a worst-case scenario for coupling between the respective flow paths.

For the simulation of the system using the sliding mode controller, the smoothing control function represented by equations (147) and (148) is implemented to smooth-out the response of the system operating in sliding mode. The first section presents the comparison results from the effect of interaction disturbances on the two controllers.

### A. Interaction Disturbance

The first comparison case for the two controllers involves generating a nominal time-varying flow profile in path 1 and a constant profile in paths 2 and 3. This simulates an interaction disturbance within the TCS system. In this case, decoupled performance is indicated by perfect tracking of the flow profiles in paths 1, 2, and 3.

The flight controller defined in equation (149) is implemented in each of the three flow paths. Simulation results to defined flow profiles in paths 1, 2, and 3 are shown in figures 30, 31, and 32, respectively. After which, the sliding mode controller illustrated in figure 11 with the smoothing function is implemented in each of the three flow paths. Simulation results to defined flow profiles in paths

1, 2, and 3 are shown in figures 33, 34, and 35, respectively. The dotted lines represent the defined flow profiles and the solid lines represent the actual flow tracking responses.

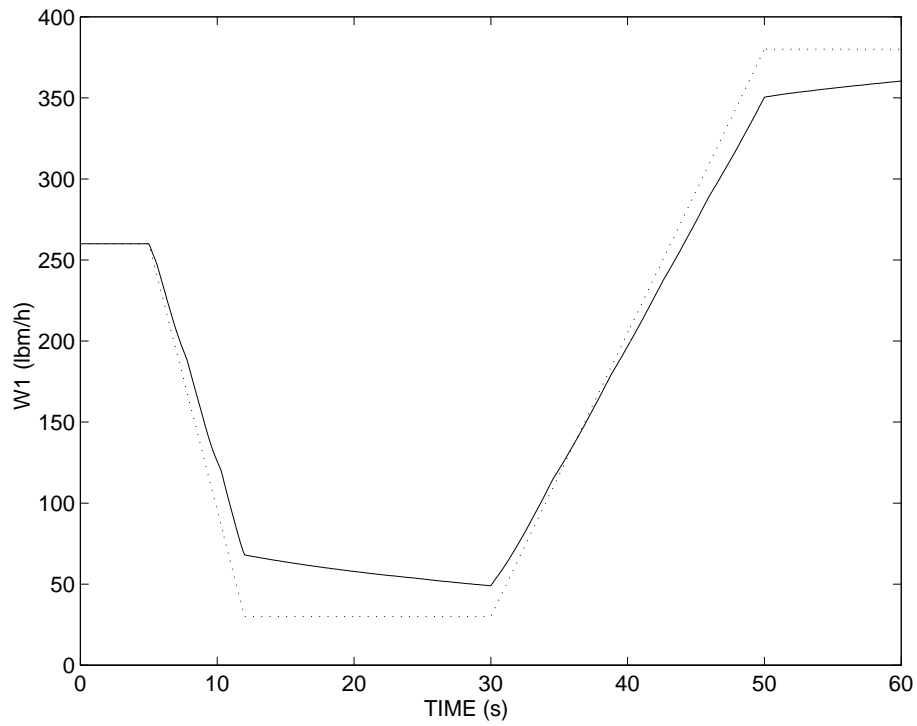


Figure 30. Flow response in path 1 for flight controller with interaction disturbance.

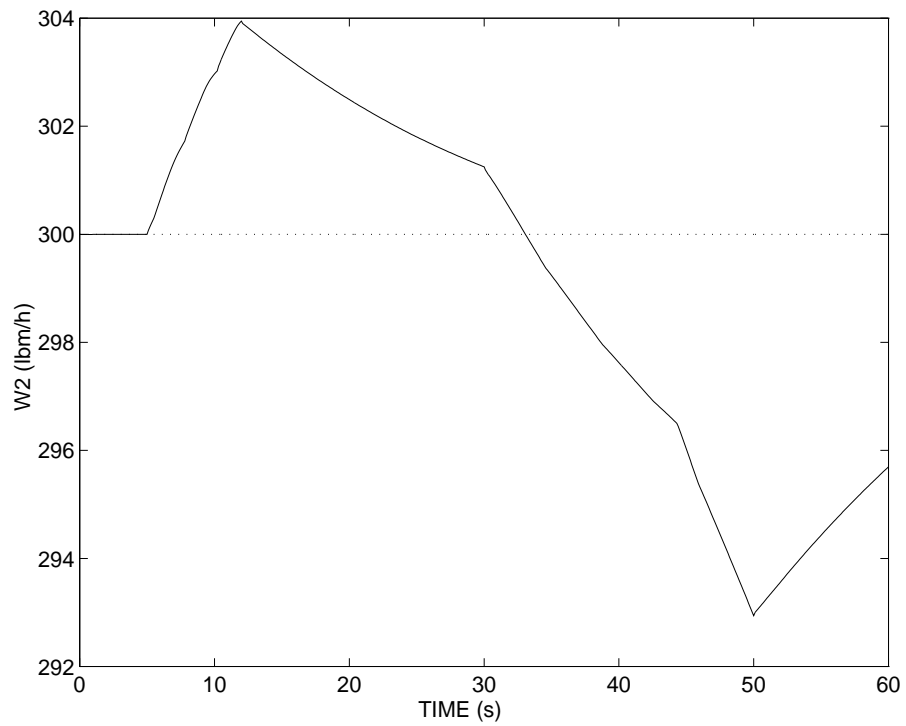


Figure 31. Flow response in path 2 for flight controller with interaction disturbance.

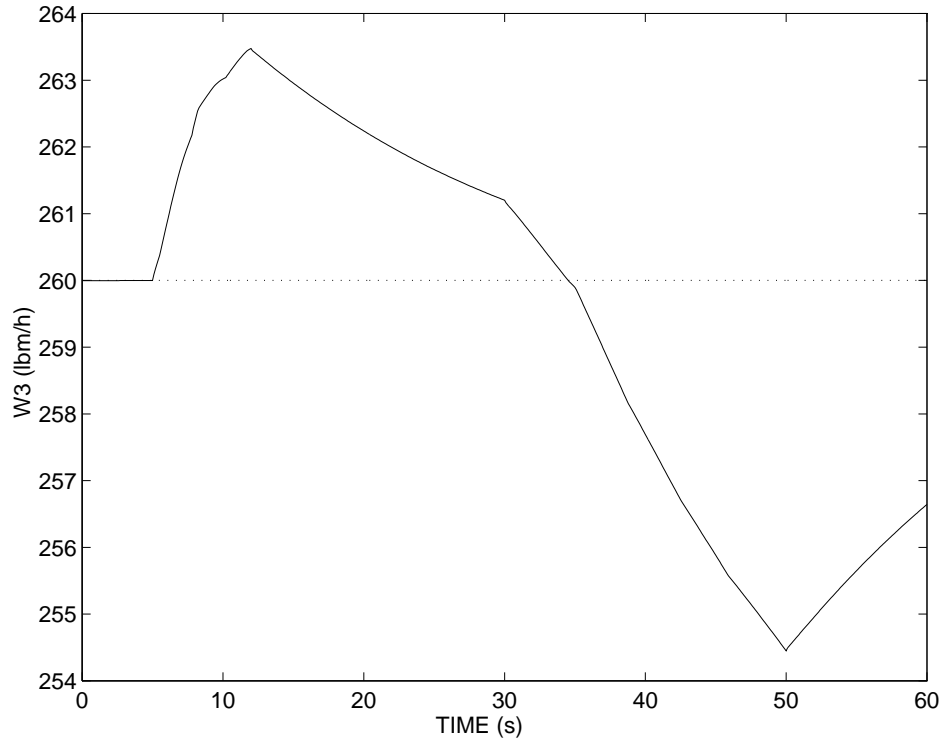


Figure 32. Flow response in path 3 for flight controller with interaction disturbance.

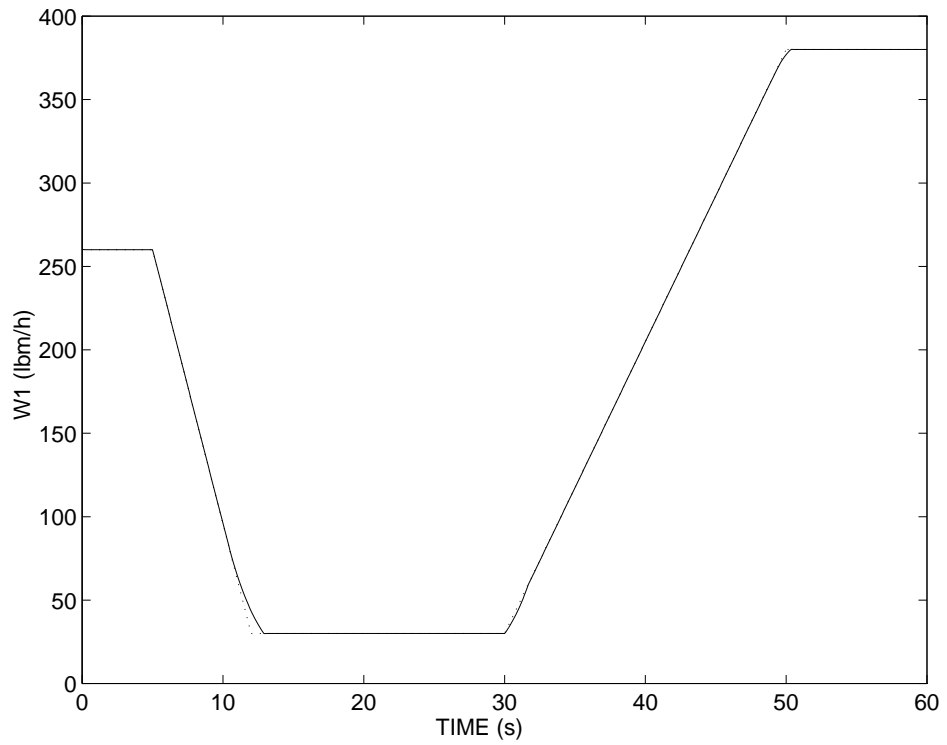


Figure 33. Flow response in path 1 for sliding controller with interaction disturbance.

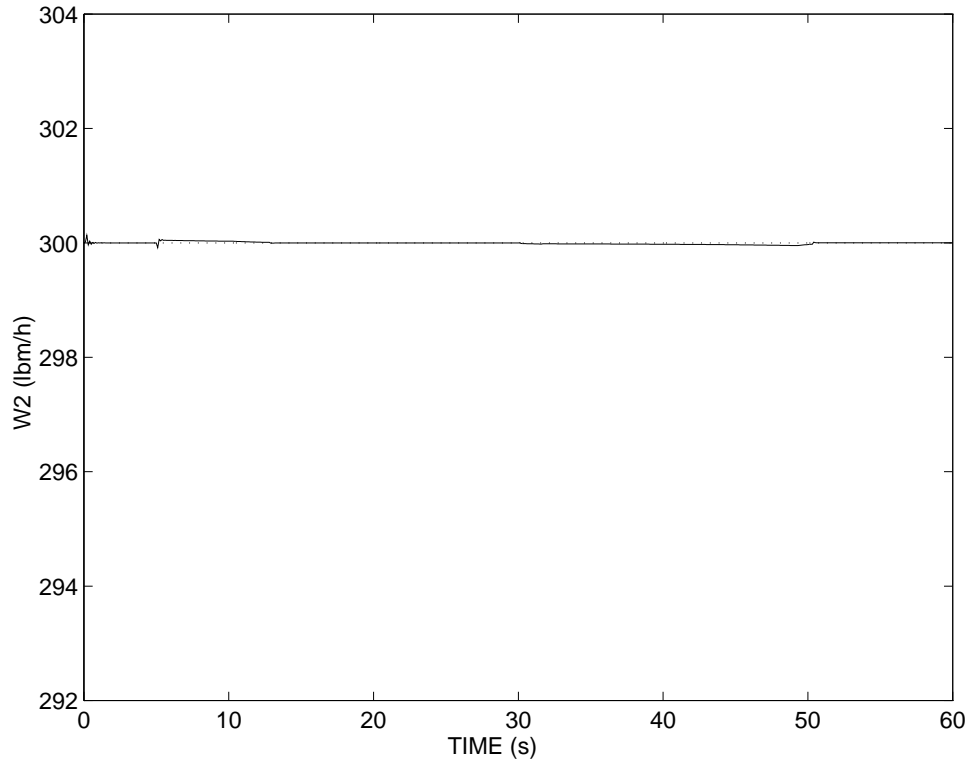


Figure 34. Flow response in path 2 for sliding controller with interaction disturbance.

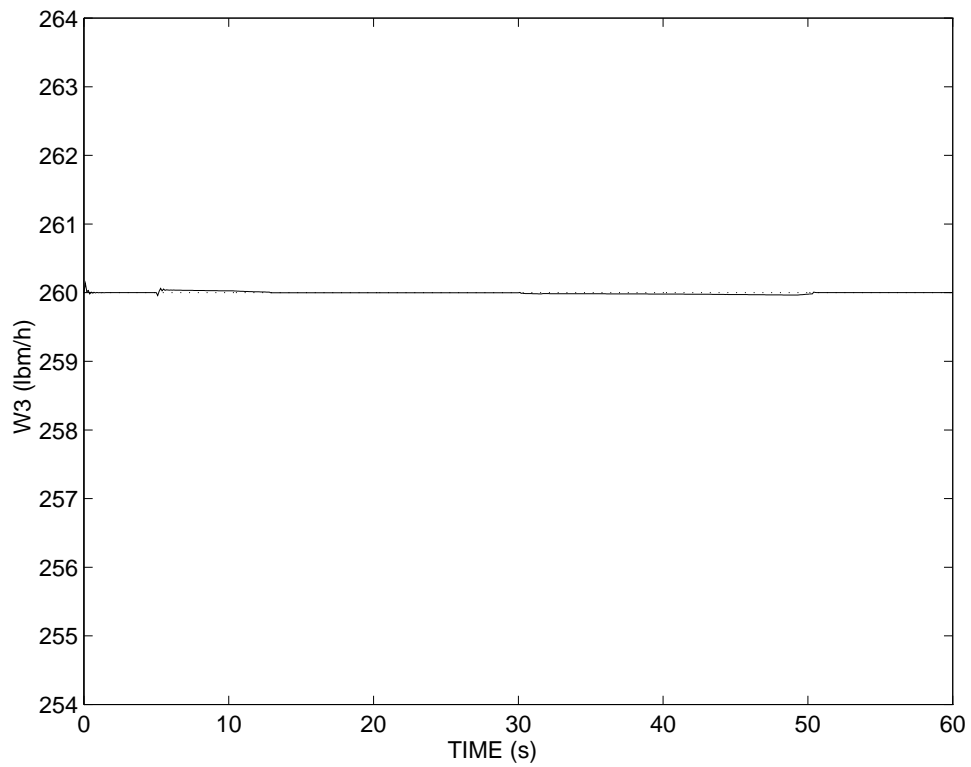


Figure 35. Flow response in path 3 for sliding controller with interaction disturbance.

Comparing the tracking performance of both controllers in path 1, it is obvious that the tracking provided by the flight controller shown in figure 30 is not as accurate as that of the sliding mode controller shown in figure 33. It is also obvious from figures 31 and 32 that the flight controller does not provide accurate decoupled tracking compared with that shown in figures 34 and 35 for the sliding mode controller. The second section discusses the effect of external disturbances on the two controllers.

### B. External Disturbance

The second comparison case involves injecting an external disturbance torque into the TCS through so-called normalized control forces that are added to the two controller input signals. In reality, these disturbance torques occur internal to the valve actuators; however, they are normalized and applied at the control inputs for simulation purposes. This effect is accomplished by adding the signal shown in figure 20 to the controller input signals in path 2. This external disturbance torque causes the actual control signal to deviate 30 percent from the nominal control input signal.

The simulation results using the flight controller to track defined flow profiles in paths 1, 2, and 3 are shown in figures 36, 37, and 38, respectively. The simulation results using the sliding mode controller to track defined flow profiles in paths 1, 2, and 3 are identical to the ones shown in figures 33, 34, and 35, respectively; hence, these results are not repeated in this section. As in the last section, the dotted lines represent the defined flow profiles and the solid lines represent the actual flow tracking responses.

From figures 36, 37, and 38, it is obvious that the flight controller displays very poor performance in the face of external disturbance torques. The resulting flows deviate as much as 30 percent from their desired flow profiles. The system pressure shown in figure 39 drops over 60 percent from its nominal set-point due to the effect of these disturbances. As seen from the flight controller performance, the strong coupling of the respective paths through the nonlinear pump source is a potential disastrous combination when subjected to disturbance torques of this magnitude.

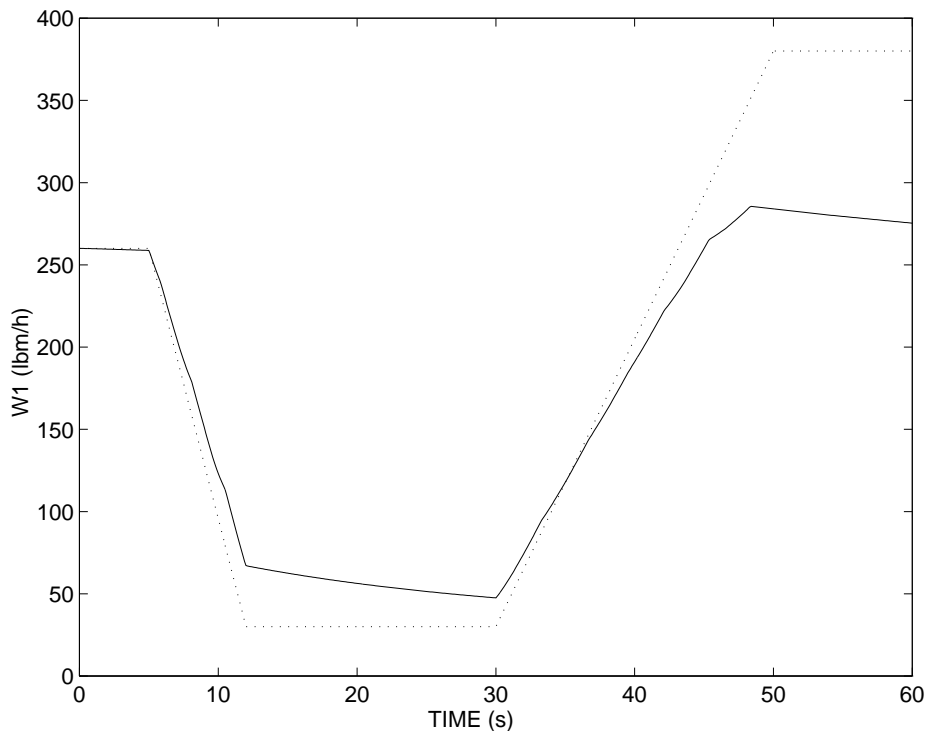


Figure 36. Flow response in path 1 for flight controller with external disturbance.

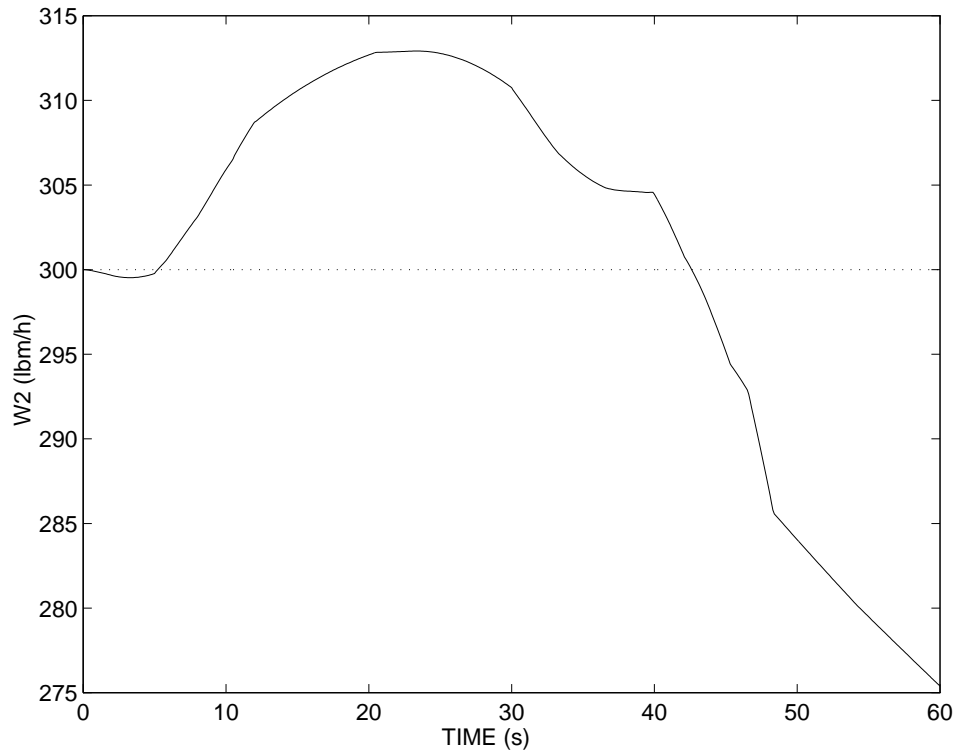


Figure 37. Flow response in path 2 for flight controller with external disturbance.

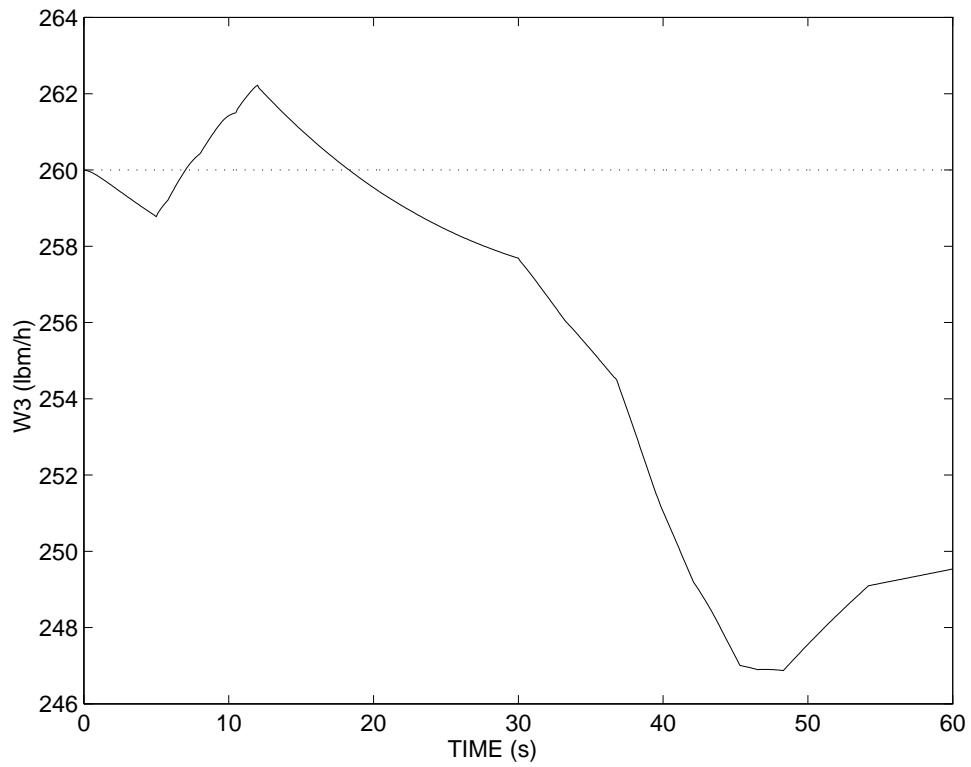


Figure 38. Flow response in path 3 for flight controller with external disturbance.

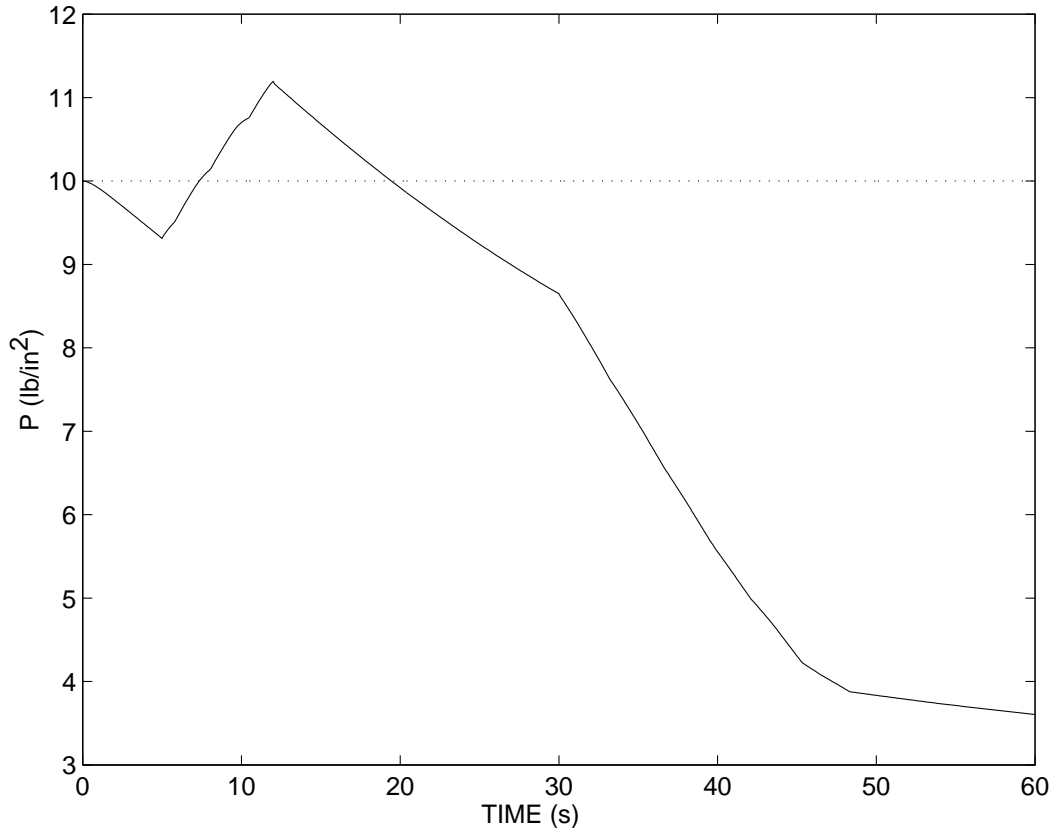


Figure 39. System pressure drop for flight controller with external disturbance.

From figures 33, 34, 35, it is obvious that the sliding mode controller displays very good performance in the face of external disturbance torques. The resulting flows display perfect decoupled set-point tracking performance in the presence of the large disturbance torques, time-varying profiles, and system nonlinearities.

### C. Summary

This section presented the results of the sliding mode controller and flight controller, both applied to the TCS system. It is clear that the sliding mode controller excels at accurate robust decoupled tracking in the presence of internal and external disturbances compared with that of the PID flight controller. The sliding mode controller achieves this performance over the full operating range of the TCS and without having to linearize the system at various operating points. This section showed that application of sliding mode control techniques to MIMO nonlinear systems such as the TCS significantly improves the performance of the system over traditional PID controllers.

## VIII. CONCLUSION

This report formulates the TCS control problem and solves the problem using the methods of sliding mode control. The problem solving process begins with the development of a TCS mathematical model using first principle laws of continuity of mass and momentum. The resulting model is classified as a nonlinear MIMO system with partially known parameters. The basics of sliding mode control, a subclass of VSS control, are reviewed through a phase plane illustration of an unstable second-order

system. The theory of sliding mode control is presented and applied to a n-dimensional nonlinear MIMO system. This theory is presented in three steps: (1) transformation of the system to the normal form to obtain the vector relative degree and to analyze the stability of the internal dynamics; (2) synthesis of the sliding surfaces upon which the output motion is restricted; and (3) development of the control functions that force the system to move to the sliding surface and to maintain the sliding surface for all subsequent time. Some useful techniques are borrowed from the method of feedback linearization in the presentation of the sliding mode control theory. The conclusions which are drawn from this work are separated into two groups: conclusions regarding the performance of sliding mode control, and conclusions regarding the advantages of sliding mode control. These conclusions are summarized in the following.

### **A. Performance**

The most significant conclusion from this work is the determination that sliding mode techniques provide precise, robust, and decoupled control of set-point flow tracking in the presence of interaction and external disturbances, parameter variations, and system nonlinearities. Sliding mode techniques provide this control over the full operating range of the system; moreover, this control is maintained with the system pump operating in a degraded mode. Excellent simulation performance of both the discontinuous and smoothing sliding mode controllers are demonstrated for the TCS system. The most striking demonstration of decoupled control is the ability of the controllers to maintain constant set-point profiles in two paths while tracking a rapidly changing set-point profile in the third path.

### **B. Advantages**

Sliding mode techniques have many distinct advantages over traditional linear and nonlinear methods for control. Realization of sliding mode control is very simple compared to many methods. For example, nonlinear methods such as feedback linearization control rely on accurate expensive real-time calculations for realizing the control function; whereas, realization of sliding mode techniques only requires that boundary conditions for such control functions be calculated a priori, not in real time. Sliding mode techniques are also robust compared to many methods. For example, the calculations required by feedback linearization, if off even a slight amount, can excite instabilities in the system. The control function boundary conditions for sliding mode techniques, however, assure system robustness throughout the operating range of the system.

Linear methods such as the popular PID controller require multiple linearizations, analyses, and simulations of the system to obtain and verify system robustness and performance. Sliding mode techniques are applied directly to the nonlinear system and robustness and stability are shown without multiple linearizations of the system. The linear PID controller is limited in its decoupled tracking robustness to external and interaction disturbances because of the slow nature of the integral action of the controller. Sliding mode techniques respond at a very high rate to maintain local performance in sliding mode; hence, maintaining perfect decoupled tracking robustness for the system.

## APPENDIX

### TCS MARSYAS Program

The following is the MARSYAS program that is used to numerically simulate and analyze the TCS mathematical and sliding mode controller models.

```
* global constant definitions $
CONSTANT: PI = 3.14159 $
* conversion constant (lbf-ft/sec**2-lbf) $
CONSTANT: GC = 32.174 $
* this is a pump map (lbf/hr versus psi) obtained at "rspeed" rpm. rspeed/pspeed scales-up the flow to
use a "rspeed" rmp map. (pspeed/rspeed)**2 scales-down the output pressure to a "pspeed" rmp map. $
DEFINE: PUMP (FLOW,PSPEED,RSPEED) = ((PSPEED/RSPEED)**2) *
      AF([
          0.0, 78.50,
          250.2, 78.50,
          500.5, 78.50,
          1001.0, 78.50,
          1251.2, 78.25,
          1501.5, 78.00,
          1751.7, 77.00,
          2002.0, 76.00,
          2252.2, 74.50,
          2502.5, 72.50,
          2752.7, 69.50,
          3003.0, 66.00,
          3253.2, 61.50,
          3503.5, 54.00,
          3603.6, 50.00 ], FABS(FLOW)*(RSPEED/PSPEED)) $

* main model definition $
* inputs:
* pset - system pressure set-point (psi) $
* pump\ref\speed - 100 pump speed (rpm) $
* wset1 - flow set-point profile for path 1 (lbf/hr) $
* wset2 - flow set-point profile for path 2 (lbf/hr) $
* wset3 - flow set-point profile for path 3 (lbf/hr) $
* outputs: * p - system pressure (psi) $
* w1 - flow response for path 1 (lbf/hr) $
* va1 - sliding mode control input to path 1 (volts) $
* va1\filtered - val filtered (volts) $
* av1 - control valve angle for path 1 (degrees) $
* w2 - flow response for path 2 (lbf/hr) $
* va2 - sliding mode control input to path 2 (volts) $
* va2\filtered - va2 filtered (volts) $
* av2 - control valve angle for path 2 (degrees) $
* w3 - flow response for path 3 (lbf/hr) $
* va3 - sliding mode control input to path 3 (volts) $
* va3\filtered - va3 filtered (volts) $
* av3 - control valve angle for path 3 (degrees) $
* w4 - flow response for path 4 (lbf/hr) $
MODEL: MAIN $
INPUTS: PSET,PUMP\REF\SPEED,WSET1,WSET2,WSET3 $
```

OUTPUTS: P \$  
OUTPUTS: WSET1,W1,VA1,VA1\FILTERED,AV1\$  
OUTPUTS: WSET2,W2,VA2,VA2\FILTERED,AV2 \$  
OUTPUTS: WSET3,W3,VA3,VA3\FILTERED,AV3 \$  
OUIPUTS: W4 \$

\* source model definition \$  
\* inputs: \$  
\* w# - flow responses in paths (lbm/hr) \$  
\* pump\ref\speed - 100 pump speed (rpm) \$  
\* pset - system pressure set-point (psi) \$  
\* outputs; \$  
ws - source flow response (lbm/hr) \$  
\* p - system pressure drop (psi) \$  
\* ps - high pressure of the source pump (psi) \$  
\* h5 - variable for calculating umax \$  
SUBMODEL: SOURCE;  
INPUTS: W1,W2,W3,W4,PUMP\REF\SPEED,PSET;  
OUTPUTS: WS,P,P5,H5 \$

\* flow path submodels \$  
\* inputs: \*  
p - system pressure (psi) \$  
\* va# - control valve inputs (volts) \$  
\* outputs \$  
\* w# - response of the flow in path # (lbm/hr) \$  
\* av# - angle of valve in path # (degrees) \$  
SUBMODEL: LEG1;  
IPUTS: P,VA1;  
OUTPUTS: W1,AV1 \$

SUBMODEL: LEG2;  
INPUTS: P,VA2;  
OUTPUTS: W2,AV2 \$

SUBMODEL: LEG3;  
INPUTS: P,VA3;  
OUTPUTS: W3,AV3 \$

SUBMODEL: STATIC;  
INPUTS: P ;  
OUTPUTS: W4 \$

\* sliding mode controller submodels \$  
\* inputs: \$  
\* w# - response of flow in path # (lbm/hr) \$  
\* wset# - flow set-point profile in path # (lbm/hr) \$  
\* outputs: \$  
\* va# - valve command in path # (volts) \$  
\* va#\filtered - filtered va# (volts) \$  
SUBMODEL: LEG1\CONT;  
INPUTS: W1,WSET1;  
OUTPUTS: VA1,VA1\FILTERED \$

SUBMODEL: LEG2\CONT;  
INPUTS: W2,WSET2;  
OUTPUTS: VA2,VA2\FILTERED \$

SUBMODEL: LEG3\CONT;  
INPUTS: W3,WSET3;  
OUTPUTS: VA3,VA3\FILTERED \$

\* existence condition submodels \$  
\* f## - variables to calculate umax \$  
\* h5 - variable to calculate umax \$

SUBMODEL: EXIST1;  
INPUTS: W1,AV1,WSET1,WS,W2,W3,W4,H5,F11,F21,F12,F13,F14;  
OUIPUTS: UEQ1,WV1 \$

SUBMODEL EXIST2;  
INPUTS: W2,AV2,WSET2,WS,W1,W3,W4,H5,F12,F22,F11,F13,F14;  
OUTPUTS: UEQ2,WV2 \$

SUBMODEL: EXIST3;  
INPUTS: W3,AV3,WSET3,WS,W1,W2,W4,H5,F13,F23,F11,F12,F14;  
OUTPUTS: UEQ3,WV3 \$  
END \$

\* path 1 flow submodel \$

MODEL: LEG1 \$

INPUTS: P,VA \$

OUTPUTS: W,AV \$

\* flow response equation (lbm/hr) \$

EQUATION:  $W' = 1/L * (-(ALPHA * EXP(-BETA * AV) + DELTA) * W^{**2} - K * W^{**2} + P)$  \$

\* valve angle response equation (degree) \$

:  $AV' = WV$  \$

\* valve speed response equation (deg/sec) \$

:  $WV' = 1/TAU * (KV * VA - WV)$  \$

\* flow resistance constant (lbf-hr<sup>\*\*2</sup>/lbm-in<sup>\*\*2</sup>) \$

:  $K = 3.57E-5$  \$

\* valve speed time constant (secs) \$

:  $TAU = 0.01$  \$

\* flow inertance (hr-sec-lbf/lbm-in<sup>\*\*2</sup>) \$

:  $L = 15.0 / (3600 * 144 * GC * PI * (0.5/24)^{**2})$  \$

\* valve resistance coefficient (lbf-hr<sup>\*\*2</sup>/lbm<sup>\*\*2</sup>-in<sup>\*\*2</sup>) \$

:  $ALPHA = 0.129$  \$

\* valve resistance coefficient (lbf-hr<sup>\*\*2</sup>/lbm<sup>\*\*2</sup>-in<sup>\*\*2</sup>) \$

:  $BETA = 0.1695$  \$

\* valve resistance coefficient (1/deg) \$

:  $DELTA = 1.14E-5$  \$

\* conversion constant between volts and degrees (deg/sec-volt) \$

:  $KV = 1.0$  \$

END \$

\* path 2 flow submodel \$

MODEL: LEG2 \$

INPUTS: P,VA \$

OUTPUTS: W,AV \$

```

* flow response equation (lbm/hr) $
EQUATION : W' = 1/L * (-(ALPHA*EXP(-BETA*AV)+DELTA)*W**2 - K*W**2 + P) $
* valve angle response equation (degree) $
  : AV' = WV$
* valve speed response equation (deg/sec) $
  : WV' = 1/TAU * (KV*VA- WV) $
* flow resistance constant (lbf-hr**2/lbm-in**2) $
  : K = 3.57E-5 $
$ valve speed time constant (secs) $
  TAU = 0.01 $
* flow inertance (hr-sec-lbf/lbm-in**2) $
  : L = 15.0/(3600*144*GC*PI*(0.5/24)**2)$
* valve resistance coefficient (lbf-hr**2/lbm**2-in**2) $
  : ALPHA = 0.129 $
* valve resistance coefficient (lbf-hr**2/lbm**2-in**2) $
  : BETA = 0.1695 $
* valve resistance coefficient (1/deg) $
  : DELTA = 1.14E-5 $
* conversion constant between volts and degrees (deg/sec-volt) $
  : KV= 1.0 $
END $

```

```

* path 3 flow submodel $
MODEL: LEG3 $
INPUTS: P,VA $
OUTPUTS: W,AV $
* flow response equation (lbm/hr) $
EQUATION: W' = 1/L * (-(ALPHA*EXP(-BETA*AV)+DELTA)*W**2 - K*W**2 + P) $
* valve angle response equation (degree) $
  : AV'-WV$
* valve speed response equation (deg/sec) $
  : WV' = 1/TAU * (KV*VA- WV) $
* flow resistance constant (lbf-hr**2/lbm-in**2) $
  : K = 3.57E-5 $
* valve speed time constant (secs) $
  : TAU = 0.01 $
* flow inertance (hr-sec-lbf/lbm-in**2) $
  : L = 15.0/(3600*144*GC*PI*(0.5/24)**2)$
* valve resistance coefficient (lbf-hr**2/lbm**2-in**2) $
  : ALPHA = 0.129 $
* valve resistance coefficient (lbf-hr** 2/lbm**2-in**2) $
  : BETA = 0.1695 $
* valve resistance coefficient (1/deg) $
  : DELTA=1.14E-5 $
* conversion constant between volts and degrees (deg/sec-volt) $
  : KV = 1.0 $
END $

```

```

* path 4 flow submodel $
MODEL: STATIC $
IPUTS: P $
OUTPUTS: W $
* flow response equation (lbm/hr) $
EQUATION: W' = 1/L * (-(ALPHA*EXP(-BETA*AV)+DELTA)*W**2 - K*W**2 + P) $
* valve resistance coefficient (lbf-hr**2/lbm**2-in**2) $

```

```

      : ALPHA = 0.129 $
* valve resistance coefficient (lbf-hr**2/lbm**2-in**2) $
      : BETA = 0.1695 $
* valve resistance coefficient (1/deg) $
      : DELTA = 1.14E-5 $
* flow resistance constant (lbf-hr**2/lbm-in**2) $
      : K = 3.57E-5 $
* flow inertance (hr-sec-lbf/lbm-in**2) $
      : L = 7.03E-4$
* fixed (static) angle of valve (degrees) $
      : AV = 37.0 $
END $

* source submodel $
MODEL SOURCE $
INPUTS: W1,W2,W3,W4,PUMP\REF \SPEED,PSET $
OUTPUTS: WS,P,PS,H5 $
MATRICES: XC[2,1], A[1,2], F[2,2], G[2,3], H[3,1], Z[1,1]$
* system pressure equation (psi) $
EQUATION: P' = 2/C * (WS - W1 - W2 - W3 - W4) $
* system flow equation (lbm/hr) $
      : WS' = 1/LS * (-RS*WS + PS - P) $
* high pressure side of the pump equation (psi) $
      : PS = (PUMP(WS,PUMP\SPEED*60/(2*PI),PUMP\REF\SPEED)) $
* source resistance (lbf-hr**2/lbm-in**2) $
      : RS = 1.0E-5*WS $
* source inertance (hr-sec-lbf/lbm-in**2) $
      : LS = 1.129230E-03 $
* source capacitance (lbf-hr/lbm-in**2-sec) $
      : C = 0.1$
* existence variable $
      : H5 = 1/LS * (-RS*WS + PS - P) $
* speed of pump equation (rads/sec) $
      : PUMP\SPEED' = 1/JML*(KT*IA-KI*PUMP\SPEED**2) $
* motor current $
      : IA' = 1/LM*(-RM*IA-KE*PUMP\SPEED-K2*(P-PSET)-K3*SPEED\FBK+ Z[1,1]) $
* speed feedback from pump sensor (rads/sec) $
      : SPEED\FBK' = 1/TAUF*(PUMP\SPEED-SPEED\FBK) $
* pump and pressure controller vector $
      : XC' = F*XC + G*H $
* source constants and matrices $
      : Z = A*XC $
      : KT = 0.3312 $
      : JML = 3.125E-5 $
      : LM = 0.0012 $
      : KE = 0.0418 $
      : RM = 0.618 $
      : K2 = 0.00213 $
      : TAUF = 0.00796 $
      : KI = 5.07E-7 $
      : K3 = 0.021 $
      : A = MAT(1,2, .0213, 400) $
      : F = MAT(2,2, 0, 0, 4.3E4, 0) $
      : G = MAT(2,3, 0, -1, .1, 4.3E-4, 4.3E-5, 4.3E-5) $
      : H = MAT(3,1,SPEED\FBK, P, PSET) $

```

END \$

\* sliding mode controller for path 1 \$

MODEL: LEG1\CONT \$

INPUTS: W,WSET \$

OUTPUTS: VA,VA\FILTERED \$

\* sliding surface coefficients \$

EQUATION : C1 = 225.0 \$

: C2 = 21.0 \$

\* sliding surface equation \$

: SIGMA = (EDD + C2\*ED + C1\*E)/100 \$

: VA = 5.0 IF (SIGMA.GE.EPS) ELSE

-5.0 IF (SIGMA.LE.-EPS) ELSE

(5/EPS)\*SIGMA \$

\* boundary condition \$

: EPS = 1.0 \$

\* flow error (lbm/hr) \$

: E = WSET - W \$

\* first derivative of error (lbm/hr/sec) \$

: ED' = (E-ED)/.1 \$

\* second derivative of error (lbm/hr/sec\*\*2) \$

: EDD' = (ED - EDD)/.1 \$

\* filtered control input (volts) \$

: VA\FILTERED' = (VA - VA\FILTERED)/0.2 \$

END \$

\* sliding mode controller for path 2 \$

MODEL: LEG2\CONT \$

INPUTS: W,WSET \$

OUTPUTS: VA,VA\FILTERED \$

\* sliding surface coefficients \$

EQUATION : C1 = 225.0 \$

: C2 = 21.0 \$

\* sliding surface equation \$

: SIGMA = (EDD + C2\*ED + C1\*E)/100 \$

: VA = 5.0 IF (SIGMA.GE.EPS) ELSE

-5.0 IF (SIGMA.LE.-EPS) ELSE

(5/EPS)\*SIGMA \$

\* boundary condition \$

: EPS = 1.0 \$

\* flow error (lbm/hr) \$

: E = WSET - W \$

\* first derivative of error (lbm/hr/sec) \$

: ED' = (E - ED)/.1 \$

\* second derivative of error (lbm/hr/sec\*\*2) \$

: EDD' = (ED - EDD)/.1 \$

\* filtered control input (volts) \$

: VA\FILTERED' = (VA - VA\FILTERED)/0.2 \$

END \$

\* sliding mode controller for path 3 \$

MODEL: LEG3\CONT \$

INPUTS: W,WSET \$

OUTPUTS: VA,VA\FILTERED \$

```

* sliding surface coefficients $
EQUATION : C1 = 225.0 $
          : C2 = 21.0$
* sliding surface equation $
          : SIGMA = (EDD + C2*ED + C1*E)/100 $
          : VA = 5.0 IF (SIGMA.GE.EPS) ELSE
            -5.0 IF (SIGMA.LE.-EPS) ELSE
            (5/EPS)*SIGMA $
* boundary condition $
          : EPS = 1.0$
* flow error (lbm/hr) $
          : E = WSET - W $
* first derivative of error (lbm/hr/sec) $
          : ED' = (E - ED)/.1 $
* second derivative of error (lbm/hr/sec**2) $
          : EDD' = (ED - EDD)/.1 $
* filtered control input (volts) $
          : VA\FILTERED' = (VA- VA\FILTERED)/0.2 $
END $

* existence condition submodel $
MODEL: EXIST $
INPUTS: W1,AV1,WV1,VA1,K1,TAU,L1,ALPHA,BETA,DELTA,KV,C1,C2,WSET1,P,W2,W3,
        W4,WT,H5,H6,H7,H8 $
OUTPUTS: U,SIGMA,SIGMAD,E,ED,EDD,EDDD $
* calculation of error and its derivatives $
EQUATION: E = WSET1 - W1 $
          : ED = WSET1D - 1/L1 * F1 $
          : EDD = WSET1DD - 1/L1 * DF1 $
          : EDDD = WSET1DDD - 1/L1 * DDF1 $
* calculation of the set-point profile derivatives $
          : WSET1D = 0 IF TIME.LE.5 ELSE
            -32.86 IF TIME.LE.12 ELSE
            0 IF TIME.LE.30 ELSE
            17.5 IF TIME.LE.50 ELSE
            0 $
          : WSET1DD = 0 $
          : WSET1DDD = 0 $
* calculation of existence variables $
          : F1 = F3*W1**2 + P $
          : F3 = -((ALPHA*EXP(-BETA*AV1)+DELTA)+K1) $
          : DF1 = G1+G2+G3 $
          : G1 = ALPHA*BETA*WV1*(W1**2)*EXP(-BETA*AV1) $
          : G2 = 2/L1 * W1*F1*F3 $
          : G3 = 2/CEQ * (WT-(W1+W2+W3+W4)) $
          : DDF1 = H1+H2+H3+H4+2/CEQ*(HS-H6-H7-H8) $
          : H1 = -ALPHA*(BETA**2)*(WV1**2)*(W1**2)*EXP(-BETA*AV1)+ 2/L1*
            (F3*(W1**3)+F1*W1)*ALPHA*BETA*WV1 *EXP(-BETA*AV1) $
          : H2 = 2/L1*ALPHA*BETA*WV1*W1*F1*EXP(-BETA*AV1) + F1/(L1**2)*
            (4*(W1**2)*(F3**2)+2*F1*F3) - 2*F1/(L1*CEQ) $
          : H3 = 4/(L1*CEQ)*F3*W1*(WT-(W1+W2+W3+W4)) $
          : H4 = ALPHA*BETA*(W1**2)*(EXP(-BETA*AV1))*(1/TAU*(KV*VA1 - WV1)) $
* calculation of sigma and sigma dot $
          : SIGMA = EDD + C2*ED + C1*E $
          : SIGMAD = EDDD + C2*EDD + C1*ED $

```

```

* calculation of umax $
  : U = (-WSET1DDD+1/L1*(H1+H2+H3+2/CEQ*(H5-H6-H7-H8)+ALPHA
    *BETA/TAU*WV1*(W1**2)*EXP(-BETA*AV1))-C2*EDD-C1*ED)/
    (1/(TAU*L1)*ALPHA*BETA*KV*(W1**2)*EXP(-BETA*AV1)) $
* system capacitance $
  : CEQ = 0.1 $
END $

* simulation submodel $
SIMULATE: MAIN $
* excite pump reference speed (rpm) $
EXCITE: PUMP\REF\SPEED = 18900.0 $
* excite of the input set-point profiles $
EXCITE: WSET1 = AF([0,260,5,260,12,30,30,30,50,380,60.1,380],TIME) $
  : WSET2 - AF([0,2.987103E+02,10,2.987103E+02,17,400,25,400,33,50,45,50,52,250,
    60.1,250],TIME) $
  : WSET3 - AF([0,260,7,260,15,350,35,350,45,30,50,30,55,100,60.1,100],TIME) $
* excite of the pressure set-point $
  : PSET = 10.0 $
* excite of the disturbance torque $
  : TD = AF([0,0.0,
    2,0.0,
    10,1.5,
    12,1.5,
    20,1.2,
    23,1.2,
    30,0.2,
    32,0.2,
    38,1.4,
    40,1.4,
    48,-1.0,
    52,-1.0,
    58,0.0, 60.1,0.0],TIME) $
* initialize integrators for states $
INITIALIZE: SOURCE,
  P = 1.000002E+01,
  WS = 1.004140E+03,
  PUMP\SPEED = 1.016179E+03,
  IA = 1.580731E+00,
  SPEED\FBK = 1.016179E+03,
  XC = MAT (2, 1,1.016179E+03, 1.078708E-01) $
  : LEG1,
  W = 2.600000E+02,
  AV = 4.220731E+01,
  WV=0.0$
  : LEG1\CONT,
  ED = 0.0,
  EDD = 0.0,
  VA\FILTERED = 0.0 $
  : LEG2,
  W = 2.987103E+02,
  AV = 4.479999E+01,
  WV = 0.0 $
  : LEG2\CONT,
  ED = 0.0,

```

```
EDD = 0.0,  
VA\FILTERED = 0.0 $  
: LEG3,  
W = 2.600000E+02,  
AV = 4.220731E+01,  
WV = 0.0 $  
: LEG3\CONT,  
ED = 0.0,  
EDD = 0.0,  
VA\FILTERED = 0.0 $  
: STATIC,  
W = 1.854298E+02 $  
* integrate using runge-kutta 4th order $  
INTEGRATE: RK4,TIMESTEP,0.001 $  
STOPIF: TIME.GE.60.0 $  
SAMPLE: STEP,100 $  
PLOT: LINEAR(0,1000,100),\OUTPUTS\ $  
END $
```

## REFERENCES

1. Ogata, K.: "System Dynamics." Prentice-Hall, Englewood Cliffs, NJ, 1978, pp. 184–195.
2. Cruz, J.B.: "Feedback Systems." McGraw Hill, New York, NY, 1971.
3. Athans, M.: "Special Issue on Linear-Quadratic-Gaussian Control." IEEE Transactions Automatic Control, vol. 16(6), 1971.
4. Brogan, W.L.: "Modern Control Theory, Second Edition." Prentice-Hall, Englewood Cliffs, NJ, 1985, pp. 350–356.
5. Landau, I.D.: "Adaptive Control: The Model Reference Approach." Marcel Dekker, New York, 1979.
6. Basar, T.: "H $\infty$ -Optimal Control and Related Minimax Design Problems: A Dynamic Game Approach." Birkhäuser, Boston, 1991.
7. Isidori, A.: "Nonlinear Control Systems." Springer-Verlag, Berlin, 1989, pp. 172–292.
8. Johnson, C.D.: "Disturbance-Accommodating Control; An Overview." Proceedings of the 1986 American Control Conference, vol. 1, Seattle, WA, June, 1986, pp. 526–536.
9. Slotine, J.E., and Li, W.: "Applied Nonlinear Control." Prentice Hall, Englewood Cliffs, NJ, 1991, pp. 191–275.
10. Itkis, U.: "Control Systems of Variable Structure." John Wiley & Sons, New York, NY, 1976, pp. 1–214.
11. Utkin, V.I.: "Variable Structure Systems With Sliding Modes." IEEE Transactions on Automatic Control, vol. AC-22, No. 2, April, 1977, pp. 212–222.
12. DeCarlo, R.A., Zak, S.H., and Mathews, G.P.: "Variable Structure Control of Nonlinear Multivariable Systems: A Tutorial." IEEE Proceedings, vol. 76, 1988, pp. 212–232.
13. Streeter, V.L., and Wylie, B.E.: "Fluid Mechanics." McGraw-Hill, Inc., New York, NY, 1975, pp. 109–127.
14. Van Wylen, G.J., and Sonntag, R.E.: "Fundamentals of Classical Thermodynamics." John Wiley and Sons, Inc., New York, NY, 1985, p. 24.
15. Irwin, J.D.: "Basic Engineering Circuit Analysis," Macmillan Publishing Company, New York, NY, 1984, pp. 24–25.
16. Jackson, M.E.: "Preliminary Control System Design and Analysis for the Space Station Furnace Facility Thermal Control System." NASA Technical Memorandum 108476, January 1995.
17. Strang, G.: "Linear Algebra and Its Applications." Third edition, Harcourt Brace Jovanovich, Inc., 1986, pp. 153–156.
18. Wyle, C.R., and Barret, L.C.: "Advanced Engineering Mathematics." Fifth edition, McGraw-Hill Book Co., New York, NY, 1982, pp. 295–296.

19. Elmali, E., and Olgac, N.: "Robust Output Tracking Control of Nonlinear MIMO Systems Via Sliding Mode Technique." *Automatica*, vol. 28, No. 1, Pergamon Press, 1992, pp. 145–151.
20. Johnson, C.D.: "Another Note on the Transformation to Canonical (Phase-Variable) Form." *IEEE Transactions on Automatic Control*, vol. AC-11, No. 3, January 1966, p. 609.
21. Byrnes, C., and Isidori, A.: "Local Stabilization of Minimum Phase Nonlinear Systems." *System Control Letter* 11, pp. 9–11.
22. Shtessel, Y.B., and Jackson, M.E.: "Sliding Mode Thermal Control System for Space Station Furnace Facility." *Proceedings of the 27th Southeastern Symposium on System Theory*, IEEE Computer Society Press, Los Alamitos, CA, March 1995, pp. 164–168.
23. Dorf, C.F.: "Modern Control Systems." Addison-Wesley Publishing Co., New York, NY, 1989, p. 155.
24. Utkin, V.I.: "Equations of Sliding Mode in Discontinuous System." *Automat. Remote Contr.*, vol. 's I and II, No. 12, 1972, pp. 1897–1907, No. 2, pp. 211–219.
25. Wonham, W.M., and Johnson, C.D.: "Optimal Bang-Bang Control With Quadratic Performance Index." *Proceedings of JACC*, 1963, pp. 101–112.
26. Sarpturk, S.Z., Istefanopulos, Y., and Kaynak, O.: "On the Stability of Discrete-Time Sliding Mode Control Systems." *IEEE Transactions on Automatic Control*, vol. AC-32, No. 10, October 1987, pp. 930–932.